

ความสัมพันธ์ระหว่างอิมพีแดนซ์ของเสียงและค่าความพูนของหมวดหินประดู่เต่าในปริมาตรลประดู่เต่า
แอ่งพิษณุโลก ประเทศไทย



นางสาว สุหทัยา แก้วละเอียด

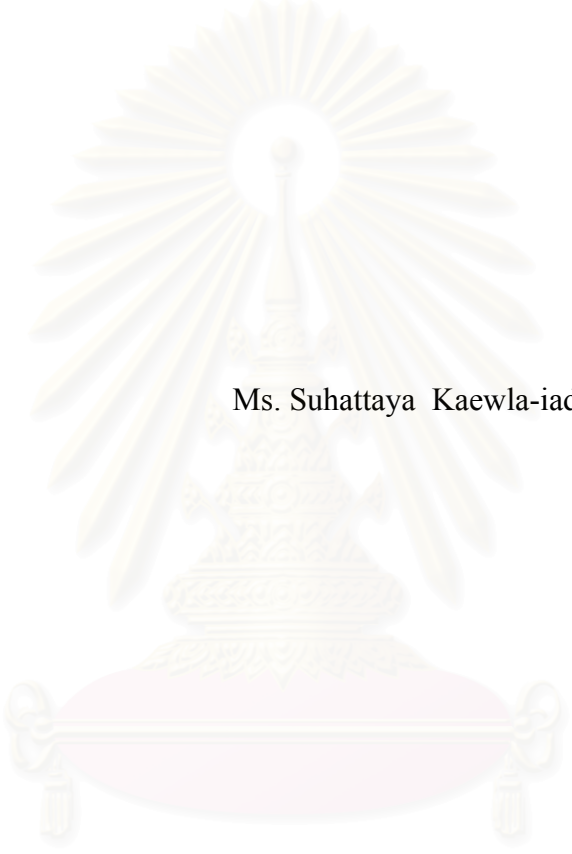
สถาบันวิทยบริการ
วิทยานิพนธ์นี้เป็นส่วนหนึ่งของการศึกษาตามหลักสูตรปริญญาวิทยาศาสตรมหาบัณฑิต
จุฬาลงกรณ์มหาวิทยาลัย
สาขาวิชาธรณีวิทยา ภาควิชาธรณีวิทยา
คณะวิทยาศาสตร์ จุฬาลงกรณ์มหาวิทยาลัย

ปีการศึกษา 2545

ISBN 974-17-3051-9

ลิขสิทธิ์ของจุฬาลงกรณ์มหาวิทยาลัย

RELATIONSHIP BETWEEN ACOUSTIC IMPEDANCE AND POROSITY
OF PRATU TAO FORMATION IN THE GREATER PRATU TAO AREA,
PHITSANULOK BASIN, THAILAND



Ms. Suhattaya Kaewla-iad

สถาบันวิทยบริการ
จุฬาลงกรณ์มหาวิทยาลัย

A Thesis Submitted in Partial Fulfillment of the Requirements
for the Degree of Master of Science in Geology

Department of Geology

Faculty of Science

Chulalongkorn University

Academic Year 2002

ISBN 974-17-3051-9

Thesis Title Relationship Between Acoustic Impedance and Porosity
of Pratu Tao Formation in the Greater Pratu Tao Area,
Phitsanulok Basin, Thailand
By Ms. Suhattaya Kaewla-iaad
Field of Study Geology
Thesis Advisor Associate Professor Punya Charusiri, Ph.D.
Thesis Co-advisor Somchai Poom-im, M.S.

Accepted by the Faculty of Science, Chulalongkorn University in Partial
Fulfillment of the Requirements for the Master's Degree

..... Dean of Faculty of Science
(Associate Professor Wanchai Phothiphichitr, Ph.D.)

THESIS COMMITTEE

..... Chairman
(Assistant Professor Veerote Daorerk, M.Sc.)

..... Thesis Advisor
(Associate Professor Punya Charusiri, Ph.D.)

..... Thesis Co-advisor
(Somchai Poom-im, M.S.)

..... Member
(Assistant Professor Sombat Yumuang, M.Sc.)

..... Member
(Chalermkiat Tongtaow, Ph.D.)

สุหัทธา แก้วละเอียด: ความสัมพันธ์ระหว่างอิมพีแดนซ์ของเสียงและค่าความพรุนของ
 หินประดูเต่าในปริมาตรประดูเต่าแอ่งพิบูลย์โลกประเทศไทย (RELATIONSHIP
 BETWEEN ACOUSTIC IMPEDANCE AND POROSITY OF PRATU TAO
 FORMATION IN THE GREATER PRUTU TAO AREA, PHITSANULOK BASIN,
 THAILAND) อ.ที่ปรึกษา: รศ. ดร. ปัญญา จารุศิริ, อ.ที่ปรึกษาร่วม: นาย สมชาย พุ่มอ้อม.
 124 หน้า. ISBN 974-17-3051-9.

หินประดูเต่าจัดอยู่ในกลุ่มหินชุดพิบูลย์โลกอายุยุคเทอร์เชียรี พบเฉพาะใน
 แอ่งพิบูลย์โลกเท่านั้นซึ่งอยู่ในบริเวณที่ราบลุ่มภาคกลางประเทศไทย บริษัทไทยเซลล์เอ็กพลอเรชั่น
 แอนด์โปรดักชั่นจำกัดได้รับสัมปทานในการสำรวจแหล่งปิโตรเลียมบริเวณพื้นที่สัมปทาน S1 ใน
 เดือนมีนาคม พ.ศ. 2522 ซึ่งครอบคลุมบางส่วนของแอ่งพิบูลย์โลก ผลการสำรวจพบว่าหิน
 ประดูเต่ามีศักยภาพในการกักเก็บปิโตรเลียม การศึกษาครั้งนี้กำหนดเป้าหมายในการวิเคราะห์
 ความสัมพันธ์ระหว่างอิมพีแดนซ์ของเสียง และค่าของความพรุนของหินประดูเต่าทั้งในเชิง
 ปริมาณและเชิงคุณภาพโดยใช้ข้อมูลจากหลุมเจาะ 11 หลุม และประกอบด้วยข้อมูลการหยัง
 ธรณีฟิสิกส์ ซึ่งได้แก่ รังสีแกมมา ความหนาแน่น นิวตรอน และแคลิเปอร์ โดยที่ข้อมูล
 จากการหยังธรณีฟิสิกส์ในช่วงปี พ.ศ. 2524 – 2527 มีคุณภาพต่ำกว่าข้อมูลที่ได้ในปี พ.ศ. 2544
 อันเนื่องมาจากสภาพหลุมเกิดความเสียหายบางส่วนจากการขุดเจาะ นอกจากนี้ได้ทำการวิเคราะห์
 ข้อมูลการสำรวจคลื่นแผ่นดินไหวสะท้อนสามมิติแบบสะท้อนในรูปแบบของอิมพีแดนซ์เทียม

ผลการศึกษาเชิงปริมาณพบว่า อิมพีแดนซ์ของเสียงอันเกิดจากการสังเคราะห์จากข้อมูล
 หยังธรณีฟิสิกส์มีความสัมพันธ์เชิงเส้นตรงกับค่าความพรุน ในขณะที่อิมพีแดนซ์เทียมจากข้อมูล
 สำรวจคลื่นแผ่นดินไหวสะท้อนแบบสะท้อนไม่แสดงความสัมพันธ์เชิงเส้นตรงกับค่าความพรุน ซึ่ง
 ทำให้ไม่สามารถใช้ข้อมูลดังกล่าวในการทำนายการกระจายตัวของหินกักเก็บ ในหินประดูเต่าได้

ส่วนผลการศึกษาเชิงคุณภาพพบว่า อิมพีแดนซ์ของเสียงจากข้อมูลหยังธรณีฟิสิกส์เมื่อนำ
 มาแสดงความสัมพันธ์กับความลึกในรูปแบบของกราฟ สามารถนำมาแบ่งหน่วยของหินโดย
 เบื้องต้นได้ 4 หน่วย ซึ่งจะเป็นข้อมูลสนับสนุนเพื่อช่วยในการศึกษาลักษณะการสะสมตัวและ
 การลำดับชั้นหินของหินประดูเต่าต่อไปในอนาคต

ภาควิชา	ธรณีวิทยา	ลายมือชื่อนิสิต.....
สาขาวิชา	ธรณีวิทยา	ลายมืออาจารย์ที่ปรึกษา.....
ปีการศึกษา	2545	ลายมือชื่ออาจารย์ที่ปรึกษาร่วม.....

4372515123 : MAJOR GEOLOGY
 KEY WORD : ACOUSTIC IMPEDANCE /POROSITY/ PRATUTAO
 FORMATION

SUHATTAYA KEAWLA-IAD: RELATIONSHIP BETWEEN ACOUSTIC IMPEDANCE AND POROSITY OF PRATU TAO FORMATION IN THE GREATER PRATU TAO AREA, PHITSANULOK BASIN, THAILAND. THESIS ADVISOR: ASSOCIATE PROFESSOR PUNYA CHARUSIRI, Ph.D., THESIS CO-ADVISOR: SOMCHAI POOM-IM. 124 pp. ISBN 974-17-3051-9

The Pratu Tao Formation is a Tertiary Formation of the Phitsanulok Group located in the central plain of Thailand. Thai Shell Exploration and Production Co., Ltd. was granted the S1 concession in March 1979, covering part of the Phitsanulok Basin. The exploration result presents that the Pratu Tao Formation has been proved successfully as a potential petroleum reservoir. This research aims at quantitative and qualitative analyses of the relationship between acoustic impedance and porosity of Pratu Tao Formation. The data employed in this study is composed of 11 wells with wire-line geophysical logs of gamma ray, density, neutron and caliper. The 3D seismic data with pseudo acoustic impedance (Runsum) volume is also employed in this study. The logging data acquired in the 1980s have been limited in use due to poor data quality caused from poor borehole condition, whilst the other good data acquired in 2001 are appropriate for this study.

The result of quantitative study presents that there is a linear relationship between acoustic impedance derived from the wire-line geophysical logging and porosity data. However, no linear relationship was observed between pseudo acoustic impedance (Runsum) from seismic and porosity data, the result indicates that the use of Runsum to predict a reservoir distribution cannot be applied in this seismic survey.

The result of qualitative study reveals that the values of plotting acoustic impedance versus depth in the X-Y pattern can be used to distinguish lithological units. From such new result, the Pratu Tao Formation can be subdivided into 4 distinct units (unit 1, 2, 3 and 4) based on slopes of shale impedance trend. This can be used as the supporting information for further detailed study of depositional environment and sequence stratigraphy of the Pratu Tao Formation.

Department	Geology	Student's signature:
Field of study	Geology	Advisor's signature:
Academic year	2002	Co-advisor's signature:

ACKNOWLEDGEMENTS

I would like to acknowledge Thai Shell Exploration and Production Co., Ltd. for permission to use their data. Special thanks to Mr. John Hoppe, Mr. Robert Gardham, Mr. Bernardus Johannes Van Wees, Mr. Volker Simon and Thai Shell staff for their helpful advice and support during my study.

I am very grateful to Associate Professor Dr. Punya Charusiri for sparing his precious time to provide consultancy and reviewing the thesis. I gratefully acknowledge Assistant Professor Pongsak Pongprayon, ex-advisor, for his valuable advice and all staff in the Department of Geology at Chulalongkorn University, for their support during my study.

My gratitude to Dr. Chalermkiat Tongtaow and Mr. Somchai Poom-im for their valuable time and very useful comments during my research. I am grateful to Mr. Somchai Sri-isaraporn, Mrs. Hatairat Triamwichanon, Mr. Booncherd Kongwung and Dr. Sunthorn Pumjan for their useful suggestions.

Special thanks for the generosity of the authors who for granting permission to use illustrations from their literature.

Many thanks to all my friends for their encouragement and help with the administrative work involve in this thesis, and Mr. Keith Ansell for correcting my English. Also thanks to the generosity of my colleagues who provide me their useful geological reports and theses.

This thesis is dedicated to my family whom I am very grateful for their understanding, continue support and assistance while studying.

CONTENT

	Page
ABSTRACT IN THAI.....	iv
ABSTRACT IN ENGLISH.....	v
ACKNOWLEDEMENTS.....	vi
CONTENTS.....	vii
LIST OF FIGURES.....	ix
LIST OF TABLES.....	xvi
LIST OF APPENDICES.....	xviii
CHAPTER I INTRODUCTION.....	1
1.1 Background.....	1
1.2 Study Area.....	1
1.3 Objective.....	4
1.4 Scope of Work and Methodology.....	4
1.5 Previous Investigations.....	6
1.6 Abbreviation Used.....	7
CHAPTER II REGIONAL AND GEOLOGICAL FRAMEWORK OF THE PHITSANULOK BASIN.....	9
2.1 Structural Setting.....	9
2.2 Basin Evolution.....	13
2.3 Depositional Environment and Stratigraphy.....	16
CHAPTER III DATA ACCESSIBILITY.....	23
3.1 Well Information.....	23
3.2 Lithological Classification.....	26
3.3 Logging Data.....	26
3.4 Seismic Data.....	29

CONTENT (Cont.)

	Page
CHAPTER IV DATA ANALYSIS	32
4.1 Quantitative Analysis.....	32
4.2 Qualitative Analysis.....	67
CHAPTER V DISCUSSION.....	99
4.1 Discussion of the Quantitative Results	99
4.2 Discussion of the Qualitative Results	106
CHAPTER VI CONCLUSIONS AND RECOMMENDATIONS.....	107
5.1 Conclusions.....	107
5.2 Recommendations.....	107
REFERENCES	108
APPENDICES	112
BIOGRAPHY	124

สถาบันวิทยบริการ
จุฬาลงกรณ์มหาวิทยาลัย

LIST OF FIGURES

Figure	Page
1.1 Map showing location of the study area in S1 coession covering the Phitsanulok basin, Thailand (DMR, 2002).....	2
1.2 Map showing location of the study area, Greater Pratu Tao area in the S1 concession, Thailand (Thai Shell, 2002).....	3
1.3 Summary of study workflow	5
2.1 The structural framework of the Phitsanulok Basin (Mäkel, <i>et.al</i> , 1997)...	10
2.2 The Chum Saeng depth map showing the study area	12
2.3 Structural model of the Phisanulok Basin phase I and II (Mäkel et al., 1997).....	14
2.4 Structural model of the Phisanulok Basin phase III and IV (Mäkel et al., 1997).....	15
2.5 Structural history of the Phitsanulok Basin in context of regional events (Mäkel et al., 1997)	17
2.6 Schematic stratigraphy of the Phitsanulok Basin (Bal et al., 1988)	18
2.7 Depositional environments of the Phitsanulok Basin (Bal et al., 1988)	19
2.8 K/Ar Dating data in the Pre-Tertiary Formation in S1 Concession (Thai Shell, 1985)	22
3.1 Section of normal seismic and Runsum data from the Greater Pratu Tao 3D survey	31
4.1 The parameters which are used in the Bandpass filtering process.....	33
4.2 Comparison between applying the Bandpass and the other filters into the acoustic (P-wave) impedance dataset of well NTM-C01	33
4.3a A cross-plot showing a relationship between acoustic (P-wave) impedance ($AI(Vp)$) and porosity in well NTM-A01	41
4.3b A cross-plot showing a relationship between acoustic (P-wave) impedance ($AI(Vp)$) and porosity in well NTM-B01	41
4.3c A cross-plot showing a relationship between acoustic (P-wave) impedance ($AI(Vp)$) and porosity in well NTM-C01	42
4.3d A cross-plot showing a relationship between acoustic (P-wave) impedance ($AI(Vp)$) and porosity in well KMG-A01	42

LIST OF FIGURES (Cont.)

Figure	Page
4.3e A cross-plot showing a relationship between acoustic (P-wave) impedance ($AI(V_p)$) and porosity in well PTO-A01	43
4.3f A cross-plot showing a relationship between acoustic (P-wave) impedance ($AI(V_p)$) and porosity in well PTO-A02	43
4.3g A cross-plot showing a relationship between acoustic (P-wave) impedance ($AI(V_p)$) and porosity in well PTO-A03	44
4.3h A cross-plot showing a relationship between acoustic (P-wave) impedance ($AI(V_p)$) and porosity in well WTN-A01	44
4.3i A cross-plot showing a relationship between acoustic (P-wave) impedance ($AI(V_p)$) and porosity in well WTN-B01	45
4.3j A cross-plot showing a relationship between acoustic (P-wave) impedance ($AI(V_p)$) and porosity in well NOH-A01	45
4.3k A cross-plot showing a relationship between acoustic (P-wave) impedance ($AI(V_p)$) and porosity in well NOH-A02	46
4.4a A cross-plot showing a relationship between Runsum seismic ($AI(Seismic)$) and porosity in well NTM-C01	47
4.4b A cross-plot showing a relationship between Runsum seismic ($AI(Seismic)$) and porosity in well WTN-B01	47
4.4c A cross-plot showing a relationship between Runsum seismic ($AI(Seismic)$) and porosity in well NOH-A01	48
4.4d A cross-plot showing a relationship between Runsum seismic ($AI(Seismic)$) and porosity in well NOH-A02	48
4.5a A cross-plot showing a relationship between Runsum seismic ($AI(Seismic)$) and acoustic (P-wave) impedance ($AI(V_p)$) in well NTM-C01	49
4.5b A cross-plot showing a relationship between Runsum seismic ($AI(Seismic)$) and acoustic (P-wave) impedance ($AI(V_p)$) in well WTN-B01	49
4.5c A cross-plot showing a relationship between Runsum seismic ($AI(Seismic)$) and acoustic (P-wave) impedance ($AI(V_p)$) in well NOH-A01	50
4.5d A cross-plot showing a relationship between Runsum seismic ($AI(Seismic)$) and acoustic (P-wave) impedance ($AI(V_p)$) in well NOH-A02	50

LIST OF FIGURES (Cont.)

Figure	Page
4.6a	A cross-plot showing a relationship between shear (S-wave) impedance ($AI(V_s)$) and porosity in well NTM-C01 52
4.6b	A cross-plot showing a relationship between shear (S-wave) impedance ($AI(V_s)$) and porosity in well WTN-B01 52
4.6c	A cross-plot showing a relationship between shear (S-wave) impedance ($AI(V_s)$) and porosity in well NOH-A01 53
4.6d	A cross-plot showing a relationship between shear (S-wave) impedance ($AI(V_s)$) and porosity in well NOH-A02 53
4.7a	A cross-plot showing a relationship between Runsum seismic ($AI(Seismic)$) and shear (S-wave) impedance ($AI(V_s)$) in well NTM-C01 54
4.7b	A cross-plot showing a relationship between Runsum seismic ($AI(Seismic)$) and shear (S-wave) impedance ($AI(V_s)$) in well WTN-B01 54
4.7c	A cross-plot showing a relationship between Runsum seismic ($AI(Seismic)$) and shear (S-wave) impedance ($AI(V_s)$) in well NOH-A01 55
4.7d	A cross-plot showing a relationship between Runsum seismic ($AI(Seismic)$) and shear (S-wave) impedance ($AI(V_s)$) in well NOH-A02 55
4.8a	A cross-plot showing a relationship between acoustic (P-wave) impedance ($AI(V_p)$) and shear (S-wave) impedance ($AI(V_s)$) in well NTM-C01 56
4.8b	A cross-plot showing a relationship between acoustic (P-wave) impedance ($AI(V_p)$) and shear (S-wave) impedance ($AI(V_s)$) in well WTN-B01 56
4.8c	A cross-plot showing a relationship between acoustic (P-wave) impedance ($AI(V_p)$) and shear (S-wave) impedance ($AI(V_s)$) in well NOH-A01 57
4.8d	A cross-plot showing a relationship between acoustic (P-wave) impedance ($AI(V_p)$) and shear (S-wave) impedance ($AI(V_s)$) in well NOH-A02 57
4.9a	A cross-plot showing a relationship between filtered acoustic (P-wave) impedance ($AI(V_p)$) and porosity in well NTM-C01 59
4.9b	A cross-plot showing a relationship between filtered acoustic (P-wave) impedance ($AI(V_p)$) and porosity in well WTN-B01 59
4.9c	A cross-plot showing a relationship between filtered acoustic (P-wave) impedance ($AI(V_p)$) and porosity in well NOH-A01 60

LIST OF FIGURES (Cont.)

Figure	Page
4.9d A cross-plot showing a relationship between filtered acoustic (P-wave) impedance ($AI(Vp)$) and porosity in well NOH-A02	60
4.10a A cross-plot showing a relationship between Runsum seismic ($AI(seismic)$) and filtered acoustic (P-wave) impedance ($Filtered AI(Vp)$) in well NTM-C01	61
4.10b A cross-plot showing a relationship between Runsum seismic ($AI(seismic)$) and filtered acoustic (P-wave) impedance ($Filtered AI(Vp)$) in well WTN-B01	61
4.10c A cross-plot showing a relationship between Runsum seismic ($AI(seismic)$) and filtered acoustic (P-wave) impedance ($Filtered AI(Vp)$) in well NOH-A01	62
4.10d A cross-plot showing a relationship between Runsum seismic ($AI(seismic)$) and filtered acoustic (P-wave) impedance ($Filtered AI(Vp)$) in well NOH-A02	62
4.11a A cross-plot showing a relationship between filtered shear (S-wave) impedance ($Filtered AI(Vs)$) and porosity in well NTM-C01	63
4.11b A cross-plot showing a relationship between filtered shear (S-wave) impedance ($Filtered AI(Vs)$) and porosity in well WTN-B01	63
4.11c A cross-plot showing a relationship between filtered shear (S-wave) impedance ($Filtered AI(Vs)$) and porosity in well NOH-A01	64
4.11d A cross-plot showing a relationship between filtered shear (S-wave) impedance ($Filtered AI(Vs)$) and porosity in well NOH-A02	64
4.12a A cross-plot showing a relationship between Runsum seismic ($AI(seismic)$) and filtered shear (S-wave) impedance ($Filtered AI(Vs)$) in well NTM-C01	65
4.12b A cross-plot showing a relationship between Runsum seismic ($AI(seismic)$) and filtered shear (S-wave) impedance ($Filtered AI(Vs)$) in well WTN-B01	65

LIST OF FIGURES (Cont.)

Figure	Page
4.12c A cross-plot showing a relationship between Runsum seismic ($AI(seismic)$) and filtered shear (S-wave) impedance ($Filtered AI(Vs)$) in well NOH-A01	66
4.12d A cross-plot showing a relationship between Runsum seismic ($AI(seismic)$) and filtered shear (S-wave) impedance ($Filtered AI(Vs)$) in well NOH-A02	66
4.13a A cross-plot showing a relationship between filtered acoustic (P-wave) ($Filtered AI(Vp)$) and filtered shear (S-wave) impedance ($Filtered AI(Vs)$) in well NTM-C01	68
4.13b A cross-plot showing a relationship between filtered acoustic (P-wave) ($Filtered AI(Vp)$) and filtered shear (S-wave) impedance ($Filtered AI(Vs)$) in well WTN-B01	68
4.13c A cross-plot showing a relationship between filtered acoustic (P-wave) ($Filtered AI(Vp)$) and filtered shear (S-wave) impedance ($Filtered AI(Vs)$) in well NOH-A01	69
4.13d A cross-plot showing a relationship between filtered acoustic (P-wave) ($Filtered AI(Vp)$) and filtered shear (S-wave) impedance ($Filtered AI(Vs)$) in well NOH-A02	69
4.14a A cross-plot between gamma ray and depth showing the lithological units in well NTM-C01	77
4.14b A cross-plot between acoustic (P-wave) impedance ($AI(Vp)$) and depth showing the lithological units in well NTM-C01.....	78
4.14c A cross-plot between shear (S-wave) impedance ($AI(Vs)$) and depth showing the lithological units in well NTM-C01	79
4.14d A cross-plot between Runsum seismic ($AI(Seismic)$) and depth showing the lithological units in well NTM-C01	80
4.14e A cross-plot between porosity and depth showing the lithological units in well NTM-C01	81
4.15a A cross-plot between gamma ray and depth showing the lithological units in well WTN-B01	82

LIST OF FIGURES (Cont.)

Figure	Page
4.15b A cross-plot between acoustic (P-wave) impedance (AI(Vp)) and depth showing the lithological units in well WTN-B01	83
4.15c A cross-plot between shear (S-wave) impedance (AI(Vs)) and depth showing the lithological units in well WTM-B01	84
4.15d A cross-plot between Runsum seismic (AI(Seismic)) and depth showing the lithological units in well WTN-B01	85
4.15e A cross-plot between porosity and depth showing the lithological units in well WTN-B01	86
4.16a A cross-plot between gamma ray and depth showing the lithological units in well NOH-A01	87
4.16b A cross-plot between acoustic (P-wave) impedance (AI(Vp)) and depth showing the lithological units in well NOH-A01	88
4.16c A cross-plot between shear (S-wave) impedance (AI(Vs)) and depth showing the lithological units in well NOH-A01	89
4.16d A cross-plot between Runsum seismic (AI(Seismic)) and depth showing the lithological units in well NOH-A01	90
4.16e A cross-plot between porosity and depth showing the lithological units in well NOH-A01	91
4.17a A cross-plot between gamma ray and depth showing the lithological units in well NOH-A02	92
4.17b A cross-plot between acoustic (P-wave) impedance (AI(Vp)) and depth showing the lithological units in well NOH-A02	93
4.17c A cross-plot between shear (S-wave) impedance (AI(Vs)) and depth showing the lithological units in well NOH-A02	94
4.17d A cross-plot between Runsum seismic (AI(Seismic)) and depth showing the lithological units in well NOH-A01	95
4.17e A cross-plot between porosity and depth showing the lithological units in well NOH-A02	96
5.1 Impedance (Runsum) attribute of Nelson survey displays reservoir architecture (Eocene channels) (Lechner et al., 1994)	101

LIST OF FIGURES (Cont.)

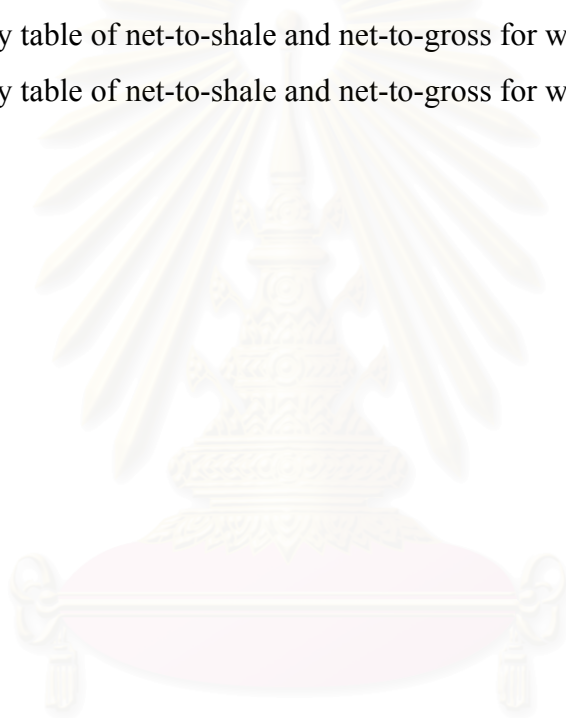
Figure		Page
5.2	Map showing Barik net sand thickness in the Greater Makarem area, the Oman (Muggli, 2000).....	101
5.3	Impedance maps with line-drawing interpretations of sand distribution and the inferred directions of sediment transport in Suphan Buri Basin, Thailand (Ronghe and Surarat, 2002)	103
5.4	The schematic plots between acoustic impedance (P-wave) against depths for wells drilled in 2001 showing the new approach to recognise the lithological units in the Pratu Tao Formation.....	104
5.5	The plots of gamma ray data against depth and acoustic impedance against depth of well NTM-C01 showing the new possible top Chum Saeng Formation.	105
5.6	The plots showing the conformable pattern with the common idealised log curve shapes interpreted as facies succession (Walker, 1992).....	106

LIST OF TABLES

Table		Page
3.1	The depth intervals (mTVDSS) of all study well in the Pratu Tao Formation.....	24
3.2	Lithological classification based on a ratio of separation between density and neutron logs.....	24
3.3	List of logging data used in this study	27
4.1	The summary of correlation coefficients obtained from the linear relationship between acoustic (P-wave) impedance and porosity	34
4.2	The summary of correlation coefficients obtained from the linear relationship between Runsum seismic and porosity	35
4.3	The summary of correlation coefficients obtained from the linear relationship between Runsum seismic and acoustic (P-wave) impedance	35
4.4	The summary of correlation coefficients obtained from the linear relationship between shear (S-wave) impedance and porosity	36
4.5	The summary of correlation coefficients obtained from the linear relationship between Runsum seismic and shear (S-wave) impedance.....	36
4.6	The summary of correlation coefficients obtained from the linear relationship between acoustic (P-wave) impedance and shear (S-wave) impedance...	37
4.7	The summary of correlation coefficients obtained from the linear relationship between filtered acoustic (P-wave) impedance and porosity.....	37
4.8	The summary of correlation coefficients obtained from the linear relationship between Runsum seismic and filtered acoustic (P-wave) impedance	38
4.9	The summary of correlation coefficients obtained from the linear relationship between filtered shear (S-wave) impedance and porosity	38
4.10	The summary of correlation coefficients obtained from the linear relationship between Runsum seismic and filtered shear (S-wave) impedance	39
4.11	The summary of correlation coefficients obtained from the linear relationship between filtered acoustic (P-wave) impedance and filtered shear (S-wave) impedance	39

LIST OF TABLES (Cont.)

Table	Page
4.12 Lithological units classified in NTM-C01	70
4.13 Lithological units classified in WTN-B01	71
4.14 Lithological units classified in NOH-A01	72
4.15 Lithological units classified in NOH-A02	73
4.16 Summary table of net-to-shale and net-to-gross for well NTM-C01	74
4.17 Summary table of net-to-shale and net-to-gross for well WTN-B01	74
4.18 Summary table of net-to-shale and net-to-gross for well NOH-A01	75
4.19 Summary table of net-to-shale and net-to-gross for well NOH-A02	75



สถาบันวิทยบริการ
จุฬาลงกรณ์มหาวิทยาลัย

LIST OF APPENDICES

Appendix		Page
A	The logging panel of well KMG-A01	113
B	The logging panel of well NOH-A01	114
C	The logging panel of well NOH-A02	115
D	The logging panel of well NTM-A01	116
E	The logging panel of well NTM-B01	117
F	The logging panel of well NTM-C01	118
G	The logging panel of well PTO-A01	119
H	The logging panel of well PTO-A02	120
I	The logging panel of well PTO-A03	121
J	The logging panel of well WTN-A01	122
K	The logging panel of well WTN-B01	123



 สถาบันวิทยบริการ
 จุฬาลงกรณ์มหาวิทยาลัย

CHAPTER I

INTRODUCTION

1.1 Background

The Greater Pratu Tao area (GPTO) is a part of the Phitsanulok Basin which is a major Tertiary extensional structure overlying a Mesozoic basement and is the largest of a string of Tertiary intracratonic extensional basins of onshore Thailand. It lies off the northern part of the S1 concession and is located to the north of the Sirikit Field which is the principal producing field in the concession (Figure 1.1). In 1981, the first well of the S1 concession, Pratu Tao A01 (PTO-A01), was drilled with only the availability of 2D seismic data in this area by Thai Shell Exploration and Production Co., Ltd. to evaluate the hydrocarbon potential in the Phitsanulok Basin. The well encountered hydrocarbon bearing sandstone in the Pratu Tao Formation which led to a further five exploration wells being drilled. However, results were less than satisfactory. Hence, consequently the 3D seismic acquisition in this area was considered as a solution to enhance the quality of subsurface information. No further wells were drilled after acquisition due to concentration on the Sirikit Field development programme. Exploration activities were resumed in 2000 and the prospectivity of the Pratu Tao Formation was reviewed.

1.2 Study Area

The study area is situated within the Bang Rakam District in Phitsanulok and Kong Krilat District in Sukhothai, both in the central plain of Thailand, and is concentrated on an area covering 160 km² in the middle and southern part of the GPTO 3D survey (Figure 1.2). The survey was carried out by Compagnie Générale de Géophysique (CGG) in 1984-1985 which covered a rectangular area of 447.53 km² (391 km² full fold). It was reprocessed in 1999-2000 to improve structural resolution and reduce exploration risk. The data from eleven wells drilled in this area was used in the study.

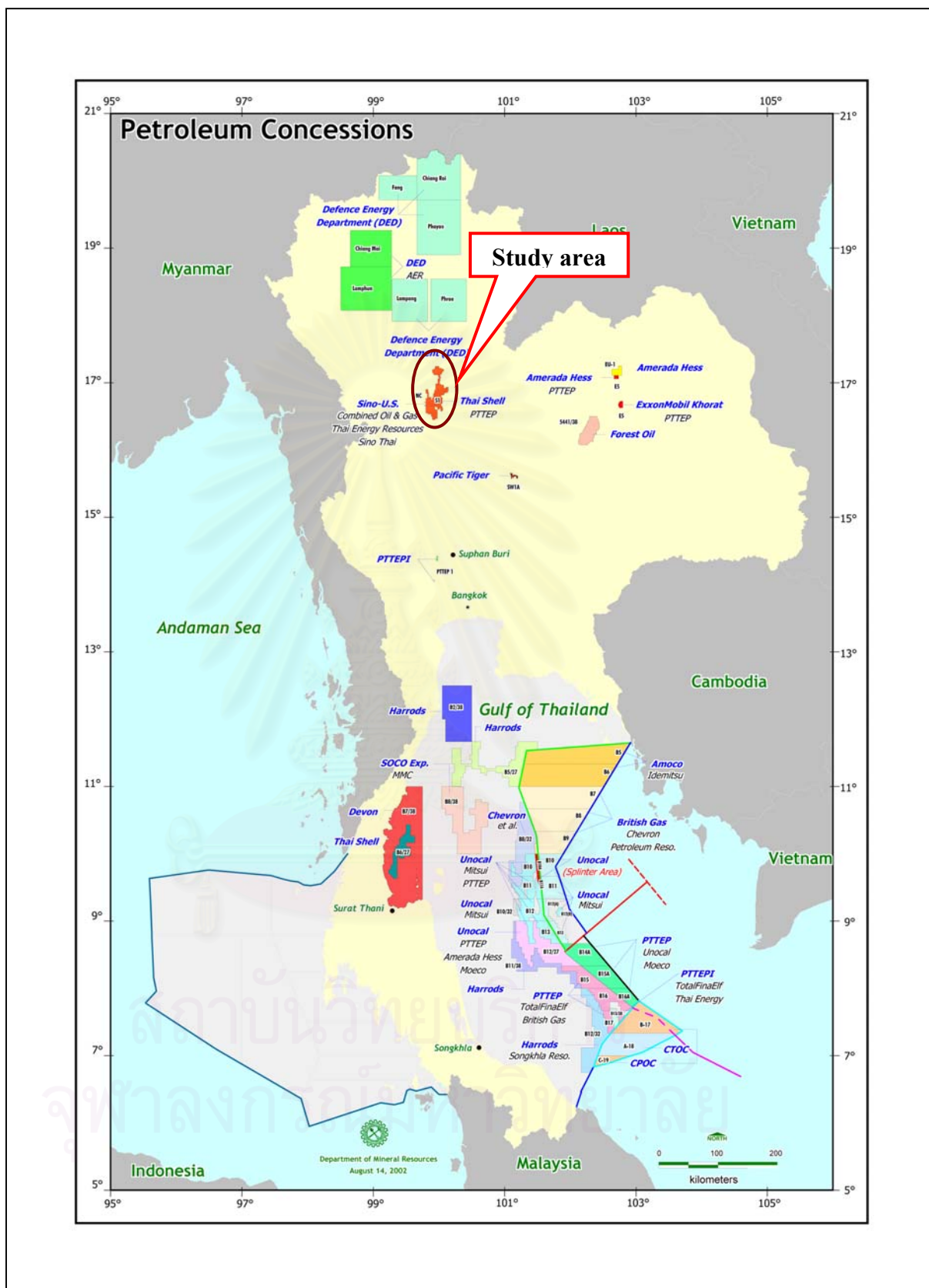


Figure 1.1 Map showing location of the study area in S1 concession covering the Phitsanulok Basin, Thailand (DMR, 2002).

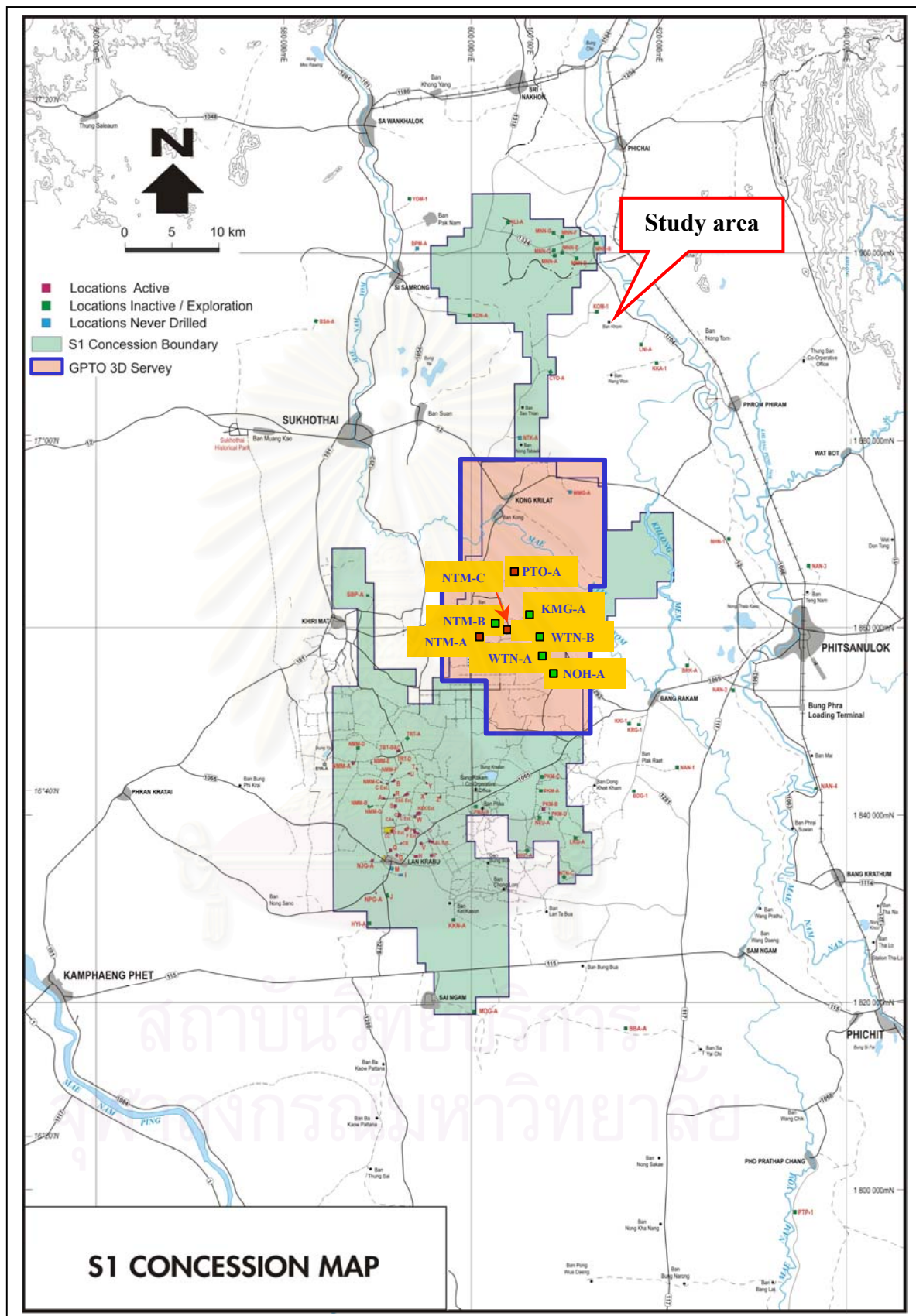


Figure 1.2 Map showing location of the study area, Greater Pratu Tao 3D survey in S1 concession, Thailand (Thai Shell, 2002).

1.3 Objective

The objective of this study is to quantitatively and qualitatively analyse the relationship between acoustic impedance and porosity of the Pratu Tao Formation in the GPTO area.

1.4 Scope of Work and Methodology

This study concentrates on data analysis only within the Pratu Tao Formation. With limitations of tools and logging data quality, a proper seismic inversion could not be applied.

The first part of the study was performed using both *LOGIC*, Shell proprietary software, and Schlumberger's seismic interpretation software package, which consist of *Charisma v.3.7.0* and *Synthetics*. The main processes are summarised as follows (Figure 1.3):

1. Gathering and quality checking of seismic and logging data
2. Extraction of Runsum seismic (pseudo acoustic impedance) from seismic depth cube
3. Acoustic impedance data computation of compressional (V_p) and shear (V_s) sonic logs
4. Data analysis using cross-plotting technique applied to create relationship between acoustic impedance (P-wave) and porosity
5. Well selection for quantitative and qualitative data analysis
6. Quantitative data analysis
 - 6.1 Cross-plotting among acoustic impedance from P-wave and S-wave (called shear impedance), Runsum seismic (AI (Seismic)) and porosity
 - 6.2 Filtering acoustic impedance (P-wave) and shear impedance (S-wave) with seismic bandwidth
 - 6.3 Cross-plotting among filtered acoustic impedance (P-wave) and shear impedance (S-wave), AI (Seismic) and porosity
- 7 Qualitative data analysis by cross-plotting among (P-wave) and shear impedance (S-wave), porosity, Runsum seismic and depth for preliminary recognition of lithological units
9. Discussion and conclusion

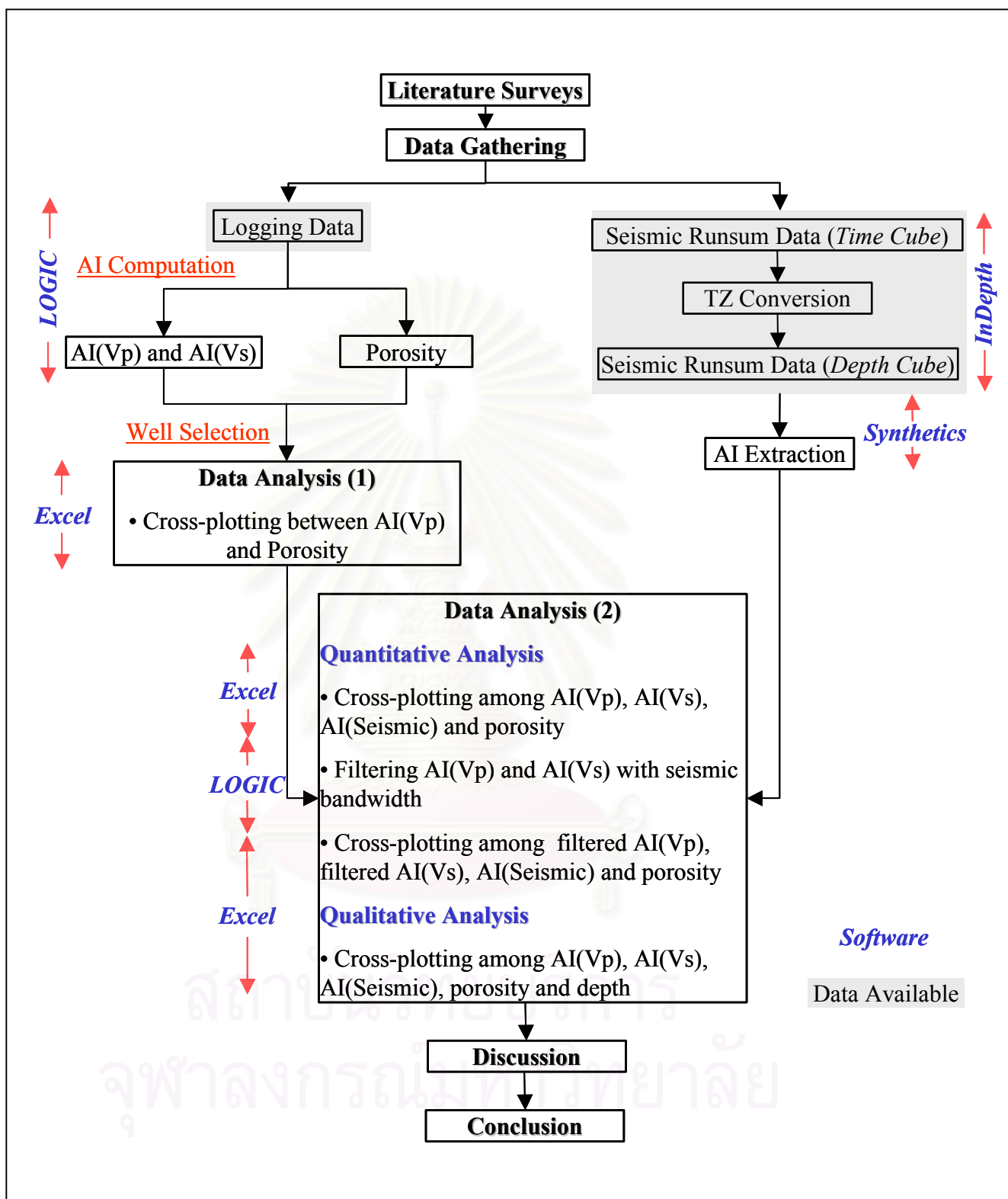


Figure 1.3 Summary of study workflow.

1.5 Previous Investigations

Study works in the GPTO area were carried out in the last two decades and are summarised as follows;

During 1984-1985, the 3D GPTO seismic survey was carried by Compagnie Générale de Géophysique (CGG).

In 1985, the survey was originally processed by Geophysical Services International (GSI) in Singapore.

In 1988, the first interpretation in the GPTO 3D survey was done using the Landmark III workstation and documented. The initial interpretation was aimed to create reasonably accurate horizon maps in the short period. In the same year, a review of the seismic processing was performed by Shell Geophysical Research in the Hague to improve a seismic quality.

In 2000, the survey was reprocessed by Shell Geoscience Services (SGS). The main objectives was to evaluate whether new processing techniques would improve the subsurface image in order to identify new prospects in the S1 concession, to improve the structural information of the GPTO 3D survey.

In 2001, a re-interpretation of the GPTO 3D survey using SGS processing data was carried as a continuation of prospectivity reviews of the Pratu Tao and Yom Formations.

There are some studies using pseudo acoustic impedances (Runsum) which are summarised as follows;

In 1994, a study of impedance conversion applied to 3D seismic dataset was carried out by Lechner et al.(1994) in Shell UK Expro. It aimed to enhance the interpretability of lithological packages allowing recognition of individual channel bodies thus facilitating an improved definition and understanding of the Nelson turbidite reservoir. A conversion of the reflectivity data to band limited pseudo acoustic impedance traces is generated by integration of the reflectivity trace using Shell proprietary software, *SIPMAP RUNSUM*. It concluded that the impedance attribute in Nelson contributed significantly to the detailed three-dimensional reservoir modelling and understanding.

A seismic inversion study was carried out over the Barik reservoir in the Greater Makarem area by Muggli (2000). The purpose of the study was to predict reservoir properties using generation of a Runsum bandlimited impedance cube. The impedance cube was a result of integration of the seismic data. The result presented a trend of sand distribution and was useful for reducing the uncertainty of the Barik property prediction.

There is a study of acoustic impedance interpretation for sand distribution adjacent to a rift boundary fault by Ronghe and Surarat (2002). This report presents a seismic inverse modeling study from an oil-producing field in the Suphan Buri basin, Thailand. Seismic data made the inverse modeling study feasible, with the objective of imaging distributions of lithology and/or hydrocarbons, depending on the data-specific discriminatory capability of acoustic impedance.

1.6 Abbreviation Used

A number of abbreviations are used in this report. For clarity they are listed below.

3D survey	Three dimension seismic survey
3D GPTO survey	Three dimension seismic survey in Greater Pratu Tao area
AI	Acoustic impedance
AI(Vp)	Acoustic impedance derived from compression (P-) wave
AI(Vs)	Shear (acoustic) impedance derived from shear (S-) wave
bopd	Barrels of oil per day
Charisma	Schlumberger's seismic interpretation software
CGG	Compagnie Générale de Géophysique. It is a company providing seismic acquisition service
DMR	Department of Mineral Resources
GPTO	The Greater Pratu Tao geographical area
GSI	Geophysical Services International. It was a company providing seismic processing service
Landmark	Halliburton's seismic interpretation software
LOGIC	Logging interpretation software invented by Shell Company
KMG	Khui Mamuang geographical area. Surface locations and wells in this area are prefixed KMG-
KMG-A01	Well Khui Mamuang A01
MMstb	Million stock tank barrels
mTVD	True vertical thickness in meters
mTVDSS	Depth below sea level in meters
NOH	Nong Ooh geographical area. Surface locations and wells in this area are prefixed NOH-

NOH-A	Nong Ooh “A” surface locations. Wells in this location are prefixed NTM-A
NOH-A01	Well Nong Ooh A01
NOH-A02	Well Nong Ooh A02
NTM	Nong Tum geographical area. Surface locations and wells in this area are prefixed NTM-
NTM-A	Nong Tum “A” surface locations. Wells in this location are prefixed NTM-A
NTM-A01	Well Nong Tum A01
NTM-B	Nong Tum “B” surface locations. Wells in this location are prefixed NTM-B
NTM-B01	Well Nong Tum B01
NTM-C	Nong Tum “C” surface locations. Wells in this location are prefixed NTM-C
NTM-C01	Well Nong Tum C01
PTO	Pratu Tao geographical area. Surface locations and wells in this area are prefixed PTO-
PTO-A	Pratu Tao “A” surface locations. Wells in this location are prefixed PTO-A
PTO-A01	Well Pratu Tao A01
PTO-A02	Well Pratu Tao A02
PTO-A03	Well Pratu Tao A03
RUNSUM	Pseudo acoustic impedance called only in Shell Company
SIPMAP	Seismic processing software invented by Shell Company
SGS	Shell Geoscience Services. It is a one of research and development departments in Shell company providing seismic processing services.
Shell UK Expro	Shell Company in United Kingdom
Thai Shell	Thai Shell Exploration and Production Co., Ltd.
WTN	Wat Tean geographical area. Surface locations and wells in this area are prefixed WTN-
WTN-A	Wat Tean “A” surface locations. Wells in this location are prefixed WTN-A
WTN-A01	Well Wat Tean A01
WTN-B	Wat Tean geographical area. Surface locations and wells in this area are prefixed WTN-
WTN-B01	Well Wat Tean B01

CHAPTER II

REGIONAL AND GEOLOGICAL FRAMEWORK OF THE PHITSANULOK BASIN

The Phitsanulok Basin is geologically very complex due to its multi-phased structural history and the interaction between faulting and deposition through time. The basin contains Tertiary sediments overlying a Mesozoic basement. The Greater Pratu Tao (GPTO) field is situated within the heavily faulted part of the Phitsanulok Basin. The depositional environments in the GPTO area are similar to the Sirikit Field which is a main oil producing area in the S1 concession. The sediments in the upper section are the product of fluvial systems whereas those in the lower section were filled in with lacustrine deposits. The alluvial plain and fan deposits were also observed in some parts of the lowest section. The Pratu Tao Formation is a result of the fluvial deposition system situated in the upper part of the Phitsanulok Basin. It is a highly potential reservoir in the GPTO area.

2.1 Structural Setting

The Phitsanulok Basin is the largest onshore Tertiary intracratonic extensional rift basin in Thailand. The rift basin is oriented approximately N-S and formed as a result of the relative movement of the Shan Thai and Indochina Blocks (Bal et al., 1988). The basin has been governed by the movements of the four main fault systems as follows (Figure 2.1):

1. The Western Boundary Fault System

These faults run as normal faults in a NNW-SSE direction. The fault system is not continuous and the separation is connected by NNE-SSW faults. They are located in the western part of the basin. The faults dip at approximately 45°. The minor sinistral oblique slip of the fault segments was found locally.

2. The Uttraradit Fault

This is situated in north of the basin and runs in ENE-WSW. It is recognised as a sinistral wrench fault moving eastward of the basement. The Uttraradit fault separates the Sukhothai Depression, downthrown to the south, from the Pichai Graben to the north.

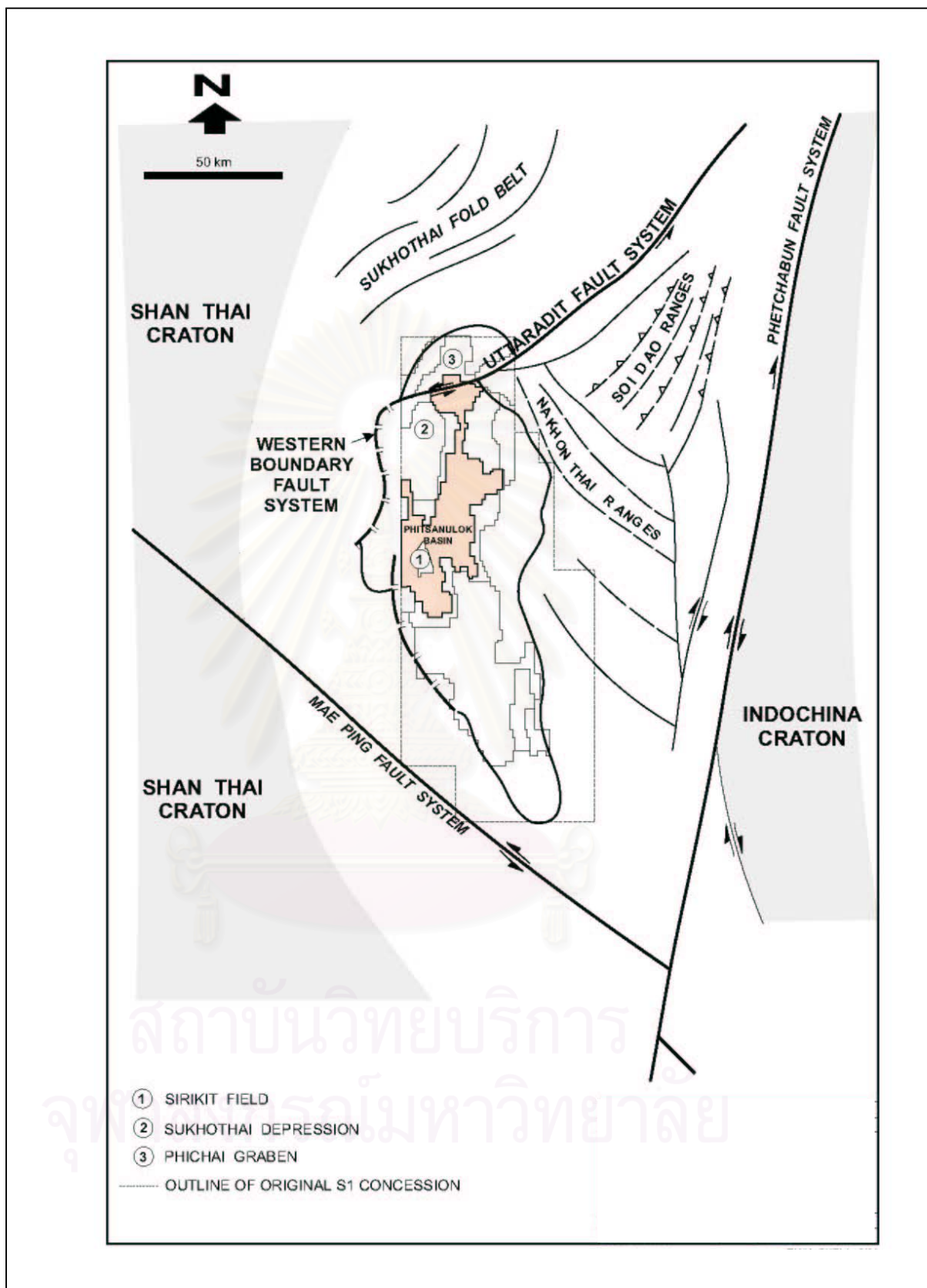


Figure 2.1 The structural framework of the Phitsanulok Basin (Mäkel et al., 1997).

3. The Mae Ping Fault

This fault is a NW-SE sinistral wrench fault located in the SW of the basin. The movement was observed primarily towards the SE of the Shan Thai Block.

4. The Phetchabun Fault Zone

This zone runs a dextral wrench fault system with a displacement of at least 50 km. It is located in the east of the basin and separates the Shan Thai Block from the Indochina Block.

The faults mentioned above are not present in the GPTO area. The fault pattern in the study area is characteristically highly dense and complex. There are two main extensional structural trends one in a NNW-SSE direction and the other in a NNE-SWW direction. The observation from the seismic interpretation in 2000 shows the tectonic outline and fault magnitude at three main horizon markers; the Pratu Tao, Chum Saeng and Pre-Tertiary Formations. The depth map of the Chum Saeng Formation shows an accomplished structural view in the GPTO area (Figure 2.2). The deepest part of the GPTO area is in the NW flank and becomes shallower relief towards the SE direction. The study area can be subdivided geographically into five areas; the Pratu Tao, Nong Tum, Khui Mamuang, Wat Tean and Nong Ooh areas (Figure 2.2).

Nong Tum Area:

There is a main SSE fault that separates Nong Tum area from Pratu Tao and Khui Mamuang areas. It is the deepest part of the western area where several blocks from a terrace. The area becomes shallower towards the NE. There are 3 wells drilled in the Nong Tum area; NTM-A01, NTM-B01 and NTM-C01, used in this study.

Pratu Tao Area:

This is in the upper part of the study area and is bounded by the SSE trending fault to the west and a number of scattering faults. There are 3 wells drilled in the Pratu Tao area; PTO-A01, PTO-A02 and PTO-A03, used in this study.

Khui Mamuang Area:

A main fault with a SSE trend separates the Nong Tum area from the Pratu Tao and Khui Mamuang areas. There is one wells drilled in the Khui Mamuang area, KMG-A01, used in this study.

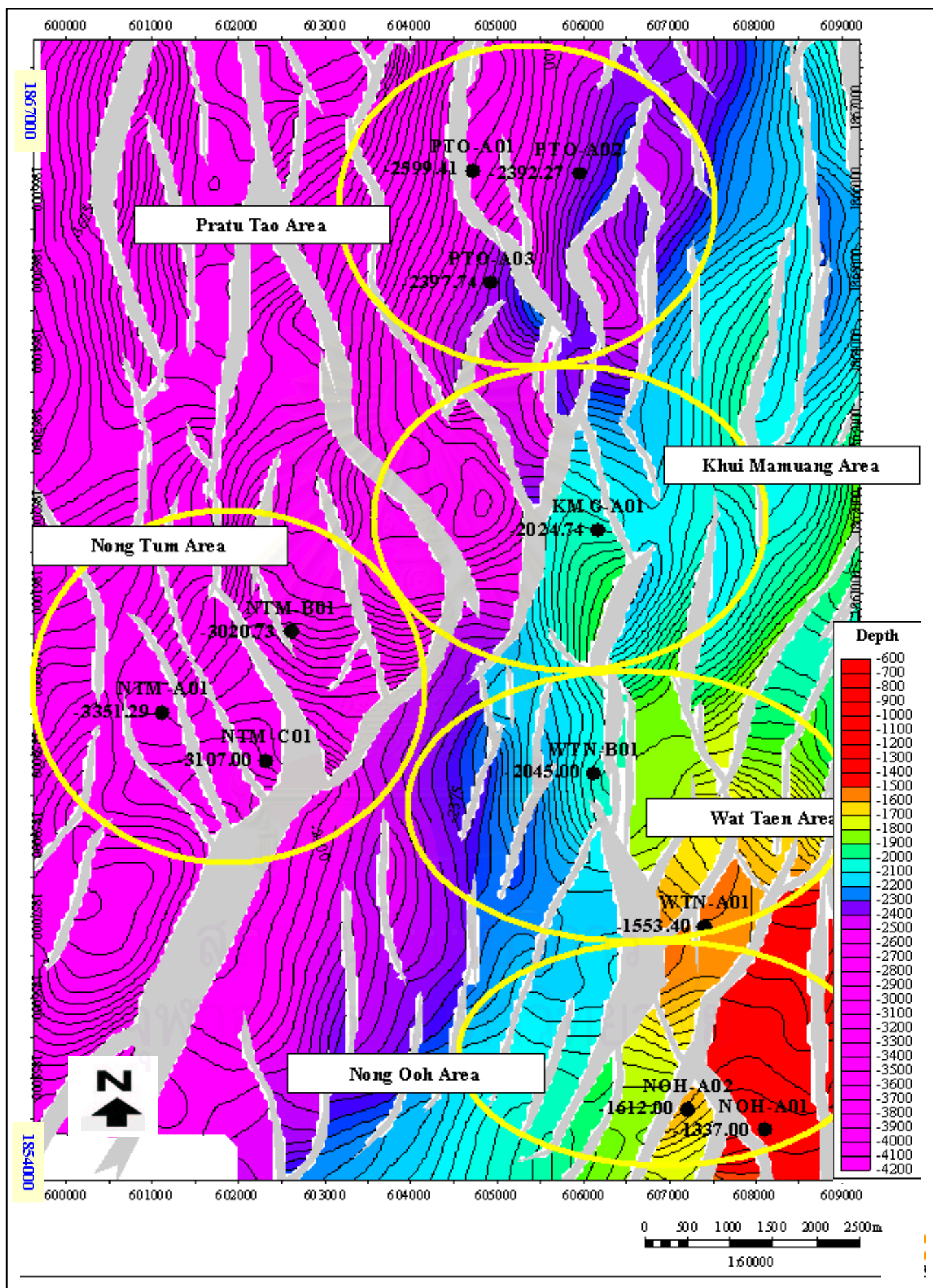


Figure 2.2 The Chum Saeng depth map showing the study area.

This is characterised by the most intense fault and is located in the eastern part of the study area. The depth is progressively shallower to the south. There are 2 wells drilled in the Wat Tean area; WTN-A01 and WTN-B01, used in this study.

Nong Ooh Area:

This area is in the southern region and the shallowest part of the study area with SE trending. There are 2 wells drilled in the Nong Ooh area; NOH-A01 and NOH-A02, used in this study.

2.2 Basin Evolution

The evolution of the Phitsanulok Basin was influenced by structural history of the four major fault systems (Mäkel et al., 1997). The sediments were derived from the Western Boundary Fault area from the north and the east. It can be subdivided in to four phases (Figures 2.3 and 2.4).

Phase I: Extension

The structural setting of the basin was an almost purely extension. It began with the extension rifting and the main extension presents along the Western Boundary Fault system. The basin was bounded by the Uttradit Fault in the North which accommodates the extension with sinistral movement. The dextral movement of the Phetchabun Fault occurred in the Northeast whilst the Mae Ping Fault presented a sinistral movement in the Southeast. The deposition of Oligocene clastic sediments (Sarabop, Nong Bua and Khom Formations) occurred over the entire basin and became progressively younger to the east. The sediments were composed of fluvial to alluvial fan and fan delta. During the Miocene, the depositional environment changed to the open lacustrine as a result of continued subsidence. The sediments of open lacustrine Chum Saeng Formation and fluvio-deltaic Lan Krabu Formation presented the interdigitating feature in this period.

Phase II: Extension and Transtension

The blocked extensional movement of the Mae Ping Fault and the continued movement along the Phetchabun Fault caused an inversion in the southern area. This leads a change in the conditions along the basin boundary faults which effected the depositional setting. The environment changed dramatically from lacustrine system to alluvial system. The Pratu Tao and Yom Formations were deposited in this changing

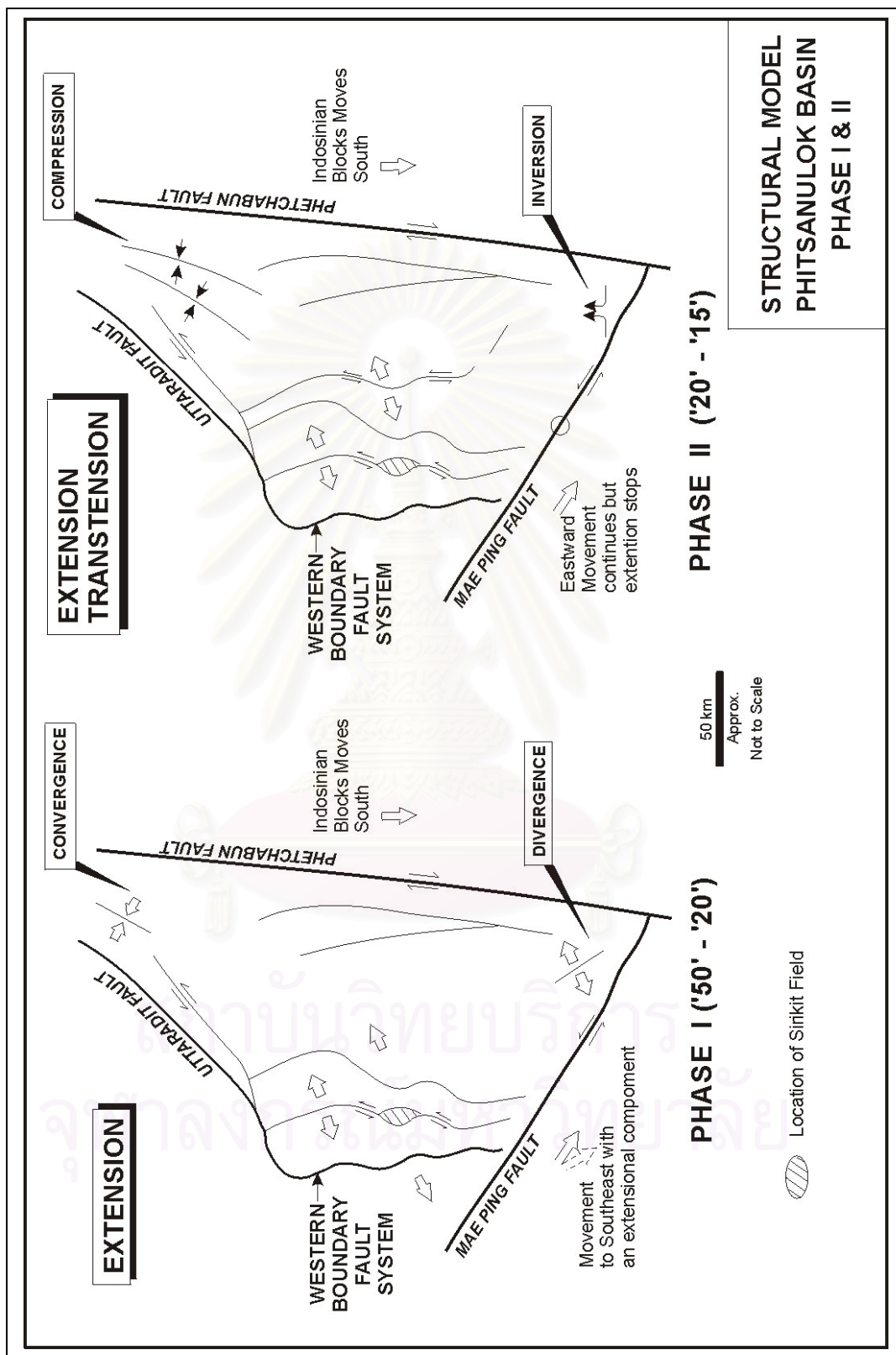


Figure 2.3 Structural model of the Phisanulok Basin phase I and II (Mäkel et al., 1997).

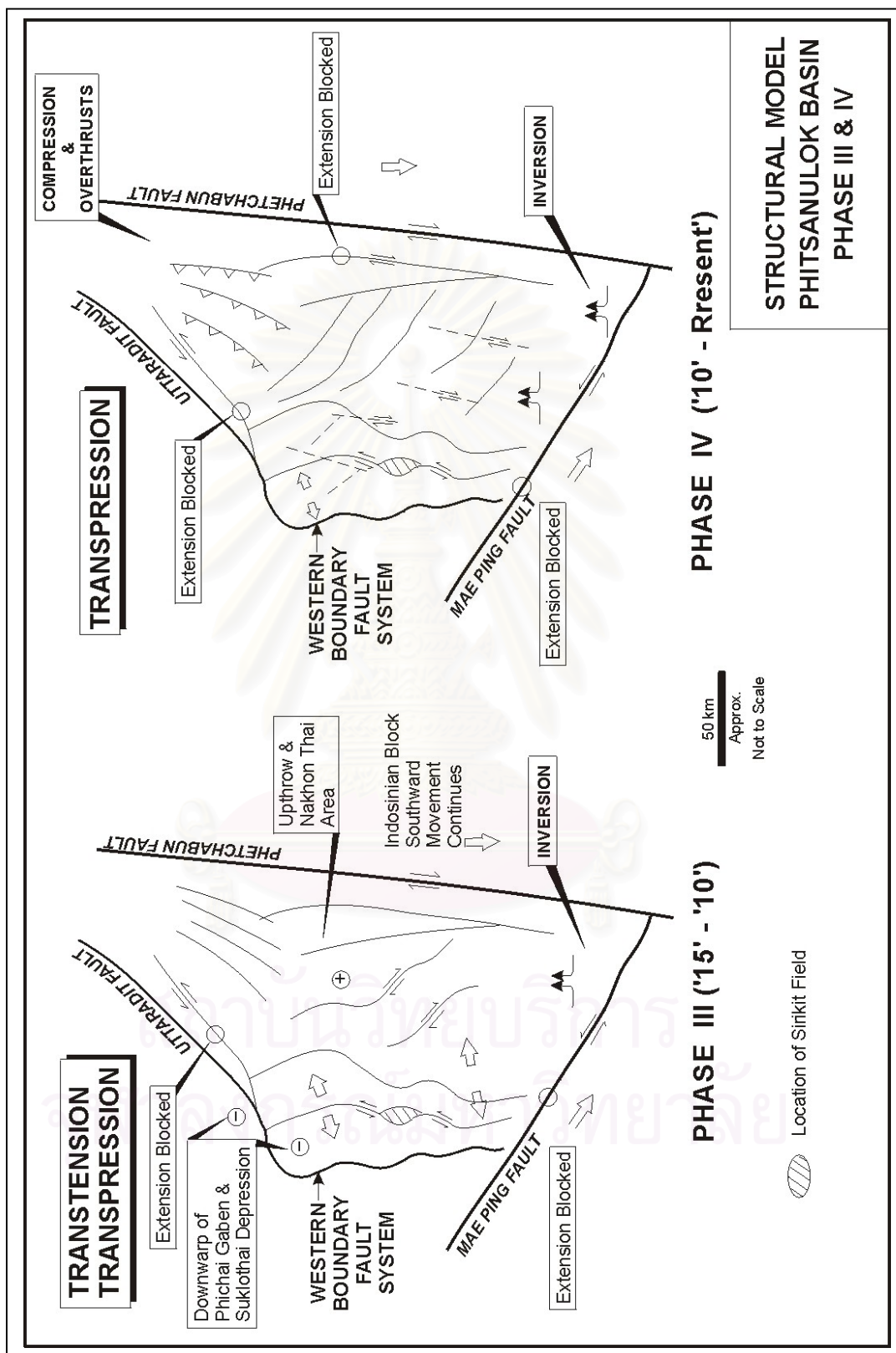


Figure 2.4 Structural model of the Phisanulok Basin phase III and IV (Mäkel et al., 1997).

tectonic regime. The clastic sediments of these formations represent braided and meandering river system.

Phase III: Transtension and Transpression

The extension of the basin ceased in the northern part of the basin, but it still continued in the south. The compression and overthrusts developed in the east. The changing of this tectonic regime might be reflected by the Yom and Ping Formation transition. This leads the dominant depositional environment switched from meandering fluvial deposition (Yom Formation) to alluvial fan and braidplain deposition (Ping Formation).

Phase IV: Transpression

The extension in the southern part was blocked. The compressional and inversion features, and wrench faulting appears to the Petchabun Fault. There are basaltic and rhyolitic rocks as a result of volcanism associated with this phase.

2.3 Depositional Environment and Stratigraphy

The Phitsanulok Basin contains non-marine the Tertiary sedimentary sequence overlying the Mesozoic basement (Figure 2.5). It represents the typical tripartite subdivision as follows:

1. The lowest section was influenced by alluvial fan and plain deposits. It consists of three equivalent formations; Sarabop, Nong Bua and Khom Formation.
2. The middle section was filled by a fluviolacustrine sedimentary wage recognised as Chum Saeng and Lan Krabu Formations.
3. The upper part consists of Yom and Pratu Tao Formations which are the product of alluvian plain deposits.

The Tertiary succession of the Phitsanulok Basin, named as Phitsanulok Group, was divided into 8 units which indicate the age between Oligocene to Recent (Bal et al., 1988). The depositional environment and stratigraphy of Phitsanulok Group are classified as follows (Figures 2.6 and 2.7):



Figure 2.5 Structural history of the Phitsanulok Basin in context of regional events (Mäkel et al., 1997).

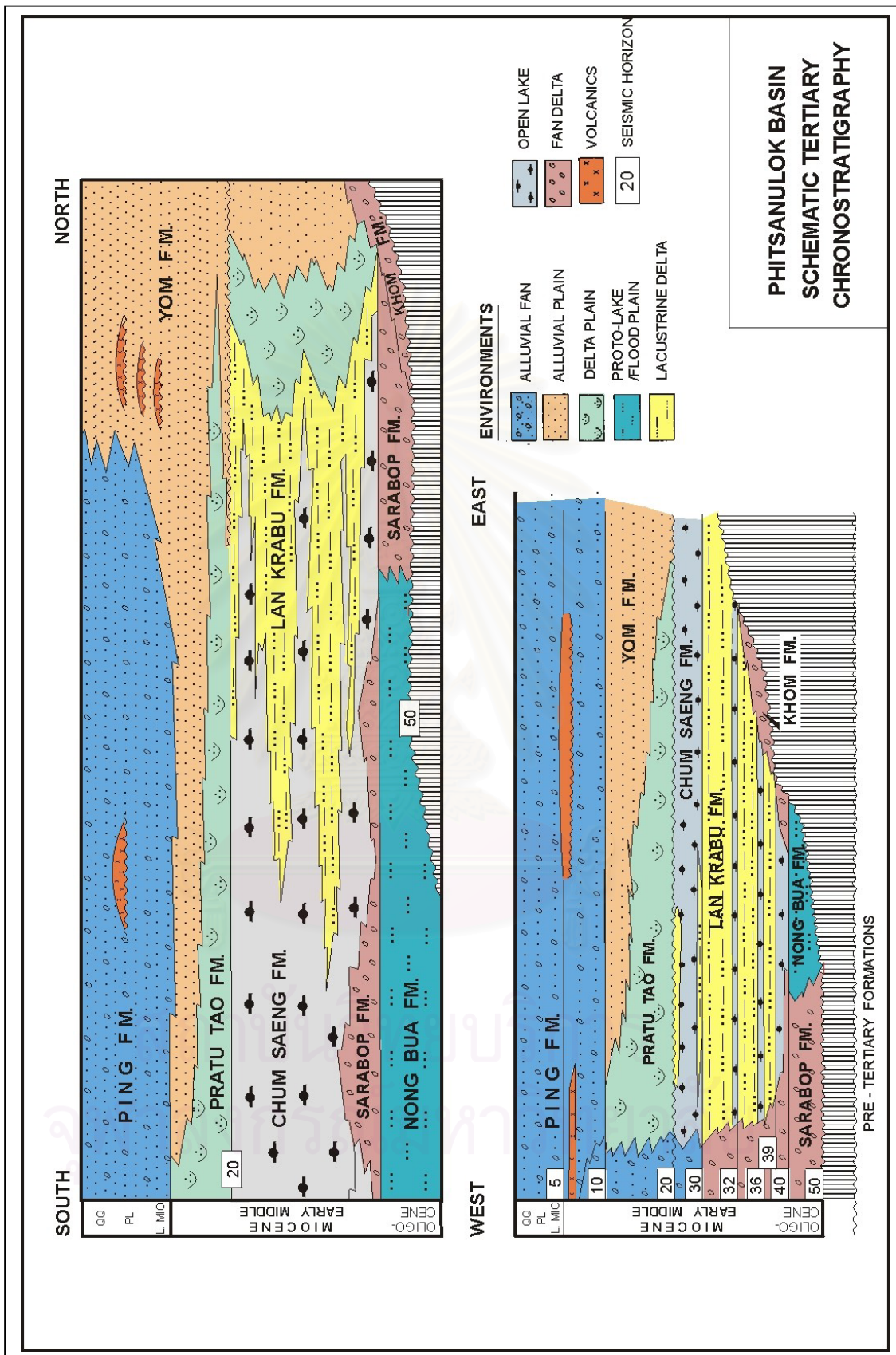


Figure 2.6 Schematic stratigraphy of the Phitsanulok Basin (Bal et al., 1988).

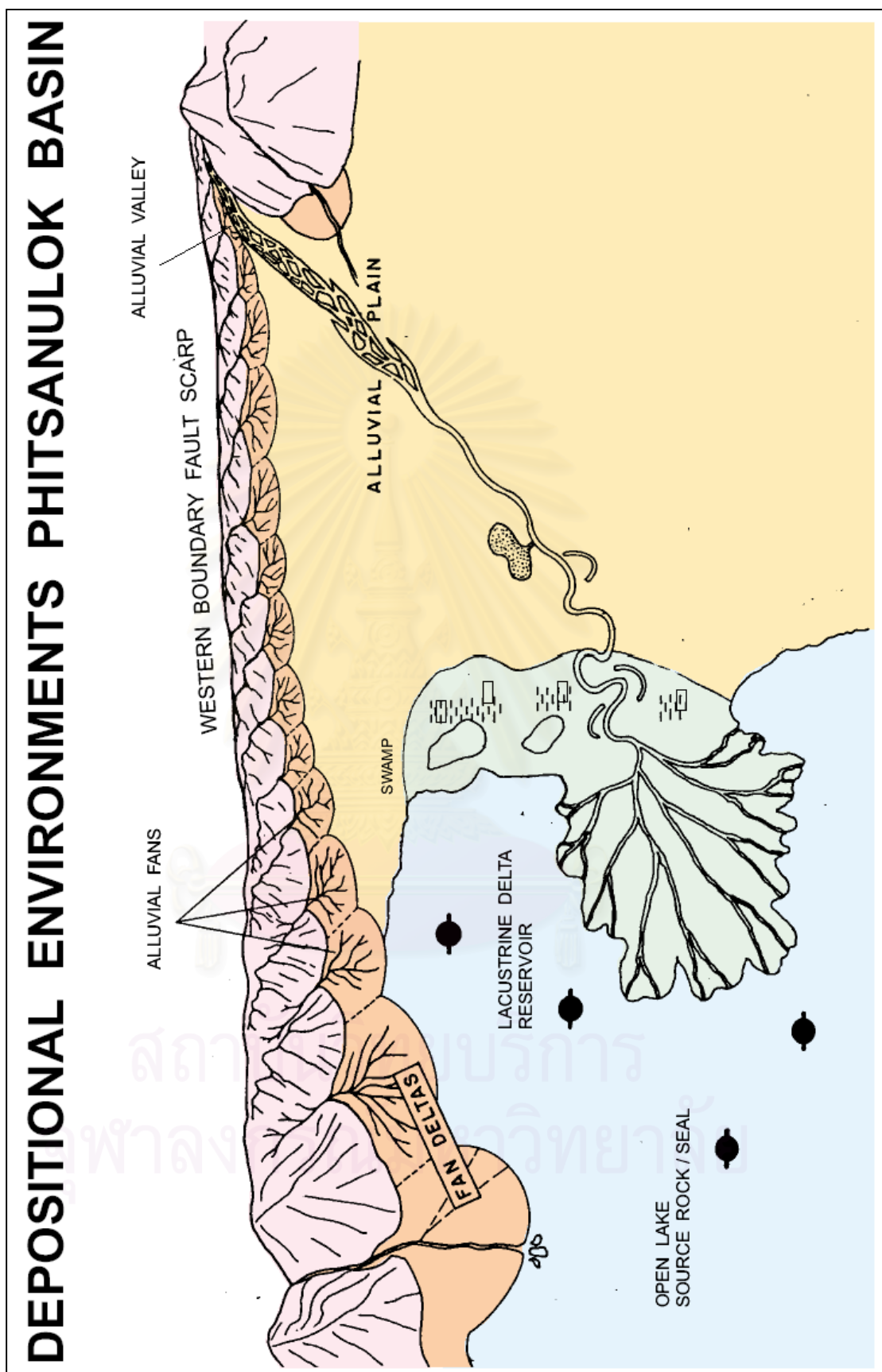


Figure 2.7 Depositional environments of the Phitsanulok Basin (Bal, et al., 1988)

Sarabop Formation: (?Oligocene - Early Miocene)

The Sarabop Formation is the oldest Tertiary rock unit in the Phitsanulok Basin. The deposition of this formation was consisted of fluvial, alluvial fan and fan delta deposits, but mainly alluvial fan type. Sediments are gravel and claystone and sandstones and were derived from the Western Boundary Fault System. The average thickness of this formation is approximately 1,400 m.

Nong Bua Formation: (?Oligocene - Early Miocene)

The Nong Bua Formation is made of predominantly low energy environment. Sediments comprise of claystone with minor fine to coarse lithic sandstone of floodplain deposit. This formation is best developed in the southeastern part of the basin.

Khom Formation: (?Early Miocene)

The Khom Formation is composed of a coarse lithofacies consisting of poorly sorted, conglomeratic sandstone from alluvial plain deposit and lacustrine claystone. It shows a diachronous onlap on the eastern flank of the basin.

Chum Saeng Formation: (?Early - Middle Miocene)

The Chum Saeng Formation is a result of open lacustrine deposit. Widespread transgressions covered the entire basin which made this formation to be a regional marker. It is high quality hydrocarbon source rock with the approximate thickness of 1,000 m.

Lan Krabu Formation: (?Early - Middle Miocene)

The Lan Krabu Formation consists of fluviolacustrine sandstones, one of main hydrocarbon reservoir targets for the basin. During Miocene, the depositional environment changed from open lacustrine to the fluvio-delta and presented interfingering deposit of Chum Saeng and Lan Krabu Formations.

Pratu Tao Formation: (?Middle Miocene)

The Pratu Tao Formation is a result of alluvial deposits. The lower member of this formation was made up of fluvial system, consisting of silty claystone with fine to coarse sands representing ephemeral lacustrine to flood plain environments with occasional fluvial systems. The upper member was dominantly vari-coloured clay fine to medium sands. This formation was confirmed to be a potential hydrocarbon reservoir in last decade. The average thickness is approximately 1,400 m.

Yom Formation: (?Middle Miocene)

The Yom Formation is indicative of a fluvial depositional system with thickness of 1,000 m. This consists of alluvial sediments comprising mainly of sandstone and claystone. A potential hydrocarbon reservoir of this formation was discovered only in the west of the Sirikit Field. In some area, the top of Yom Formation is a marked erosion surface through most of the basin. This erosion surface in exploration well Ket Kason-1, located in southeast of the Sirikit Field, is overlain by a basalt flow found and has been radiometrically dated at Late Miocene (10 million years).

Ping Formation: (?Late Miocene - Recent)

The Ping Formation is the youngest succession of this basin consisting of coarse sands and gravels with associated vari-coloured clay. This formation is 1,200 m thick of alluvial fan deposit.

The Pre-Tertiary basement in the Phitsanulok Basin has various rock types presented by sedimentary, volcanic and metamorphic rocks. The wide range of age is a variety of ?Permian to Cretaceous. However, the majority of the Pre-Tertiary rocks are assigned to Khorat group of Upper Triassic to Cretaceous age. In the GPTO area, K/Ar dating data obtained from samples of well PTO-A01 and NTM-A01 show ages of 125-157 Ma and 173 +/-9 Ma respectively (Thai Shell, 1985) (Figure 2.8).

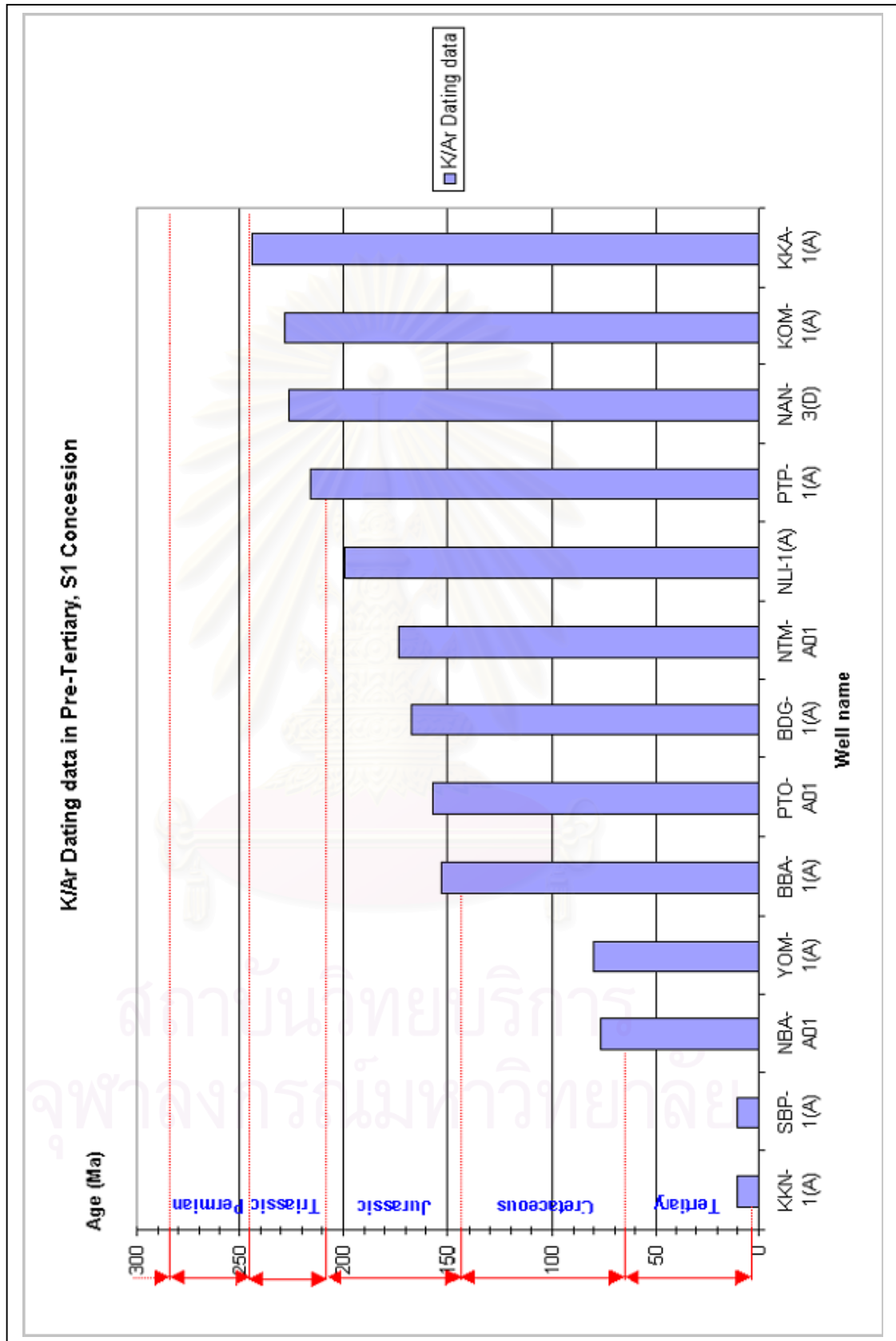


Figure 2.8 K/Ar Dating data in the Pre-Tertiary Formation in S1 Concession (Thai Shell, 1985)

CHAPTER III

DATA ACCESSIBILITY

3.1 Well Information

Eleven wells are in total used in this study. The depth intervals (mTVDSS) of each well in Pratu Tao Formation are tabulated in Table 3.1. Seven of these wells, drilled in 1980s, unfortunately have poor boreholes. The others drilled in 2001 show good borehole condition. The well locations can be seen in Figure 2.1 and below is the well information divided into geographical areas.

Nong Tum Area

- *Nong Tum-A01 (NTM-A01)*

This well was drilled June 1983 and the first well in the Nong Tum area with the aim of testing the subsurface structure and hydrocarbon presence in the Pratu Tao and Lan Krabu Formations. The well encountered 16.5 mTV and 1.7 mTV of net-oil-sand in the Pratu Tao and Lan Krabu Formations respectively. The well is currently producing approximately 200-250 bopd.

- *Nong Tum-B01 (NTM-B01)*

This was the second well in the Nong Tum area, drilled in March 1984 and had similar objectives to those of NTM-A01. Oil shows were recorded from the Pratu Tao Formation with 7.5 mTV of net-oil-sand. However, this formation is tight and the well was plugged and abandoned.

- *Nong Tum-C01 (NTM-C01)*

This well was drilled in May 2001 to appraise and develop the Pratu Tao reservoir and determine the petroleum potential of the Yom and Lan Krabu Formations in a neighbouring fault block to the NTM-A01. The well encountered 24 mTV and 2.9 mTV of net-oil-sand in the Pratu Tao and Lan Krabu Formations respectively. The production test showed a flow rate of 1,500 bopd.

Pratu Tao Area

- *Pratu Tao-A01 (PTO-A01)*

This was the first well to be drilled in S1 concession in June 1981 with the aim of testing hydrocarbon potential of the tertiary reservoir sequences overlying the

Table 3.1 The depth intervals (mTVDSS) of all study well in the Pratu Tao Formation

	KMG-A01	NOH-A01	NOH-A02	NTM-A01	NTM-B01	NTM-C01	PTO-A01	PTO-A02	PTO-A03	WTN-A01	WTN-B01
Top Pratu Tao Fm.	1482.65	891.40	1100.00	1952.07	1837.37	2060.00	1510.82	1456.19	1557.87	1211.87	1375.00
Top Chuum Saeng Fm.	2024.74	1337.00	1612.00	3351.29	3020.73	3107.00	2599.41	2392.27	2397.74	1553.40	2045.00

Table 3.2 Lithological classification based on a ratio of separation between density and neutron logs

Lithology	Density&Neutron Separation
Shale	> 10
Dirty Sand	10 > separation > 7
Shaly Sand	7 > separation > 0
Clean Sand	0 > separation > -50

Pre-Tertiary unconformity on the eastern flank of the Phitsanulok Basin. The well discovered 12.6 mTV of uneconomically producible oil in the Pratu Tao Formation and was, therefore, plugged back and suspended with the wellhead in position.

- *Pratu Tao-A02 (PTO-A02)*

This well was in the Pratu Tao area drilled in the up dip area of PTO-A01 in November 1982. The well proved unsuccessful and was consequently plugged and abandoned.

- *Pratu Tao-A03 (PTO-A03)*

This well was the third well to be drilled in the Pratu Tao area and was drilled in January 1984 to test hydrocarbon presence in the Pratu Tao Formation. The well discovered 16.5 mTV of net-oil-sand which was declared commercially viable after testing. PTO-A03 produced from 1990-1992 with a cumulative production of 0.1 MMstb before being shutdown due to pressure depletion and high water cut.

Khui Mamuang Area

- *Khui Mamuang -A01 (KMG-A01)*

The aim of this well was to test for hydrocarbon presence in the Pratu Tao, Lan Krabu Formations and Pre-Tertiary basement. The well was drilled in the Khui Mamuang area in December 1983. However, due to inadequate 2D seismic data the well was drilled outside of closure. Therefore, KMG-A01 was then plugged and abandoned.

Wat Taen Area

- *Wat Taen -A01 (WTN-A01)*

This well was the first well to be drilled in Wat Taen area in January 1984 to test hydrocarbon presence in Pratu Tao and Lan Krabu Formations. WTN-A01 was discovered 10.2 mTV of net-oil-sand in the Lan Krabu Formation. The production was ceased in 1989. The cumulative production is approximately 0.08 MMstb.

- *Wat Taen -B01 (WTN-B01)*

The aims of this well were to appraise and develop the Pratu Tao, Yom and Lan Krabu reservoirs. WTN-B01 was drilled in the Wat Taen area in June 2001. The well encountered 10.2 mTV of net-oil-sand in the Pratu Tao Formation and 6.9 mTV net-gas-sand the Lan Krabu Formation. The production test results suggest an initial production potential at approximately 1,000 bopd.

Nong Ooh Area

- *Nong Ooh -A01 (NOH-A01)*

This well was drilled in July, 2001 and the first well in Nong Ooh area to appraise the hydrocarbon potential of the Pratu Tao and Lan Krabu reservoir in a faultbounded closure adjacent to WTN-A01. Net-oil-sand with the value of 1.92 mTV was found in the Lan Krabu Formation. The well was plugged and abandoned because of insufficient recoverable reserves for an economic development.

- *Nong Ooh -B01 (NOH -B01)*

This well was the second well to be drilled in Nong Ooh area in July 2001 with those of similar objectives to NOH-A01. The well encountered 0.8 mTV net-oil-sand in the Lan Krabu Formation. NOH-A02 was plugged and abandoned because of insufficient recoverable reserves for economic development.

3.2 Lithological Classification

The lithological classification for all study wells was based on a ratio of separation density to neutron logs following Thai Shell (2000). Four rock types were classified for this study: **shale**, **dirty sand**, **shaly sand** and **clean sand**. Only shale is classified as a non-reservoir rock while the others are classified as reservoir rocks. Shale normally presents a separation ratio higher than 10. Dirty sand shows a separation ratio between 7 and 10 whereas shaly sand shows a lower separation ratio between 0 and 7. Clean sand presents the lowest separation ratio between -50 and 0. Table 3.2 shows the separation ratio applied to this lithological classification.

3.3 Logging Data

There are four log types; gamma ray, neutron, density, and sonic (P- and S-waves) used in the quantitative and qualitative studies. Appendices A-K show these logging panels for all study wells. Seven wells drilled before 2001 obtained poor quality of logging data. In particular, four wells drilled in 2001; NTM-C01, WTN-B01, NOH-A01 and NOH-B01 acquired good quality data. The gamma ray, neutron, density and compression sonic (P-wave) logging data are available for all study wells. The shear sonic (S-wave) logging data is available only in those wells drilled in 2001. The availability of logging data is tabulated in Table 3.3.

Table 3.3 List of logging data used in this study

Well	Spudded Year	Porosity data	Gamma Ray	Neutron	Density	Sonic	
						P-wave	S-wave
PTO-A01	1981	✓	✓	✓	✓	✓	-
PTO-A02	1982	✓	✓	✓	✓	✓	-
PTO-A03	1982	✓	✓	✓	✓	✓	-
NTM-A01	1983	✓	✓	✓	✓	✓	-
KMG-A01	1983	✓	✓	✓	✓	✓	-
NTM-B01	1984	✓	✓	✓	✓	✓	-
WTN-A01	1984	✓	✓	✓	✓	✓	-
NTM-C01	2001	✓	✓	✓	✓	✓	✓
WTN-B01	2001	✓	✓	✓	✓	✓	✓
NOH-A01	2001	✓	✓	✓	✓	✓	✓
NOH-A02	2001	✓	✓	✓	✓	✓	✓

3.3.1 Gamma Ray Data

The gamma ray log is a record of a formation's radioactivity emanating from naturally occurring uranium, thorium and potassium. Amongst the sedimentary rocks, shales present the strongest radiation. It is for this reason that the gamma ray logging data can be used to identify shale and correlate facies.

3.3.2 Neutron Data

The neutron log provides a reaction of a formation's neutron bombardment. This log is a measure of free pore-water which is related to a formation's hydrogen index. It is also used quantitatively to measure porosity and qualitatively to discriminate between gas and oil. The neutron log is usually combined with the density log to present the subsurface lithology indicators.

3.2.3 Density Data

The density log is a record of a formation's bulk density. The bulk density can be used as an indicator of the volume of free fluid enclosed in the formation. This log is used quantitatively to calculate porosity and acoustic impedance, and indirectly hydrocarbon density. It is also used qualitatively as a lithology indicator. The density logging data of the eleven study wells are available for data analysis.

3.3.4 Sonic Data

The sonic log shows a formation's interval transit time. The main use of the log is in seismic applications, calibration and generation of synthetics. It is also an essential parameter in the time to depth conversion of seismic data. When a transmitter of the sonic tool sends out a sound pulse, the log measures the arrival time of the pulse. The compression (P-) wave arrives ahead of the shear (S-) wave and is consequently recorded first. The compression wave travels in the same direction of motion. It propagates through the body of a medium. The particle motion of shear wave is perpendicular to the direction of propagation. The velocity of this wave is approximately one-half the velocity the compression wave. The compression wave data are available for all study wells, while the shear wave data is only available for those wells drilled in 2001.

3.3.5 Porosity Data

Porosity data is typically derived from the density log which measures the bulk density of the formation. The porosity can be defined as the percentage of voids to the total volume of rock. To calculate fractional porosities, the previous expression can be rearranged as follows:

$$\text{Porosity } (\emptyset) = \frac{\text{Volume of pores}}{\text{Total volume of rock}}$$

$$\text{Or} = \frac{\rho_{\text{ma}} - \rho_{\text{b}}}{\rho_{\text{ma}} - \rho_{\text{fl}}}$$

where ρ_{ma} = matrix (or grain) density

ρ_{fl} = fluid density

ρ_{b} = bulk density

A formation with high porosity indicates a good reservoir quality. The porosity data of the eleven study wells are available for data analysis.

3.3.6 Acoustic Impedance Data

The acoustic impedance is seismic velocity multiplied by density (Sheriff, 1997). The density data are obtained from the density log, while as the velocity data is derived from the sonic log. The acoustic impedance data indicates that rock properties can vary with lithology, porosity, fluid content and depth. These data act as an excellent tool for quantitative analysis. The calculation of acoustic impedance can be expressed as follows:

$$\text{Acoustic Impedance (AI)} = \text{Density } (\rho) \times \text{Velocity } (v)$$

This study does not only take into account the impedance from the compression (P-) wave but also for the shear (S-) wave, which it is called shear impedance. The shear impedance is a product of density and S-wave velocity.

3.4 Seismic Data

3.4.1 Normal Seismic Data

The GPTO 3D seismic survey was reprocessed four times after the acquisition was completed in 1984. The dataset used in this study was reprocessed using powerful, high resolution processing SIPMAP software and EPSI technology invented by Shell Geoscience Services (SGS) between 1999 and 2000. The objectives of this re-processing were to improve the structural resolution and to enable rock physics studies to lower the exploration risk. The normal seismic data were loaded into workstations for interpretation since year 2000. These data were interpreted later using the Charisma v.4.4.0 software package which is an application for seismic interpretation available in the GeoFrame v.3.7.1 suite.

3.4.2 Acoustic Impedance Data (Runsum Data)

After the stack procedure applied to the reflectivity data, the stack volume was converted to an acoustic impedance volume (Runsum data) using a running sum integration technique. Each input trace is integrated by adding to each data value the sum of all previous data values. This operation shifts the phase of the trace by -90 . The acoustic impedance section presents the subsurface in terms of layers, whereas seismic reflectivity data presents the subsurface in terms of interfaces between rock layers. The Runsum dataset in this study is represented in depth volume which was converted by InDepth software, one of the application in GeoFrame v.3.7.1 suite. Figure 3.1 shows the section of the normal seismic and the Runsum data from the GPTO 3D seismic survey.



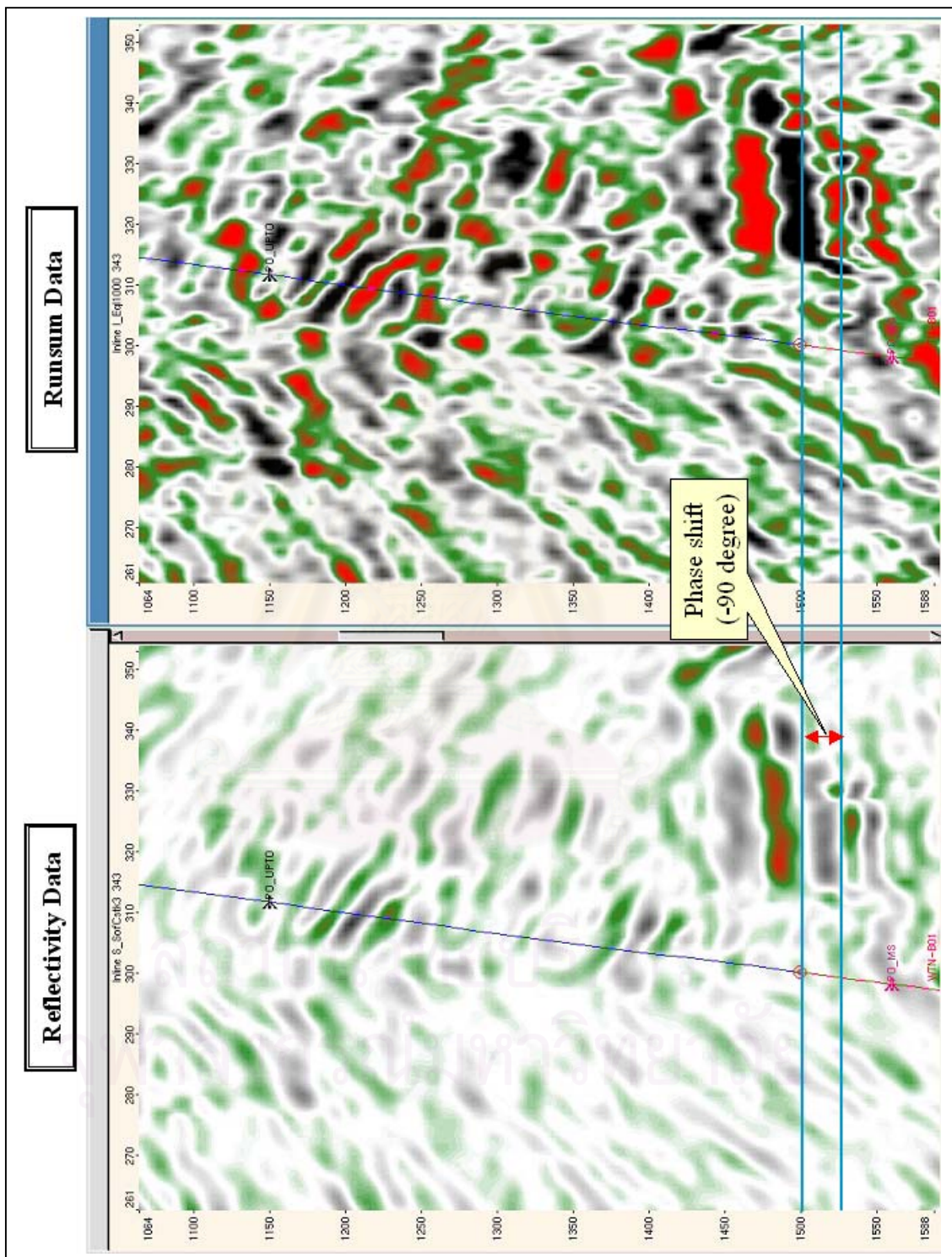


Figure 3.1 Section of normal seismic and Runsum data from the Greater Pratu Tao 3D survey

CHAPTER IV

DATA ANALYSIS

In this study, the process of data analysis has been divided into two parts; quantitative and qualitative. In this study, the quantitative analysis is defined as an analysis of lithological properties with statistic expression. For qualitative analysis, it is expressed as a quality, nature and behaviour of lithological properties without any measurements. In quantitative analysis, all seismic and logging data have been cross-plotted so that the acoustic impedance response to lithology variations can be studied. Qualitative analysis in this study aims to apply acoustic (P-wave) and shear (S-wave) impedance data to recognise lithological units.

4.1 Quantitative Analysis

The data used in qualitative study is as follows: acoustic (P-wave), shear (S-wave) impedance, porosity, The Runsum seismic, filtered acoustic (P-wave) and filtered shear (S-wave) impedance. The filtered acoustic and shear impedance data were processed by LOGIC software. The Bandpass filter was selected as the most suitable filter after trials using NTM-C01 as a tester well (Figure 4.1). This filter was able to keep closely to the original log-shape. The used Bandpass filtering parameters are illustrated in the Figure 4.2. The parameters were selected following the recommendations of the processor working on the 3D seismic survey from 1999-2000 (Marinus Klaassen, **personal communication**, February, 19, 2002).

This data was cross-plotted on a graph, on which the x -coordinate represents the value of one data type and the y -coordinate the value of the others. This cross-plot can be used to understand how two data types are related. It is also useful for observing aberrant data. The correlation coefficient (R) is the statistic that is most commonly used to summarise the relationship between two data types. It is always between -1 and $+1$ and provides an index that is independent of the magnitude of the data values. The correlation coefficient provides a measure of the linear relationship between two data types. If the relationship between two data types is not linear, the correlation coefficient may be a poor summary statistic. Tables 4.1–4.11 summarise the correlation coefficient obtained from data analysis for particular wells and lithologies.

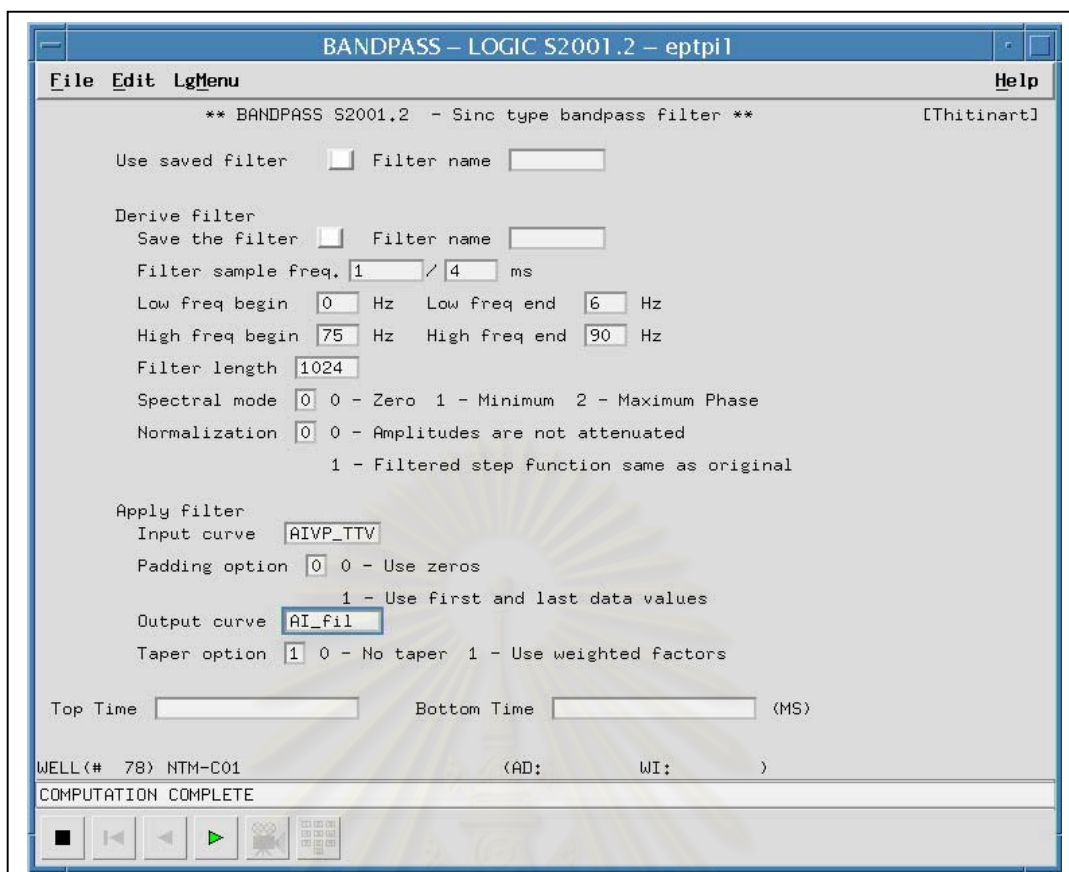


Figure 4.1 The parameters are used in the Bandpass filtering process

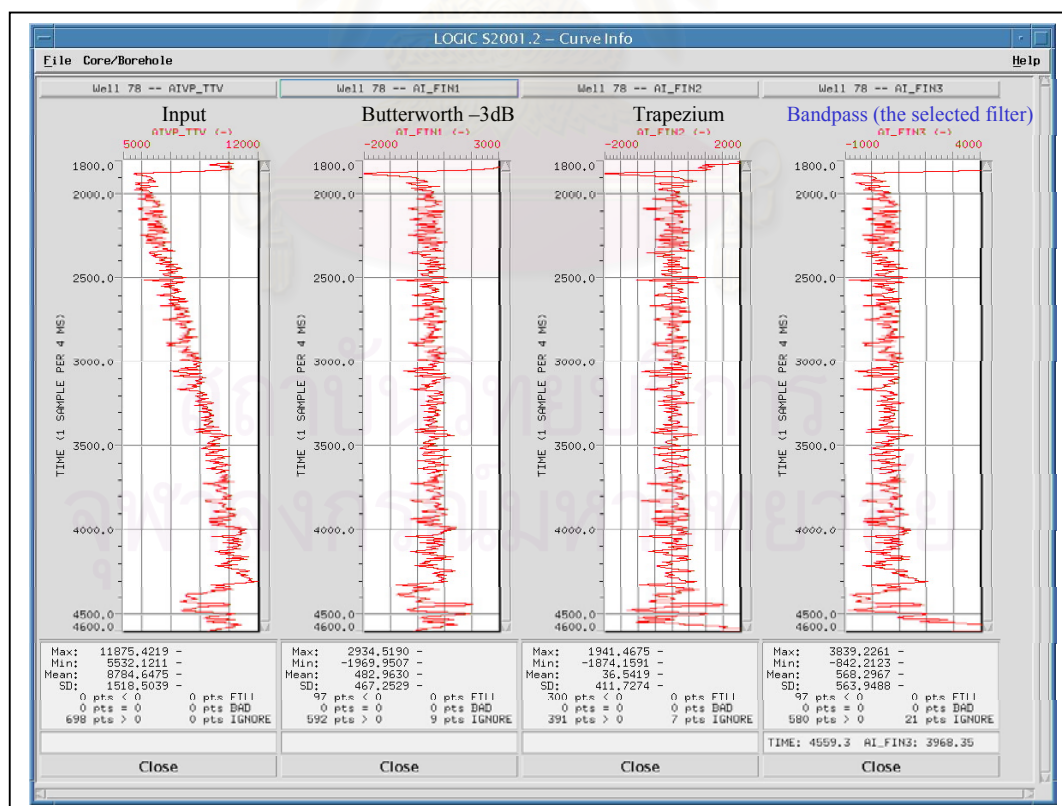


Figure 4.2 Comparison between applying the Bandpass and the other filters into the acoustic (P-wave) impedance dataset of well NTM-C01

Table 4.1 The summary of correlation coefficients obtained from the linear relationship between acoustic (P-wave) impedance and porosity

Well Name	Non-reservoir						Reservoir					
	Shale		Dirty Sand		Shaly Sand		Clean Sand					
	Number of data	Correlation Coeff.	Number of data	Correlation Coeff.	Number of data	Correlation Coeff.	Number of data	Correlation Coeff.	Number of data	Correlation Coeff.		
PTO-A01	5998	0.4271	435	0.4772	546	0.6242	113	0.6773				
PTO-A02	3150	0.5957	954	0.6166	1481	0.4030	842	0.3660				
PTO-A03	3556	0.6297	831	0.5956	1389	0.5514	676	0.3602				
NTM-A01	6729	0.6654	488	0.6762	944	0.7093	222	0.7026				
KMG-A01	2308	0.6733	398	0.6690	665	0.6686	173	0.6755				
NTM-B01	4932	0.6141	619	0.7027	977	0.6424	369	0.4932				
WTN-A01	1446	0.6452	187	0.4109	483	0.5592	128	0.6151				
NTM-C01	5419	0.6381	540	0.6878	1341	0.7947	568	0.8357				
WTN-B01	3209	0.5933	456	0.7091	902	0.8109	613	0.8356				
NOH-A01	2402	0.7520	554	0.7667	1320	0.8407	895	0.7761				
NOH-A02	2710	0.7518	491	0.7616	771	0.8899	624	0.8197				
All wells	41859	0.6652	Number of data		Number of data		Correlation Coeff.		Correlation Coeff.			
			21935		21935		0.7452					

Table 4.2 The summary of correlation coefficients obtained from the linear relationship between Runsum seismic and porosity

Well Name	Non-reservoir				Reservoir			
	Shale		Dirty Sand		Shaly Sand		Clean Sand	
	Number of data	Correlation Coeff.	Number of data	Correlation Coeff.	Number of data	Correlation Coeff.	Number of data	Correlation Coeff.
NTM-C01	5419	0.0018	540	0.0048	1341	0.0085	568	0.0007
WTN-B01	3209	0.0311	456	0.0212	902	0.0177	613	0.0006
NOH-A01	2402	0.0713	554	0.0109	1320	0.0208	835	0.0006
NOH-A02	2710	0.0518	491	0.0160	771	0.0115	624	0.0001
All wells	13740	0.0012	Number of data		Number of data		Correlation Coeff.	
			9015		9015		0.0033	

Table 4.3 The summary of correlation coefficients obtained from the linear relationship between Runsum seismic and acoustic (P-wave) impedance

Well Name	Non-reservoir				Reservoir			
	Shale		Dirty Sand		Shaly Sand		Clean Sand	
	Number of data	Correlation Coeff.	Number of data	Correlation Coeff.	Number of data	Correlation Coeff.	Number of data	Correlation Coeff.
NTM-C01	5419	0.0038	540	0.0002	1341	0.0142	568	2.E-05
WTN-B01	3209	0.0024	456	0.0227	902	0.0274	613	0.0019
NOH-A01	2402	0.0666	554	0.0134	1320	0.0153	835	0.0005
NOH-A02	2710	0.0875	491	8.E-05	771	0.0084	624	1.E-06
All wells	13740	0.0013	Number of data		Number of data		Correlation Coeff.	
			9015		9015		0.0043	

Table 4.4 The summary of correlation coefficients obtained from the linear relationship between shear (S-wave) impedance and porosity

Well Name	Non-reservoir		Reservoir					
	Shale		Dirty Sand		Shaly Sand		Clean Sand	
	Number of data	Correlation Coeff.	Number of data	Correlation Coeff.	Number of data	Correlation Coeff.	Number of data	Correlation Coeff.
NTM-C01	5419	0.5574	540	0.5287	1341	0.6396	568	0.7641
WTN-B01	3209	0.4040	456	0.3611	902	0.5066	613	0.6772
NOH-A01	2402	0.3281	554	0.2224	1320	0.4235	835	0.3704
NOH-A02	2710	0.5629	491	0.3793	771	0.6074	624	0.5032
All wells	13740	0.7845	Number of data		Number of data		Correlation Coeff.	
			9015				0.6668	

Table 4.5 The summary of correlation coefficients obtained from the linear relationship between Runsum seismic and shear (S-wave) impedance

Well Name	Non-reservoir		Reservoir					
	Shale		Dirty Sand		Shaly Sand		Clean Sand	
	Number of data	Correlation Coeff.	Number of data	Correlation Coeff.	Number of data	Correlation Coeff.	Number of data	Correlation Coeff.
NTM-C01	5419	0.0051	540	0.0018	1341	0.0252	568	8E-0.6
WTN-B01	3209	0.0010	456	0.0375	902	0.0256	613	0.0051
NOH-A01	2402	0.0216	554	0.0038	1320	0.0034	835	0.0010
NOH-A02	2710	0.0860	491	0.0008	771	0.0059	624	0.0043
All wells	13740	0.0077	Number of data		Number of data		Correlation Coeff.	
			9015				0.0047	

Table 4.6 The summary of correlation coefficients obtained from the linear relationship between acoustic (P-wave) and shear (S-wave) impedance

Well Name	Non-reservoir		Reservoir					
	Shale		Dirty Sand		Shaly Sand		Clean Sand	
	Number of data	Correlation Coeff.	Number of data	Correlation Coeff.	Number of data	Correlation Coeff.	Number of data	Correlation Coeff.
NTM-C01	5419	0.9036	540	0.8795	1341	0.8873	568	0.9137
WTN-B01	3209	0.7926	456	0.6307	902	0.7109	613	0.8199
NOH-A01	2402	0.5396	554	0.4014	1320	0.5430	835	0.4836
NOH-A02	2710	0.7951	491	0.7095	771	0.7786	624	0.7079
All wells	13740	0.9481	Number of data		Correlation Coeff.		Correlation Coeff.	
			9015				0.9179	

Table 4.7 The summary of correlation coefficients obtained from the linear relationship between filtered acoustic (P-wave) impedance and porosity

Well Name	Non-reservoir		Reservoir					
	Shale		Dirty Sand		Shaly Sand		Clean Sand	
	Number of data	Correlation Coeff.	Number of data	Correlation Coeff.	Number of data	Correlation Coeff.	Number of data	Correlation Coeff.
NTM-C01	413	0.0360	33	0.0290	93	9.E-05	34	0.0054
WTN-B01	322	0.0300	38	0.0721	93	0.0365	65	0.0782
NOH-A01	239	3.E-06	55	0.0009	139	0.0018	78	0.0002
NOH-A02	272	0.0027	50	0.0479	79	0.2161	58	0.0414
All wells	1246	0.0539	Number of data		Correlation Coeff.		Correlation Coeff.	
			815				0.0462	

Table 4.8 The summary of correlation coefficients obtained from the linear relationship between Runsum seismic and filtered acoustic (P-wave) impedance

Well Name	Non-reservoir		Reservoir					
	Shale		Dirty Sand		Shaly Sand		Clean Sand	
	Number of data	Correlation Coeff.	Number of data	Correlation Coeff.	Number of data	Correlation Coeff.	Number of data	Correlation Coeff.
NTM-C01	413	0.0088	33	0.0144	93	0.2053	34	0.2034
WTN-B01	322	0.0402	38	0.0015	93	0.0382	65	0.0006
NOH-A01	239	0.0070	55	0.1832	139	0.0012	78	0.0566
NOH-A02	272	0.0157	50	0.0968	79	0.0132	58	0.2393
All wells	1246	0.0134	Number of data		Correlation Coeff.		Correlation Coeff.	
			815				0.0083	

Table 4.9 The summary of correlation coefficients obtained from the linear relationship between filtered shear (S-wave) impedance and porosity

Well Name	Non-reservoir		Reservoir					
	Shale		Dirty Sand		Shaly Sand		Clean Sand	
	Number of data	Correlation Coeff.	Number of data	Correlation Coeff.	Number of data	Correlation Coeff.	Number of data	Correlation Coeff.
NTM-C01	413	0.0389	33	0.0293	93	0.0001	34	0.0098
WTN-B01	322	0.0363	38	0.0175	93	0.0008	65	0.0452
NOH-A01	239	0.0001	55	0.0810	139	0.0019	78	0.0002
NOH-A02	272	0.0029	50	0.0170	79	0.1796	58	0.0500
All wells	1246	0.0523	Number of data		Correlation Coeff.		Correlation Coeff.	
			815				0.0339	

Table 4.10 The summary of correlation coefficients obtained from the linear relationship between Runsum seismic and filtered shear (S-wave) impedance

Well Name	Non-reservoir			Reservoir					
	Shale			Dirty Sand		Shaly Sand		Clean Sand	
	Number of data	Correlation Coeff.		Number of data	Correlation Coeff.	Number of data	Correlation Coeff.	Number of data	Correlation Coeff.
NTM-C01	413	0.0129		33	0.0007	93	0.2232	34	0.1016
WTN-B01	322	0.0456		38	0.0015	93	0.0163	65	0.0105
NOH-A01	239	0.0109		55	0.1805	139	0.0003	78	0.0380
NOH-A02	272	0.0367		50	0.1069	79	0.0300	58	0.2267
All wells	1246	0.0165		Number of data		Number of data		Correlation Coeff.	
				815				0.014	

Table 4.11 The summary of correlation coefficients obtained from the linear relationship between filtered acoustic (P-wave) and filtered shear (S-wave) impedance

Well Name	Non-reservoir			Reservoir					
	Shale			Dirty Sand		Shaly Sand		Clean Sand	
	Number of data	Correlation Coeff.		Number of data	Correlation Coeff.	Number of data	Correlation Coeff.	Number of data	Correlation Coeff.
NTM-C01	413	0.8843		33	0.8109	93	0.6973	34	0.9007
WTN-B01	322	0.7764		38	0.6290	93	0.6990	65	0.7791
NOH-A01	239	0.5575		55	0.0019	139	0.5685	78	0.6836
NOH-A02	272	0.8233		50	0.8302	79	0.7576	58	0.8687
All wells	1246	0.8299		Number of data		Number of data		Correlation Coeff.	
				815				0.7947	

The relationship analysis of acoustic (P-wave) impedance and porosity was applied to all study wells. The other analyses were used on only four wells; NTM-C01, WTN-B01, NOH-A01 and NOH-A02, all of which have good logging data.

4.1.1 Relationship between Acoustic (P-wave) Impedance and Porosity

Eleven wells in total were used to analyse the relationship between acoustic (P-wave) impedance and porosity and have been plotted on the x - and y -axes respectively (Figures 4.3a–4.3k). The Cross-plots show that acoustic (P-wave) impedance and porosity have a linear relationship with positive correlation for all rock types. The cross-plots show that the values of the correlation coefficient of the wells drilled in 2001 are generally higher than the wells drilled before (Table 4.1). The correlation coefficients also show a higher value in the dataset of the reservoir rocks than that in the non-reservoir rock. This leads to the well selection process (Figure 1.2). In general, the wells drilled in 2001 have a better data correlation and, furthermore, shear (S-wave) sonic data is also available for these wells. Consequently, they were selected for further analyses.

4.1.2 Relationship between Runsum Seismic and Porosity

Four wells drilled in 2001 have been used to analyse the relationship between the Runsum seismic and porosity. As shown in Figures 4.4a-4.4d the dataset has been plotted and the x -axis is represented by the value of the Runsum seismic and the y -axis by porosity. The cross-plots show that the correlation coefficients are less than 0.1 (Table 4.2) and, therefore, there is a none-correlation in the linear relationship between the Runsum seismic and porosity. This is the case for all rock types implying that the porosity trend cannot be predicted from the Runsum seismic.

4.1.3 Relationship between Runsum Seismic and Acoustic (P-wave) Impedance

The relationship between the Runsum seismic and acoustic (P-wave) impedance was analysed by using the dataset of four wells drilled in 2001. The cross-plots in this analysis have been displayed and the x - and y -axes are represented by the Runsum seismic and acoustic (P-wave) impedance respectively (Figures 4.5a–4.5d). The result shows that there is no correlation between two the data types. All four wells show the correlation coefficients to be less than 0.1 for all rock types (Table

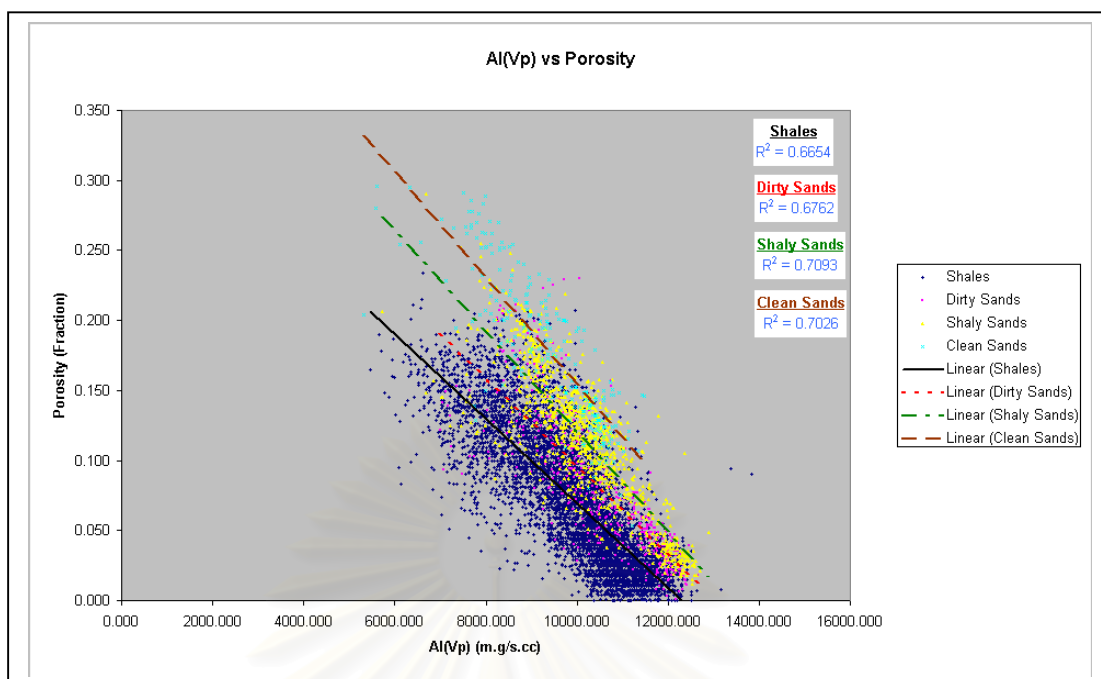


Figure 4.3a A cross-plot showing a relationship between acoustic (P-wave) impedance ($AI(Vp)$) and porosity in well NTM-A01

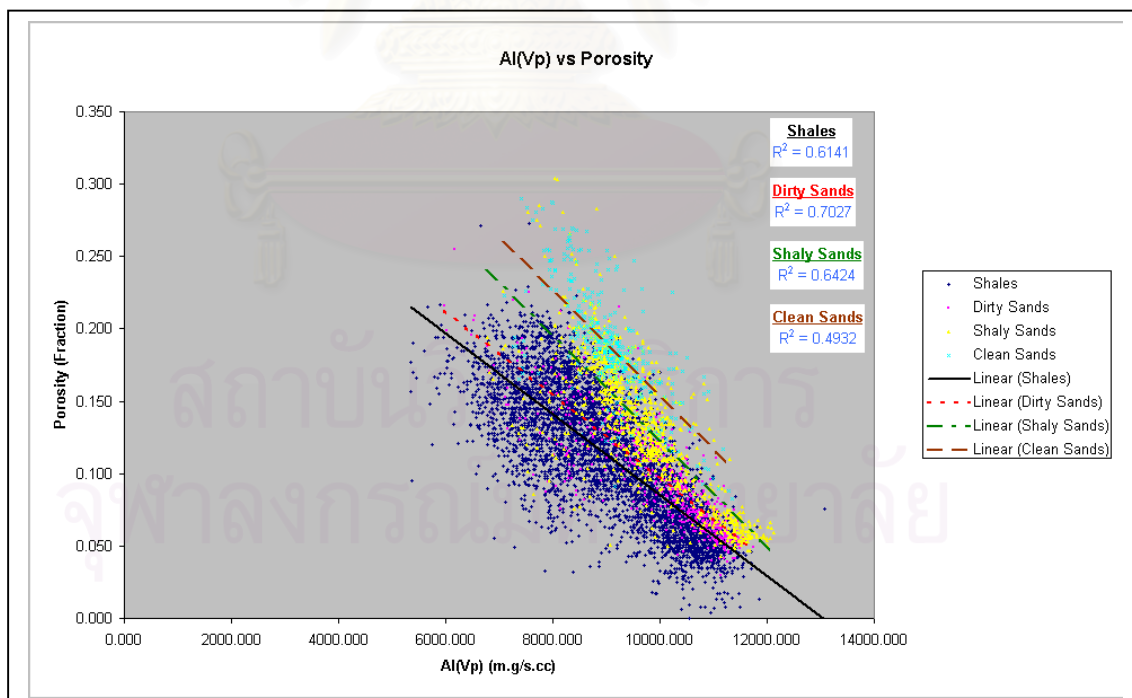


Figure 4.3b A cross-plot showing a relationship between acoustic (P-wave) impedance ($AI(Vp)$) and porosity in well NTM-B01

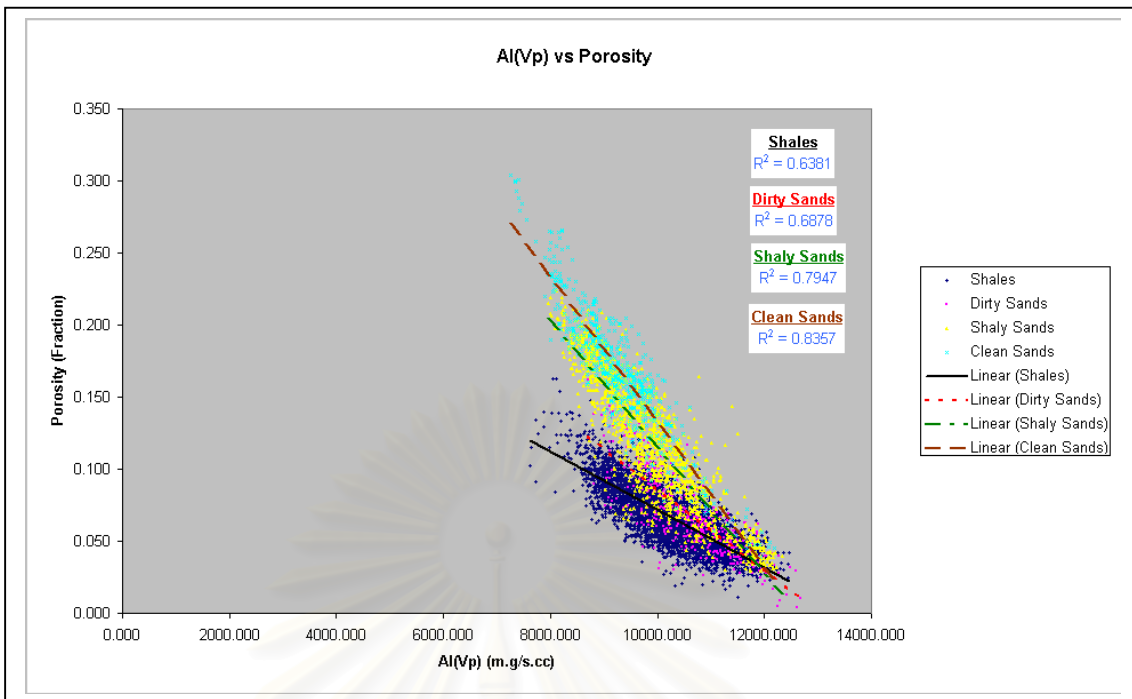


Figure 4.3c A cross-plot showing a relationship between acoustic (P-wave) impedance ($AI(Vp)$) and porosity in well NTM-C01

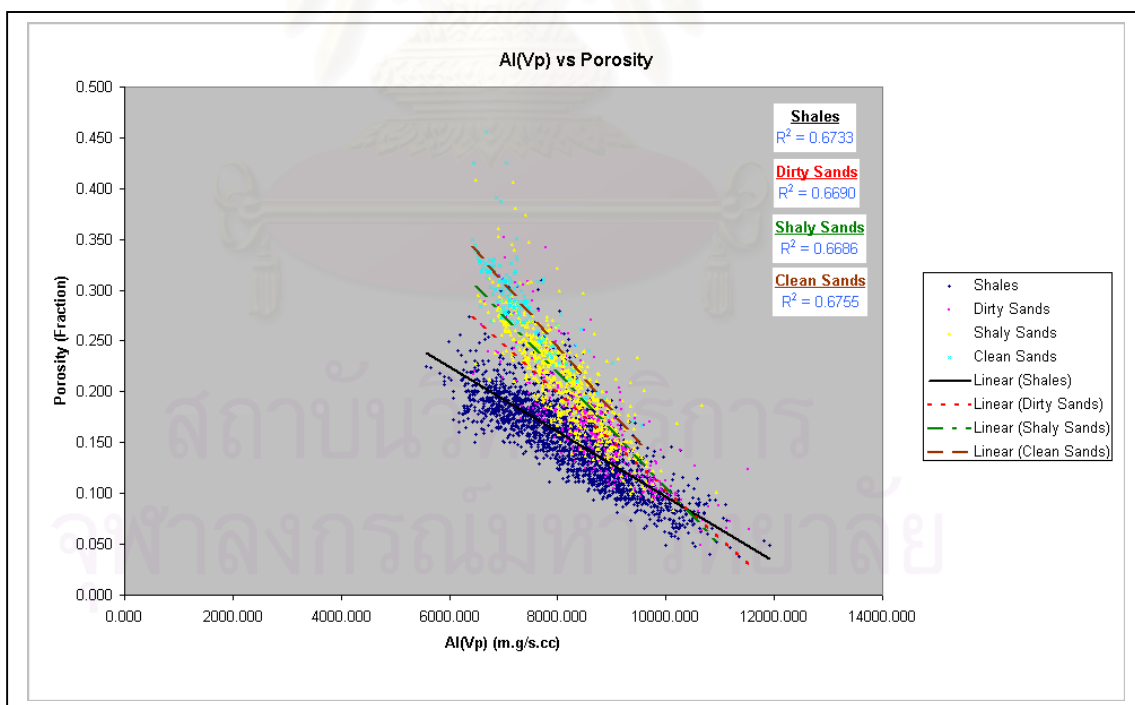


Figure 4.3d A cross-plot showing a relationship between acoustic (P-wave) impedance ($AI(Vp)$) and porosity in well KMG-A01

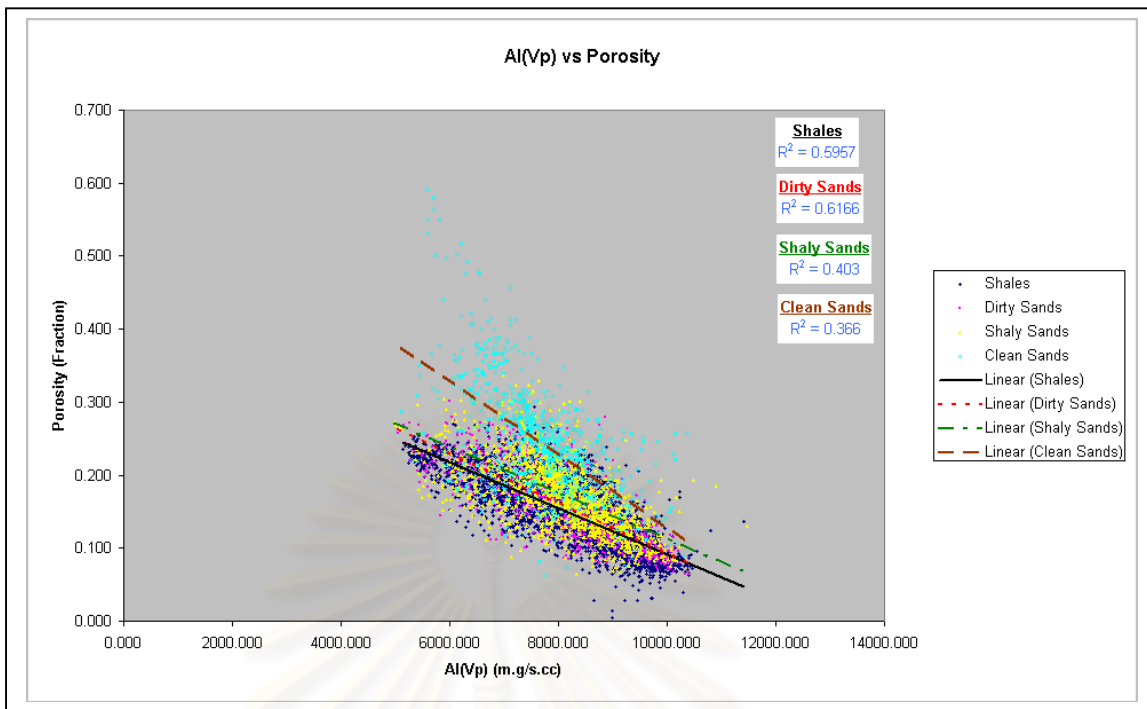


Figure 4.3e A cross-plot showing a relationship between acoustic (P-wave) impedance ($AI(Vp)$) and porosity in well PTO-A01

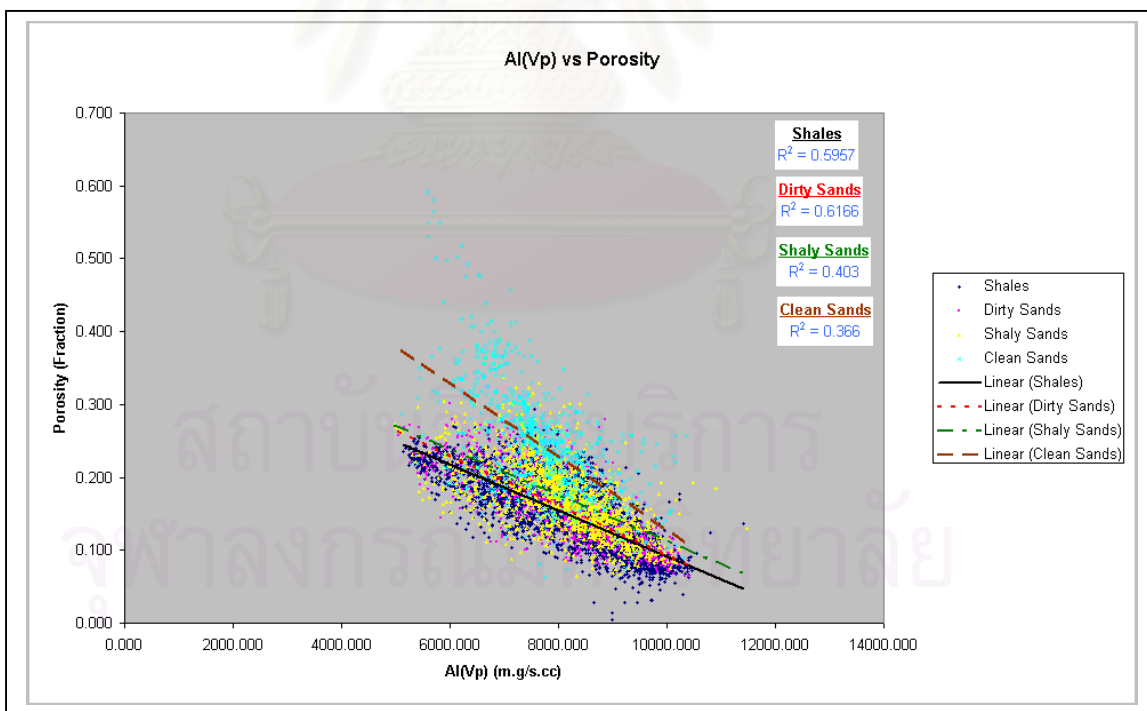


Figure 4.3f A cross-plot showing a relationship between acoustic (P-wave) impedance ($AI(Vp)$) and porosity in well PTO-A02

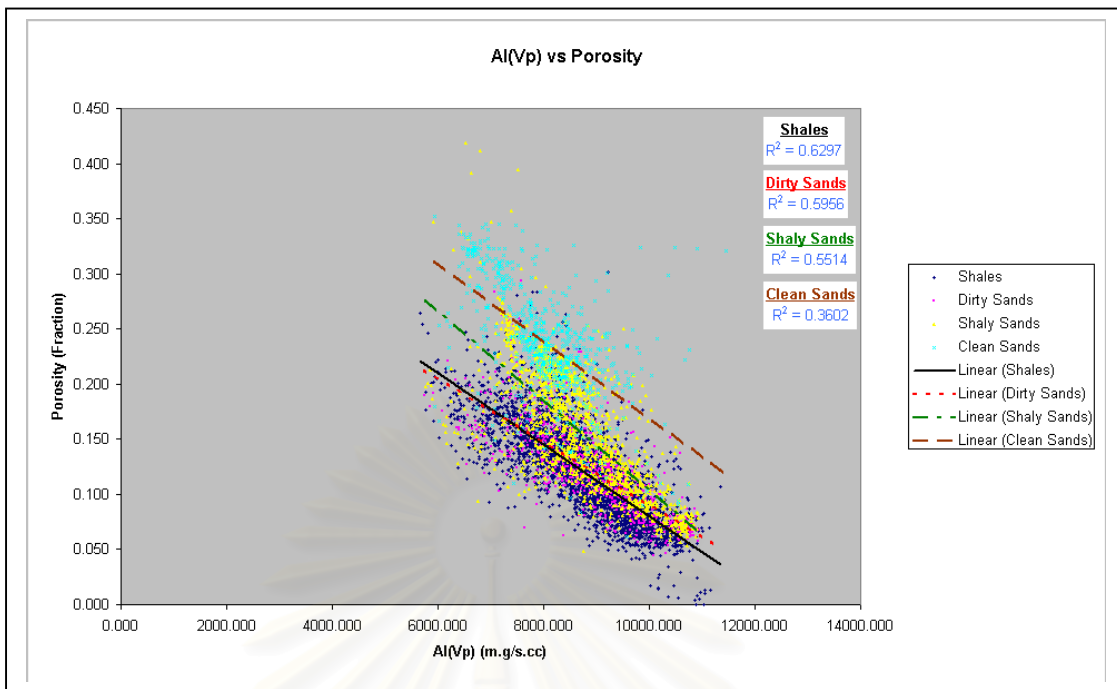


Figure 4.3g A cross-plot showing a relationship between acoustic (P-wave) impedance ($AI(Vp)$) and porosity in well PTO-A03

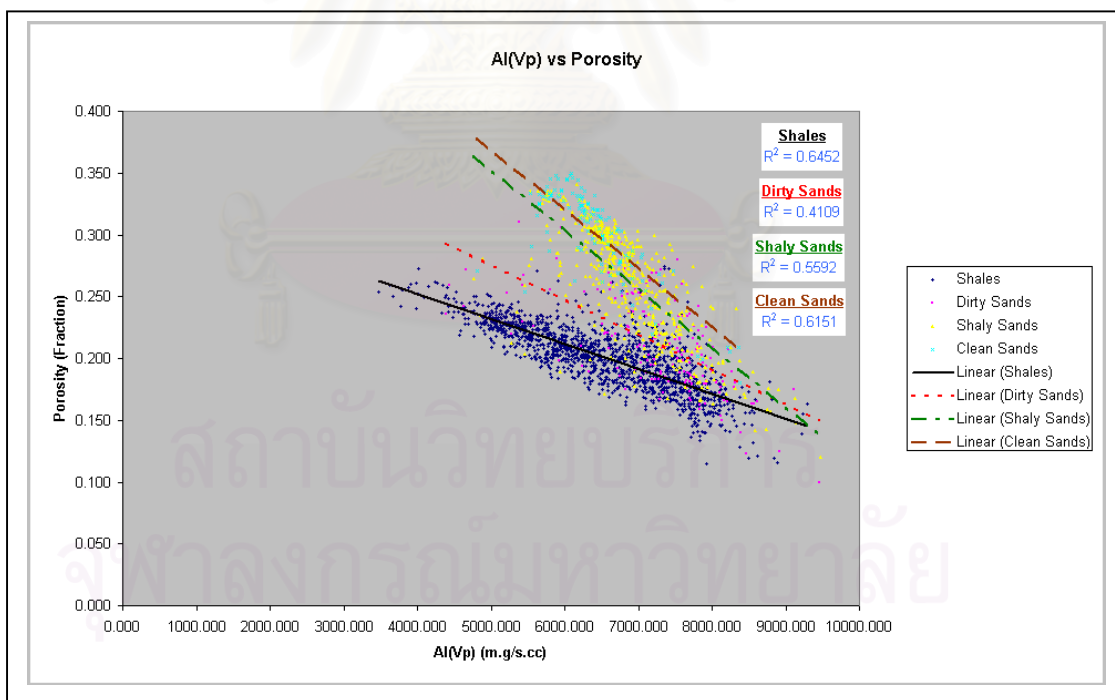


Figure 4.3h A cross-plot showing a relationship between acoustic (P-wave) impedance ($AI(Vp)$) and porosity in well WTN-A01

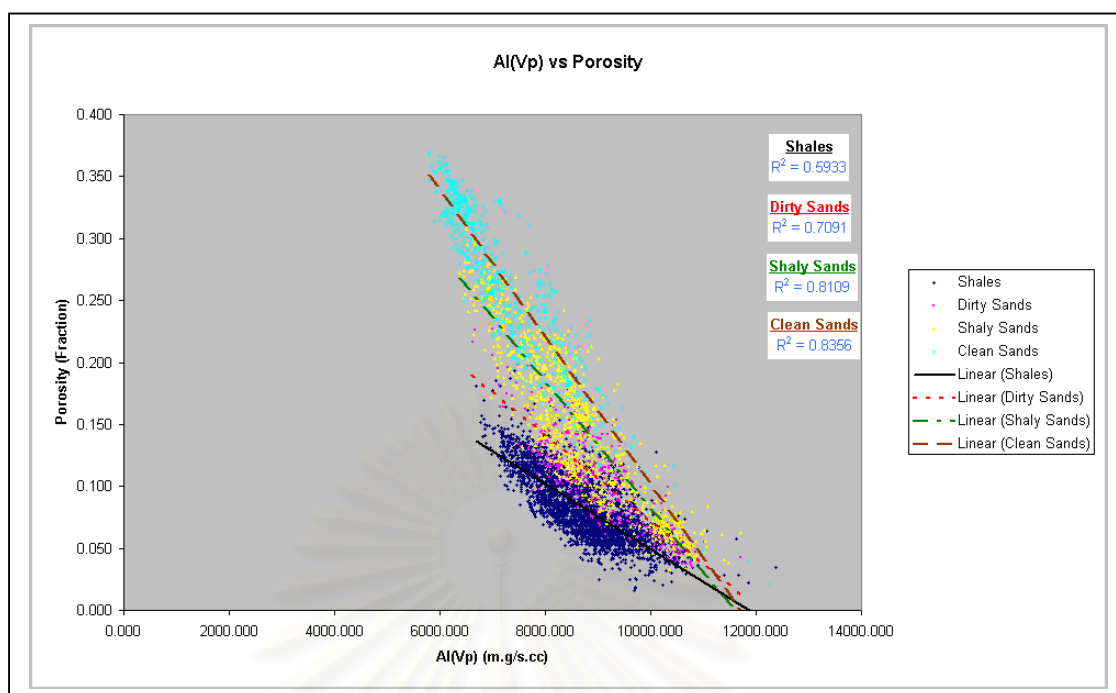


Figure 4.3i A cross-plot showing a relationship between acoustic (P-wave) impedance ($AI(Vp)$) and porosity in well WTN-B01

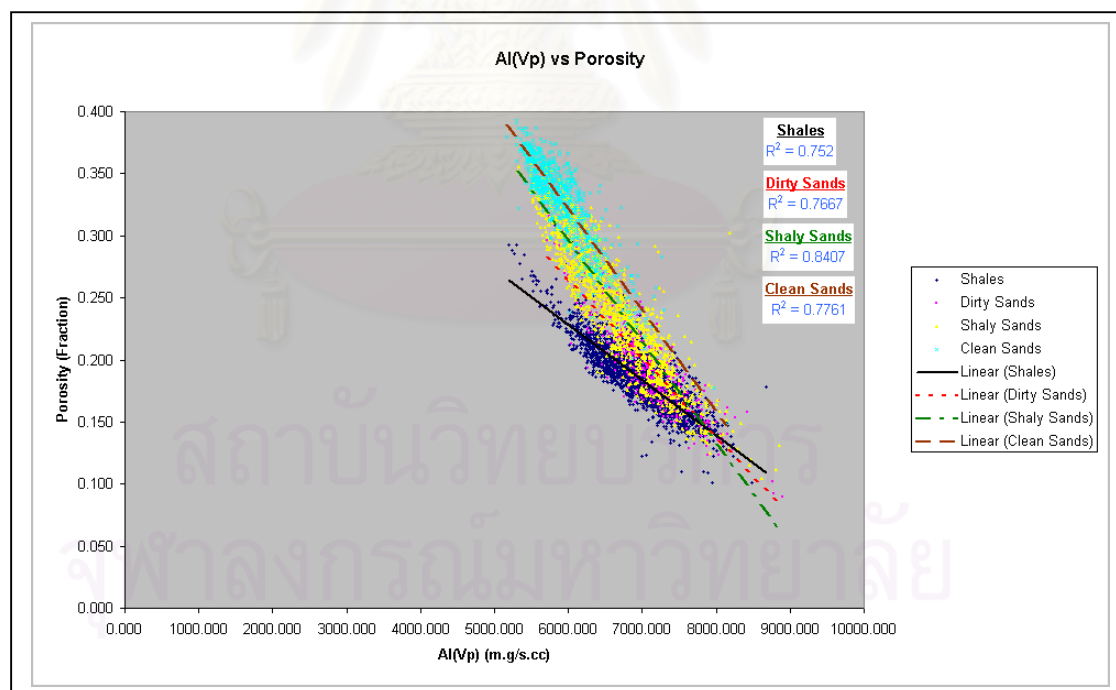


Figure 4.3j A cross-plot showing a relationship between acoustic (P-wave) impedance ($AI(Vp)$) and porosity in well NOH-A01

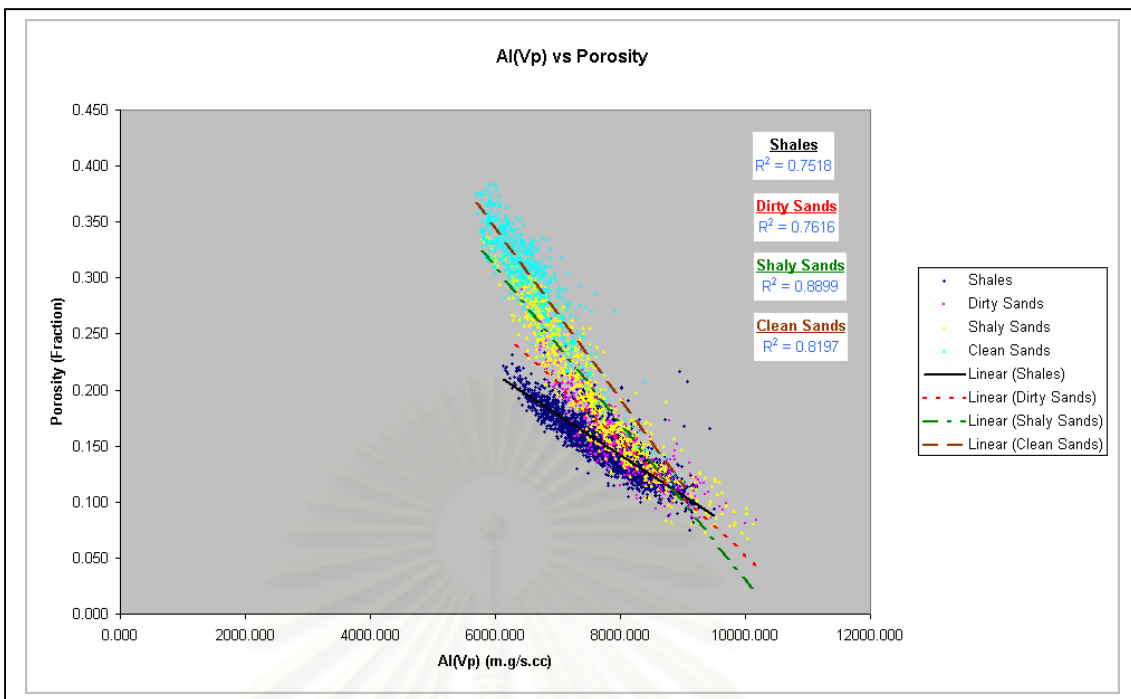


Figure 4.3k A cross-plot showing a relationship between acoustic (P-wave) impedance ($AI(Vp)$) and porosity in well NOH-A02

สถาบันวิทยบริการ
จุฬาลงกรณ์มหาวิทยาลัย

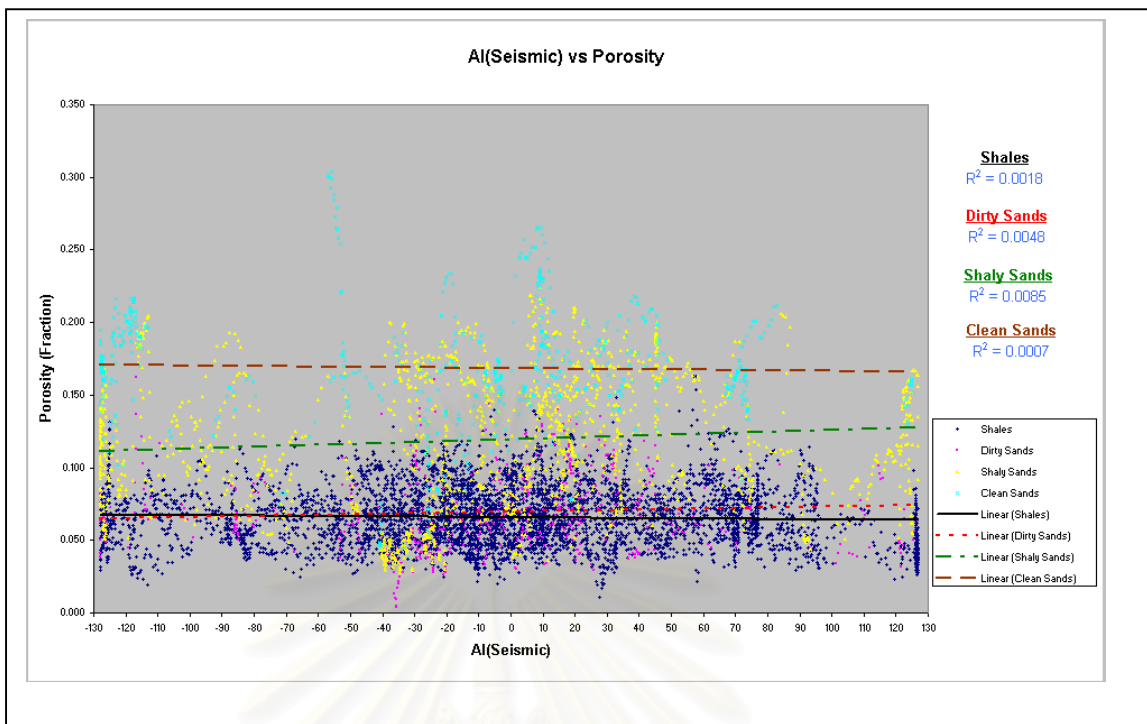


Figure 4.4a A cross-plot showing a relationship between Runsum seismic ($AI(Seismic)$) and porosity in well NTM-C01

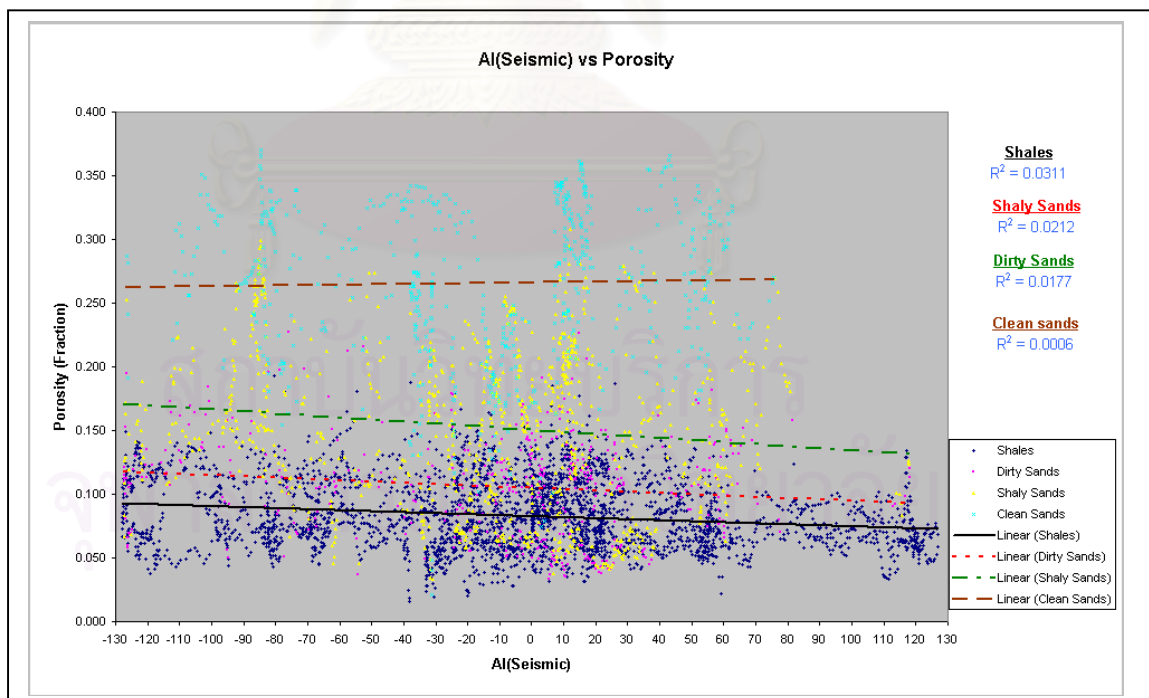


Figure 4.4b A cross-plot showing a relationship between Runsum seismic ($AI(Seismic)$) and porosity in well WTN-B01

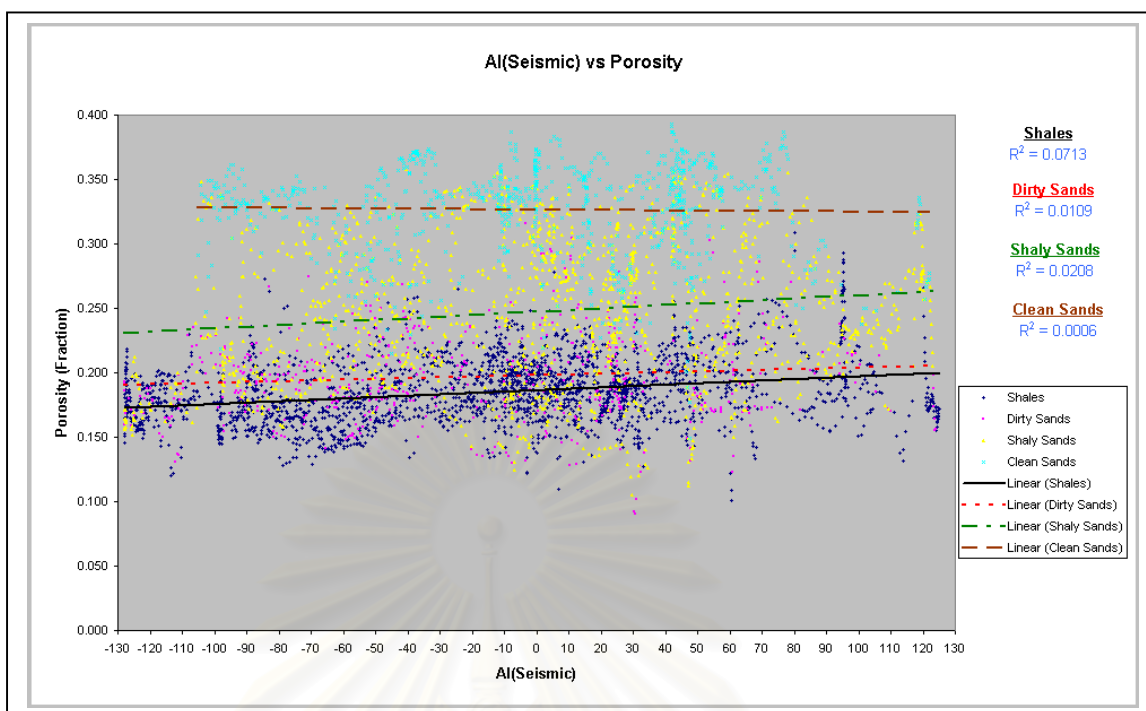


Figure 4.4c A cross-plot showing a relationship between Runsum seismic ($AI(Seismic)$) and porosity in well NOH-A01

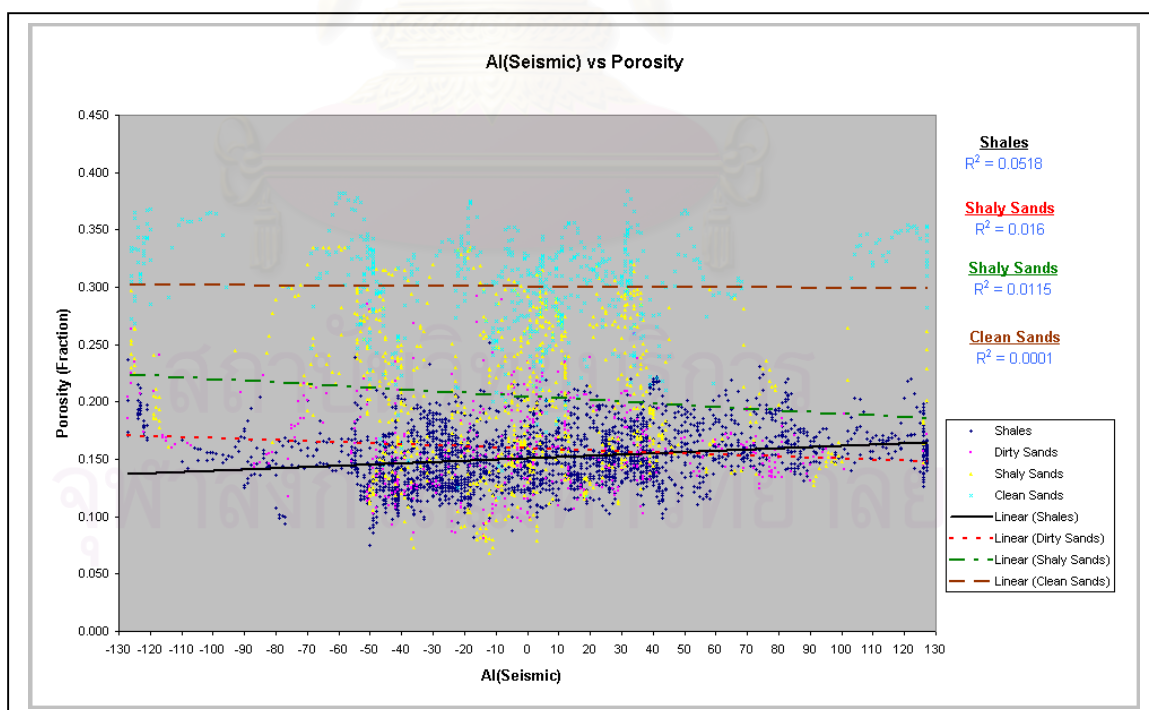


Figure 4.4d A cross-plot showing a relationship between Runsum seismic ($AI(Seismic)$) and porosity in well NOH-A02

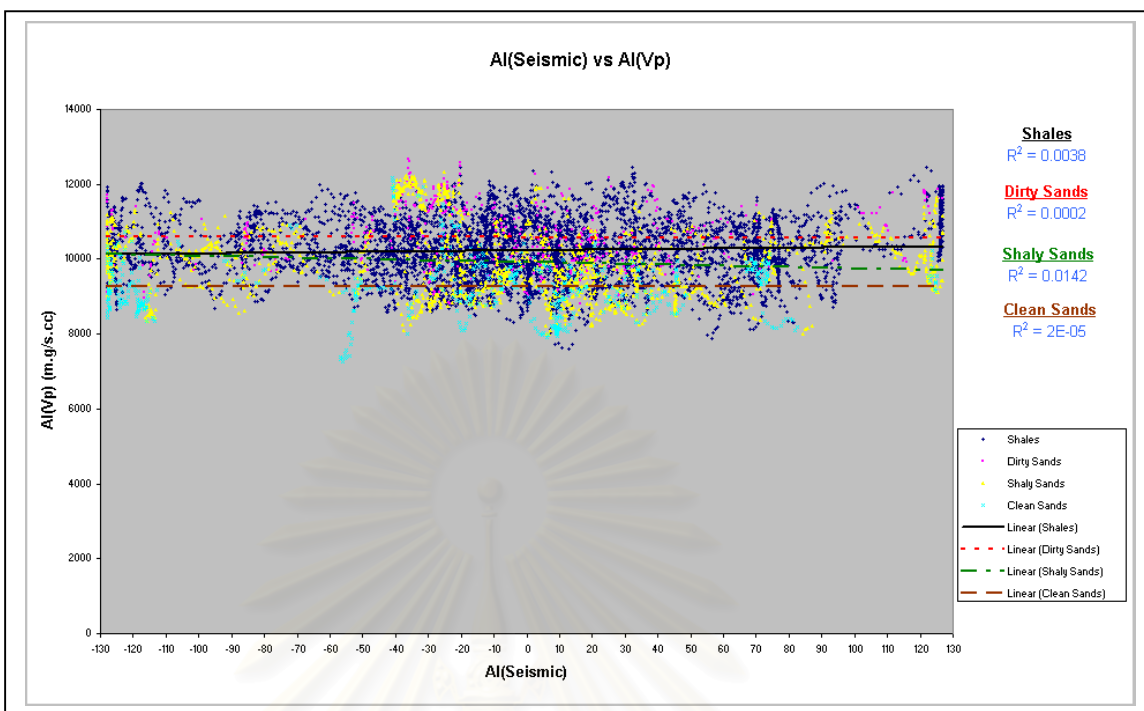


Figure 4.5a A cross-plot showing a relationship between Runsum seismic ($AI(Seismic)$) and acoustic (P-wave) impedance ($AI(Vp)$) in well NTM-C01

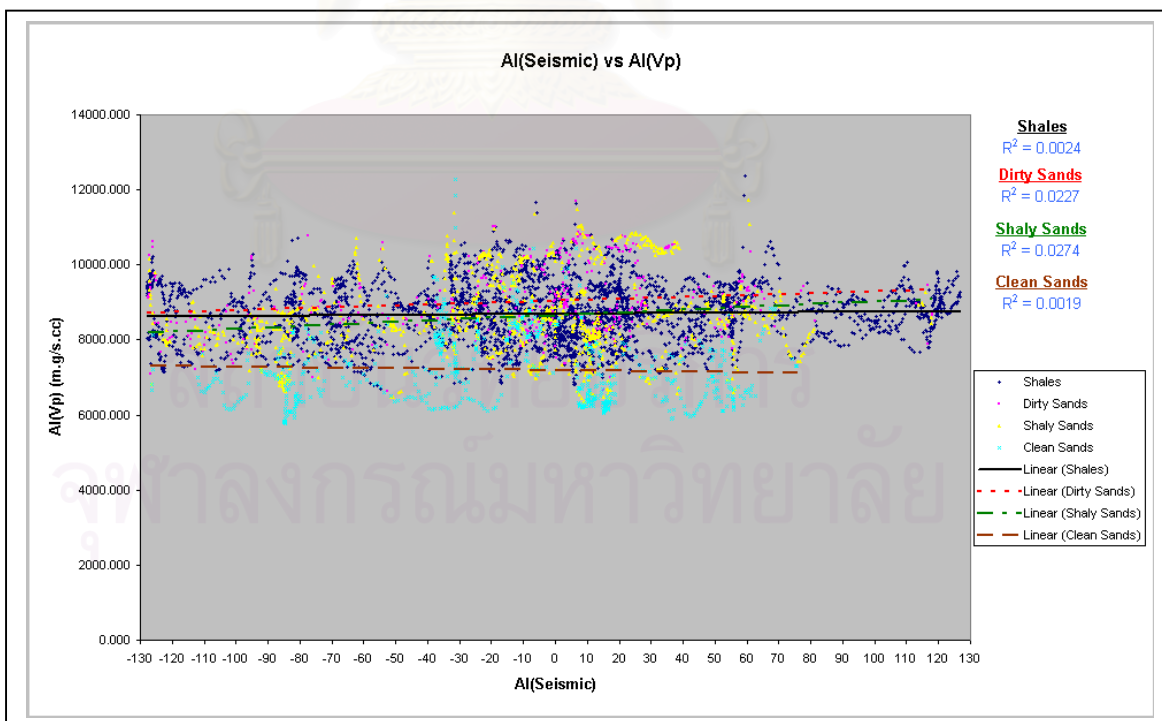


Figure 4.5b A cross-plot showing a relationship between Runsum seismic ($AI(Seismic)$) and acoustic (P-wave) impedance ($AI(Vp)$) in well WTN-B01

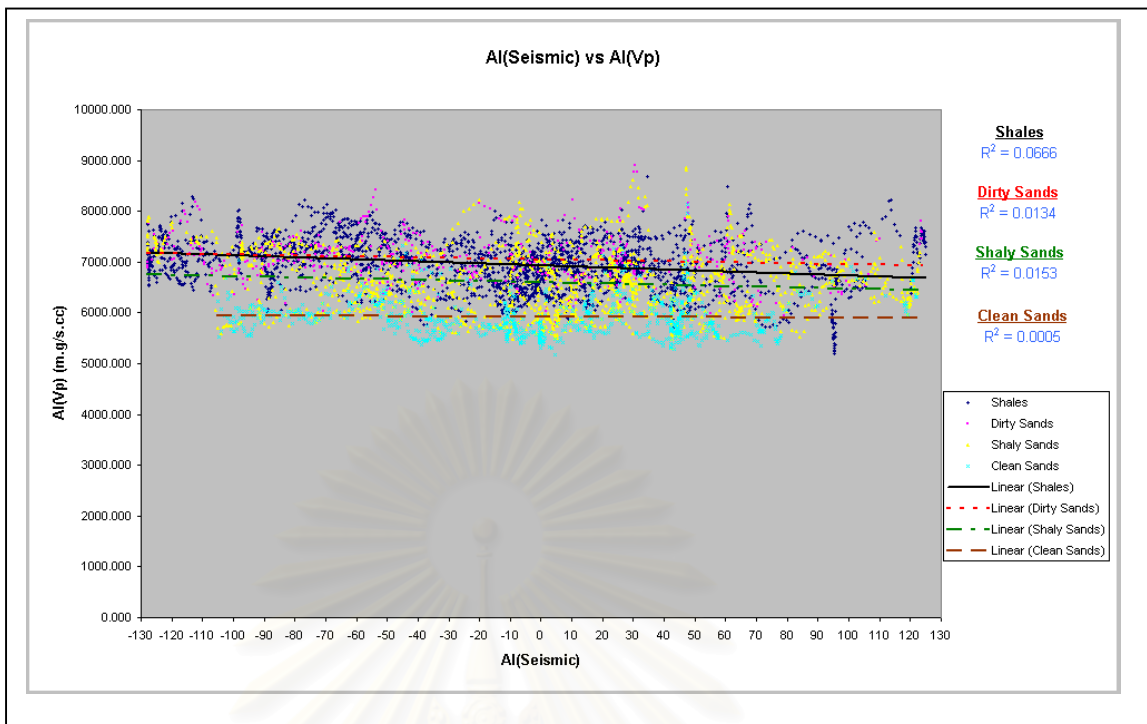


Figure 4.5c A cross-plot showing a relationship between Runsum seismic ($AI(Seismic)$) and acoustic (P-wave) impedance ($AI(Vp)$) in well NOH-A01

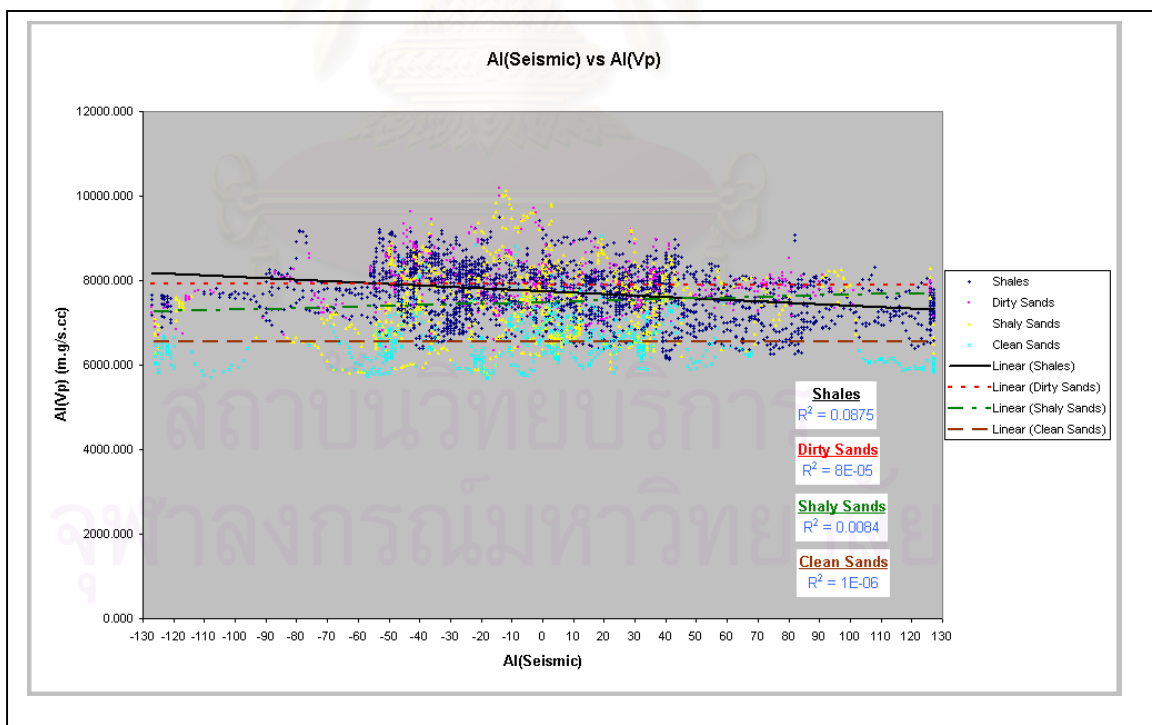


Figure 4.5d A cross-plot showing a relationship between Runsum seismic ($AI(Seismic)$) and acoustic (P-wave) impedance ($AI(Vp)$) in well NOH-A02

4.3). This means the acoustic (P-wave) impedance cannot be correlated with the Runsum seismic.

4.1.4 Relationship between Shear (S-wave) Impedance and Porosity

The shear (S-wave) impedance and porosity data were also analysed by using cross-plots. The x -axis represents shear (S-wave) impedance data whereas the y -axis shows porosity data (Figures 4.6a-4.6d). The linear relationship of these two data types is correlatable with a high coefficient number (Table 4.4). In general, non-reservoir rock shows a higher correlation coefficient value than reservoir rocks.

4.1.5 Relationship between Runsum Seismic and Shear (S-wave) Impedance

The relationship between the Runsum seismic and shear (S-wave) impedance was analysed by using the dataset of four wells drilled in 2001. A cross-plot graph has been produced from this analysis and in which the x and y axes are represented by the Runsum seismic and shear (S-wave) impedance respectively (Figures 4.7a–4.7d). The result shows that there is no correlation between the two data types. All four wells show the correlation coefficient to be less than 0.1 for all rock types (Table 4.5). This implies that the shear (S-wave) impedance cannot be correlated with the Runsum seismic.

4.1.6 Relationship between Acoustic (P-wave) and Shear (S-wave) Impedance

The dataset of acoustic (P-wave) and shear (S-wave) impedance was cross-plotted and x - and y -axes are represented by acoustic (P-wave) impedance and shear (S-wave) impedance respectively (Figures 4.8a-4.8d). The cross-plots show that the correlation coefficients are generally greater than 0.5 (Table 4.6) and, therefore, there is a linear relationship between acoustic (P-wave) and shear (S-wave) impedance. The NTM-C01 well shows the highest correlation coefficient values while NOH-A01 shows the lowest values. The graphs display clearly the separation of shale and clean sand.

4.1.7 Relationship between Filtered Acoustic (P-wave) Impedance and Porosity

The relationship between filtered acoustic (P-wave) impedance and porosity is displayed in cross-plots and in which the x - and y -axes are represented by filtered

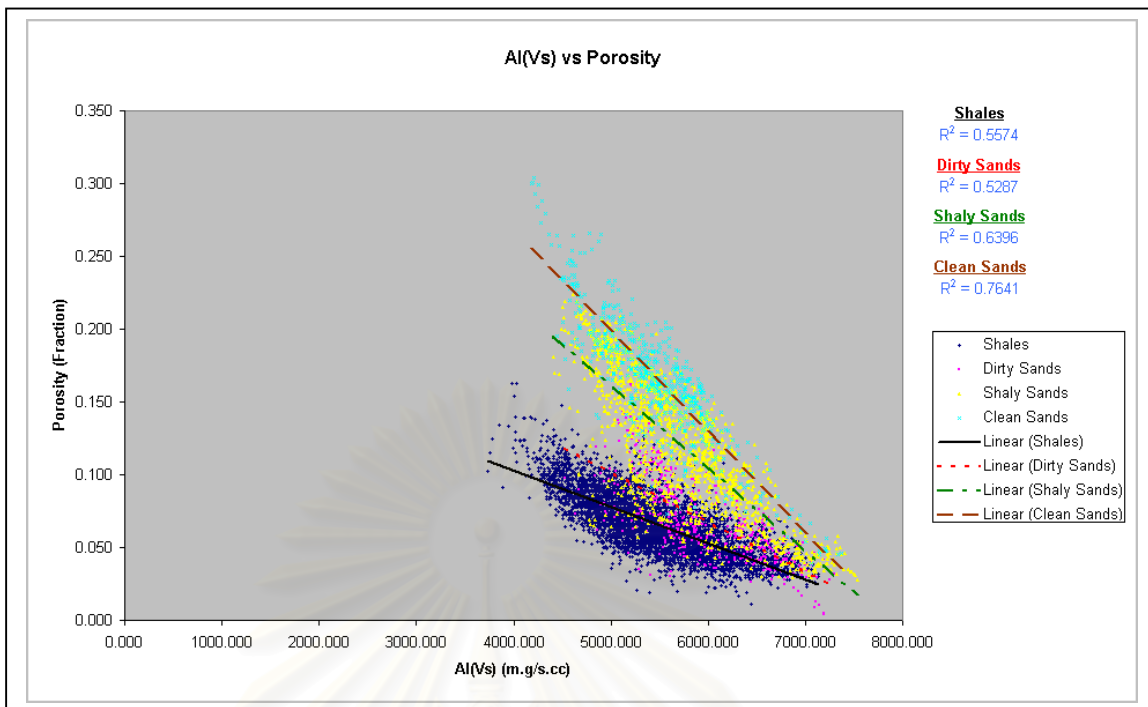


Figure 4.6a A cross-plot showing a relationship between shear (S-wave) impedance ($AI(Vs)$) and porosity in well NTM-C01

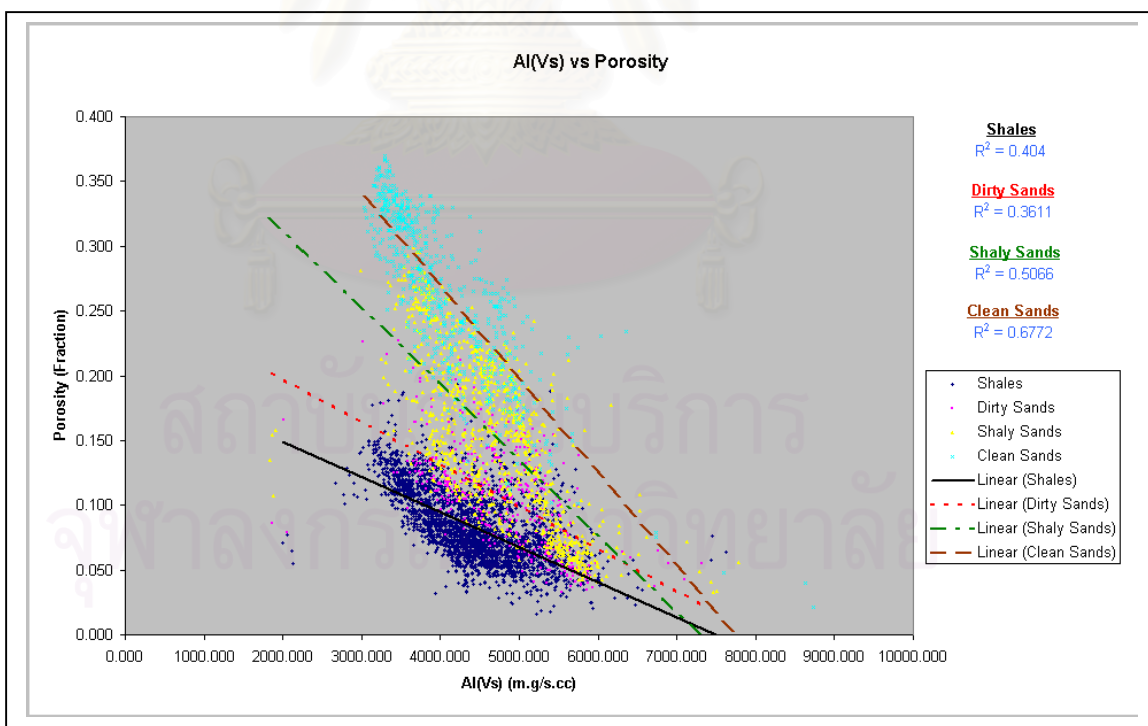


Figure 4.6b A cross-plot showing a relationship between shear (S-wave) impedance ($AI(Vs)$) and porosity in well WTN-B01

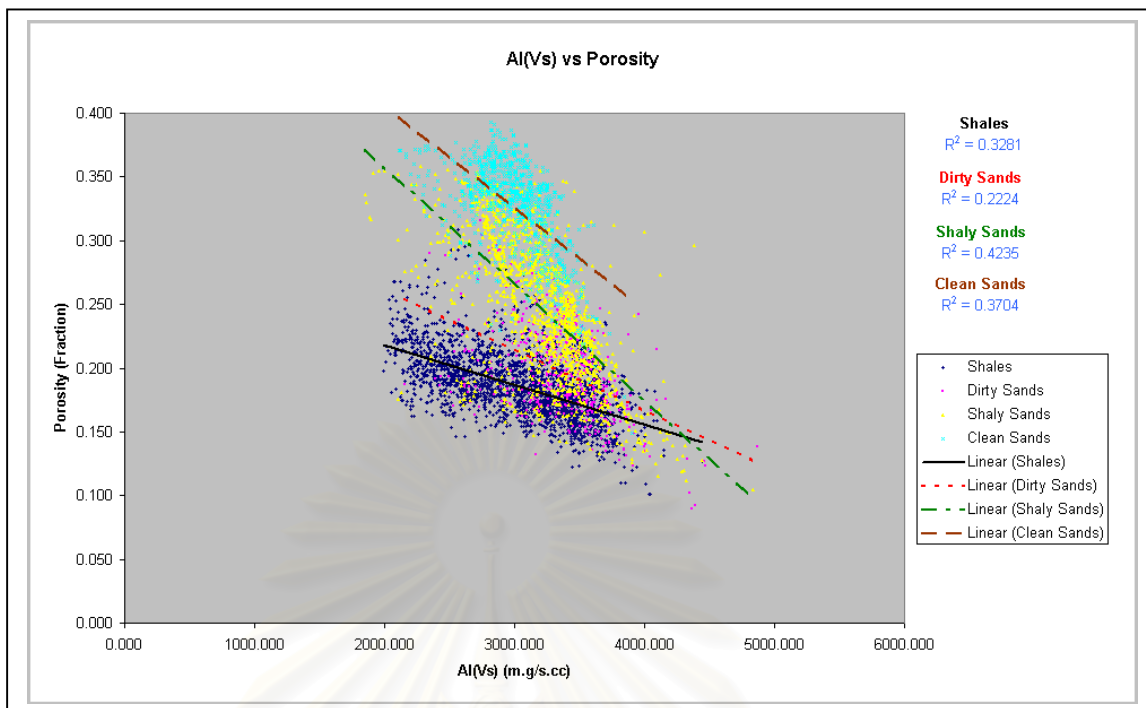


Figure 4.6c A cross-plot showing a relationship between shear (S-wave) impedance ($AI(Vs)$) and porosity in well NOH-A01

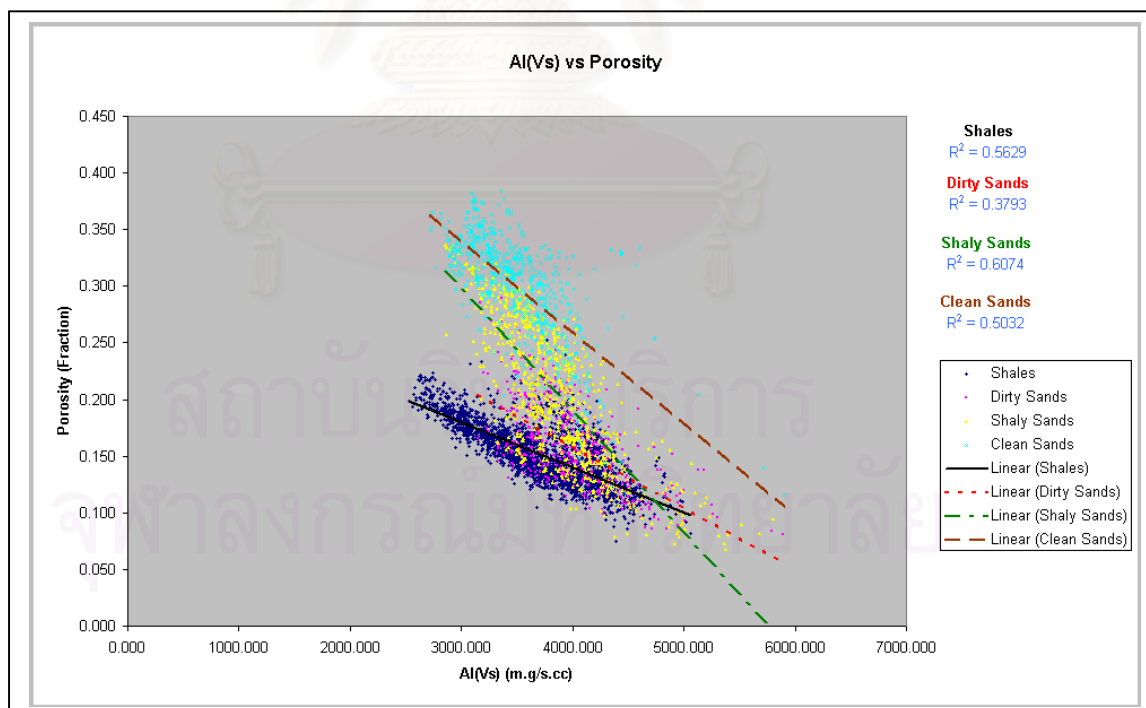


Figure 4.6d A cross-plot showing a relationship between shear (S-wave) impedance ($AI(Vs)$) and porosity in well NOH-A02

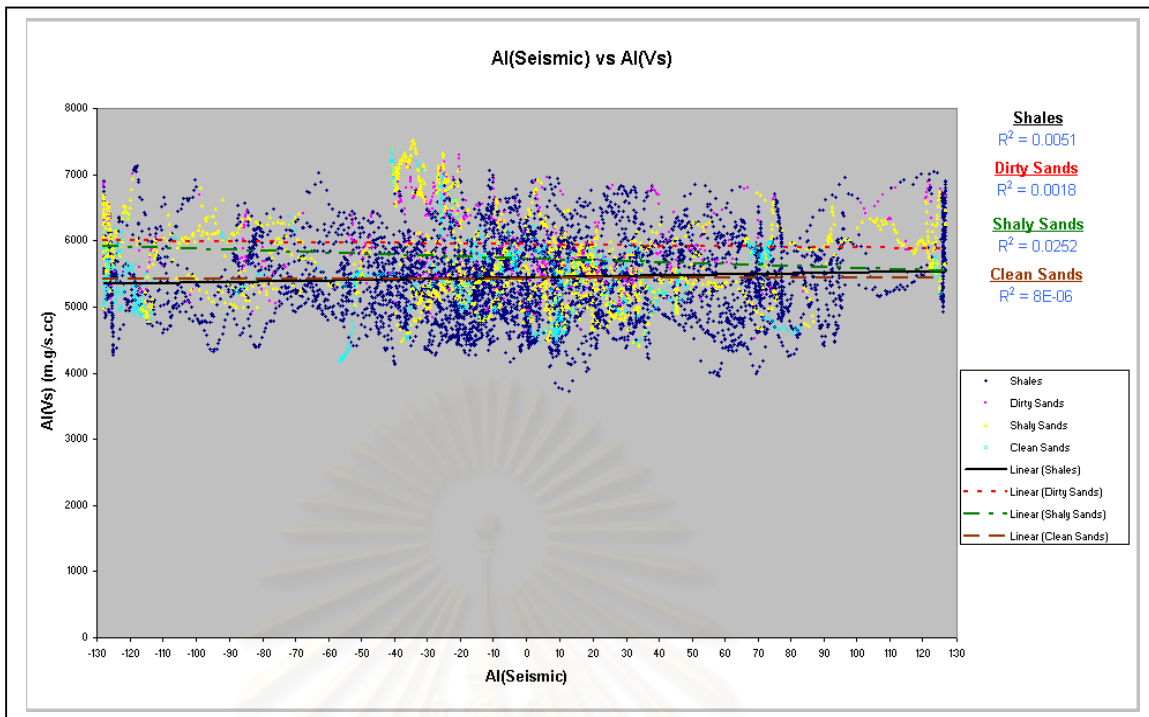


Figure 4.7a A cross-plot showing a relationship between Runsum seismic ($AI(Seismic)$) and shear (S-wave) impedance ($AI(Vs)$) in well NTM-C01

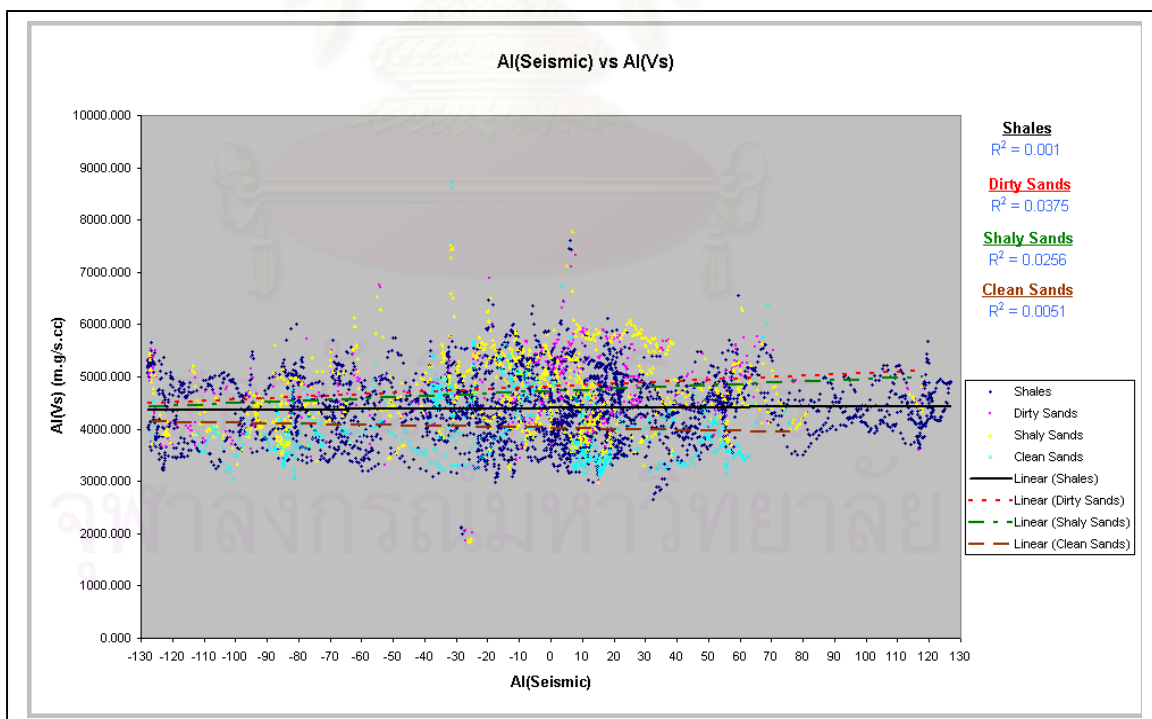


Figure 4.7b A cross-plot showing a relationship between Runsum seismic ($AI(Seismic)$) and shear (S-wave) impedance ($AI(Vs)$) in well WTN-B01

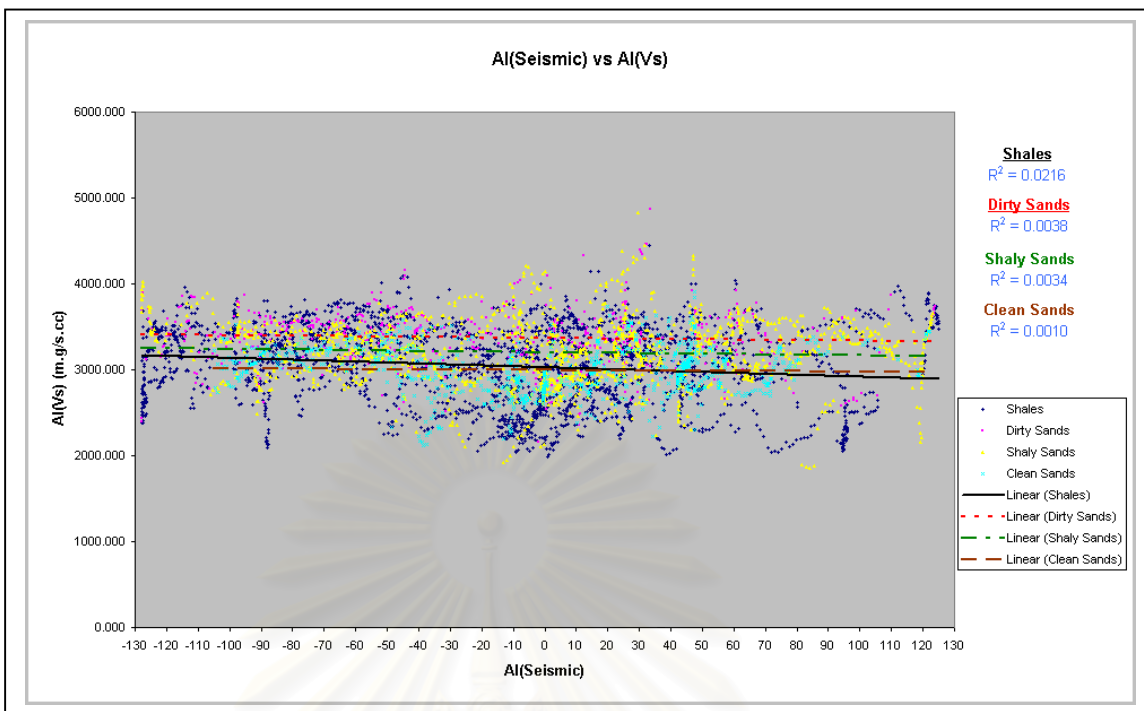


Figure 4.7c A cross-plot showing a relationship between Runsum seismic ($AI(Seismic)$) and shear (S-wave) impedance ($AI(Vs)$) in well NOH-A01

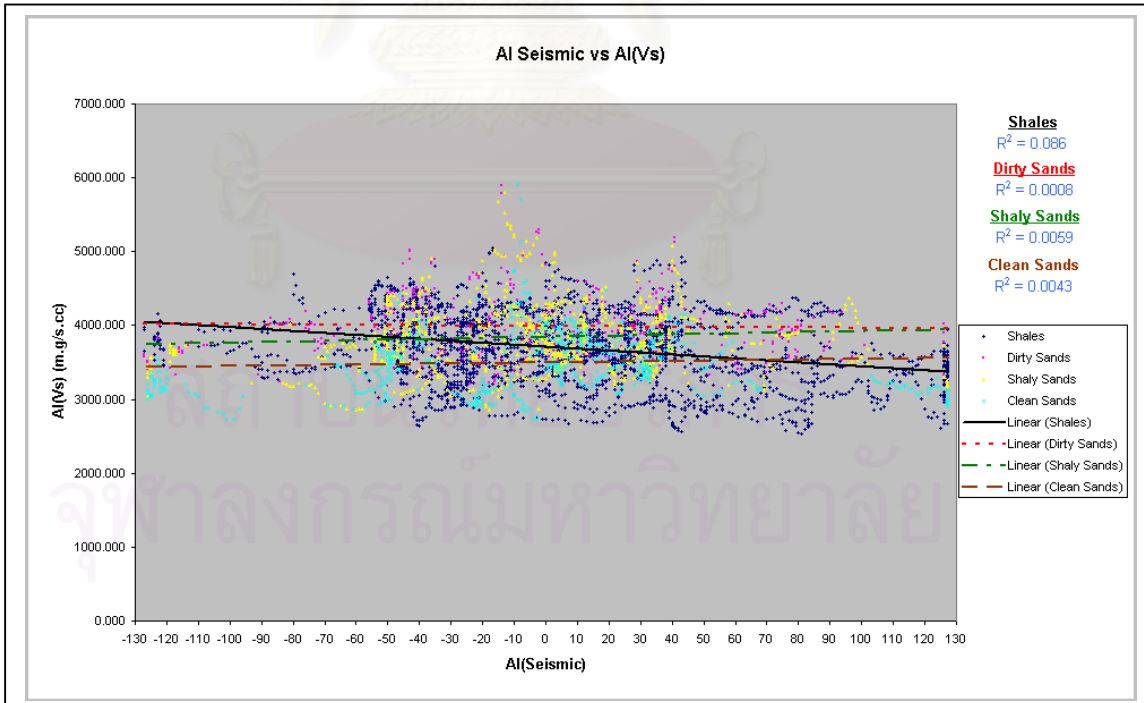


Figure 4.7d A cross-plot showing a relationship between Runsum seismic ($AI(Seismic)$) and shear (S-wave) impedance ($AI(Vs)$) in well NOH-A02

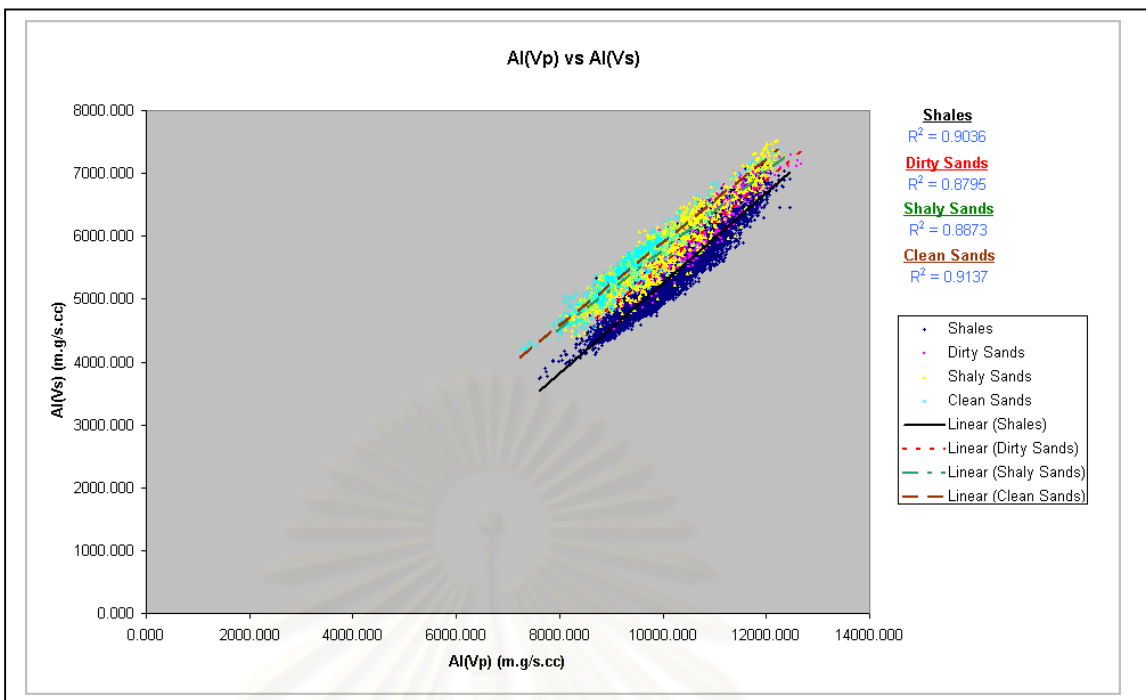


Figure 4.8a A cross-plot showing a relationship between acoustic (P-wave) impedance ($AI(Vp)$) and shear (S-wave) impedance ($AI(Vs)$) in well NTM-C01

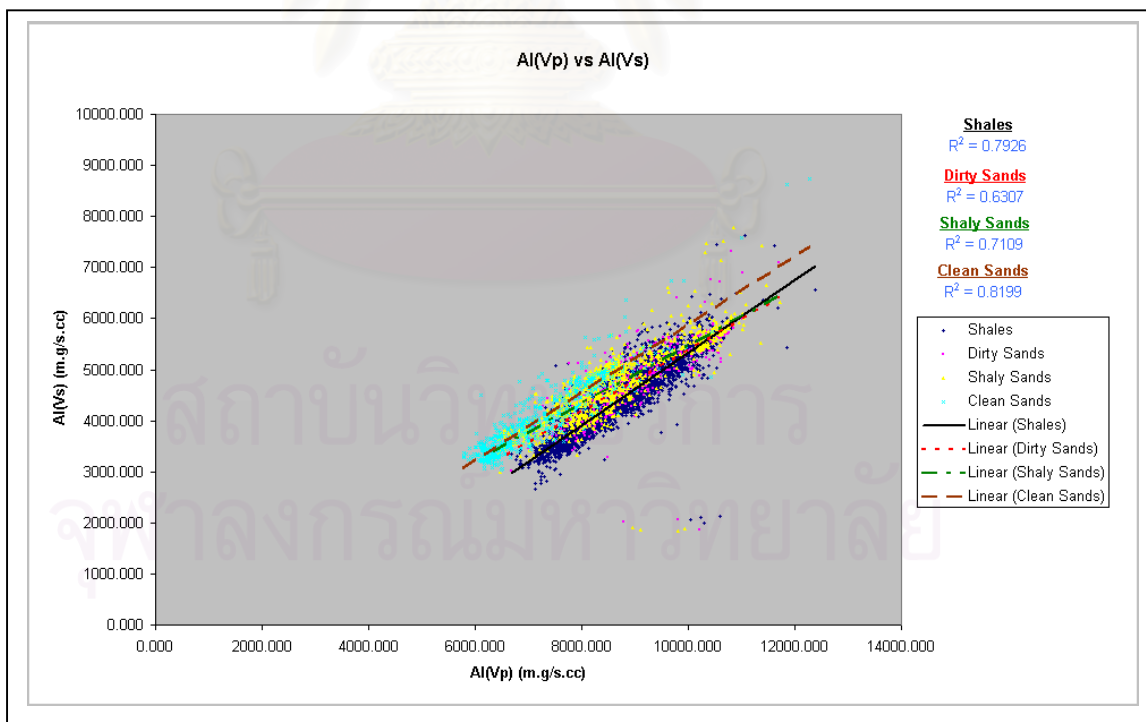


Figure 4.8b A cross-plot showing a relationship between acoustic (P-wave) impedance ($AI(Vp)$) and shear (S-wave) impedance ($AI(Vs)$) in well WTN-B01

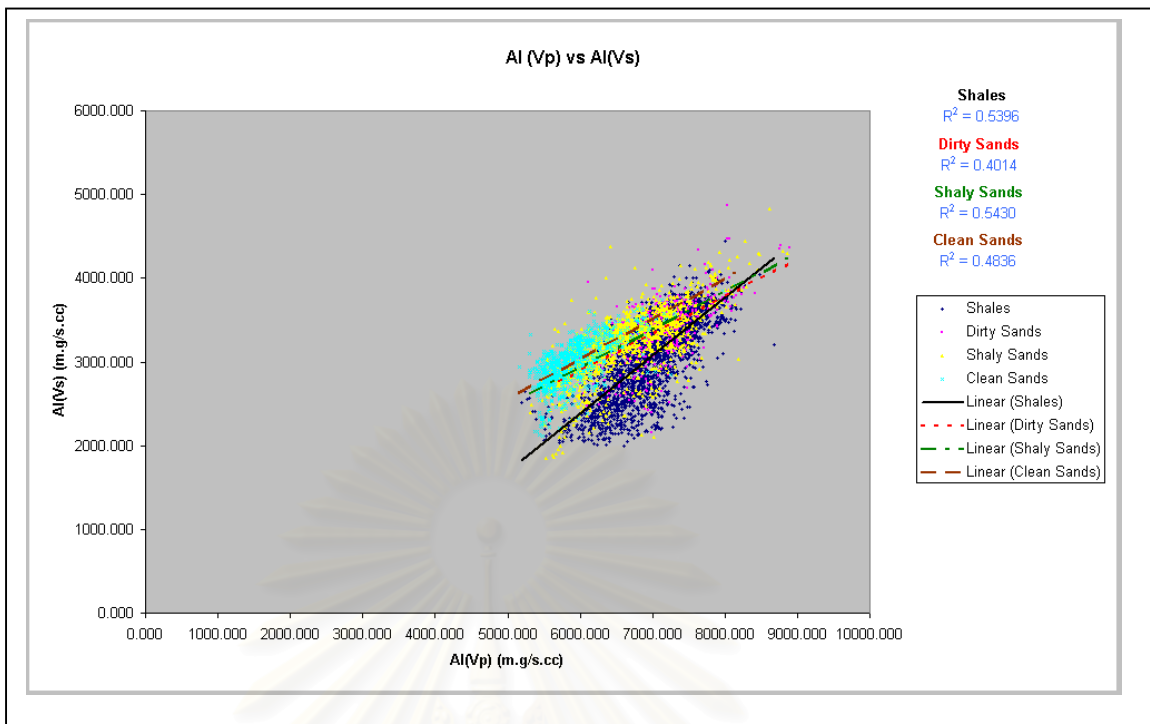


Figure 4.8c A cross-plot showing a relationship between acoustic (P-wave) impedance ($AI(Vp)$) and shear (S-wave) impedance ($AI(Vs)$) in well NOH-A01

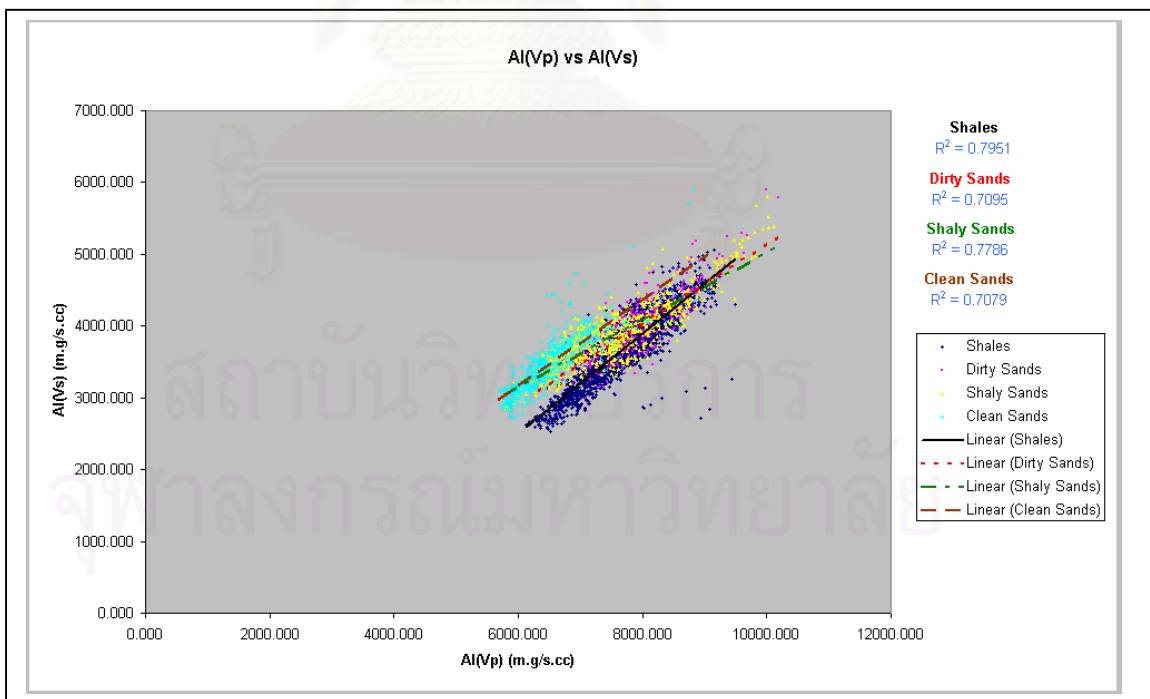


Figure 4.8d A cross-plot showing a relationship between acoustic (P-wave) impedance ($AI(Vp)$) and shear (S-wave) impedance ($AI(Vs)$) in well NOH-A02

acoustic (P-wave) impedance and porosity respectively (Figures 4.9a-4.9d). The result shows that there is no correlation between the two data types. All four wells show the correlation coefficient to be less than 0.1 for all rock types (Table 4.7). This implies that the filtered acoustic (P-wave) impedance cannot be correlated with differing porosity.

4.1.8 Relationship between Runsum Seismic and Filtered Acoustic Impedance (P-wave)

The dataset of the Runsum seismic and filtered acoustic (P-wave) impedance were cross-plotted and the x - and y -axes are represented by the Runsum seismic and filtered acoustic (P-wave) impedance respectively (Figures 4.10a-4.10d). The result shows that there is no correlation between two data types. All four wells show the correlation coefficient less than to be 0.1 for all rock types (Table 4.8). This implies that the Runsum data cannot be correlated with filtered acoustic (P-wave) impedance.

4.1.9 Relationship between Filtered Shear (S-wave) Impedance and Porosity

The relationship between filtered shear (S-wave) impedance and porosity is displayed and the x - and y -axes are represented by filtered shear (S-wave) impedance and porosity respectively (Figures 4.11a-4.11d). The result shows that there is no correlation between two data types. All four wells show the correlation coefficient less than 0.1 for all rock types (Table 4.9). This implies that the filtered shear (S-wave) impedance cannot be correlated with the differing porosity.

4.1.10 Relationship between Runsum Seismic and Filtered Shear (S-wave) Impedance

The dataset of the Runsum seismic and filtered shear (S-wave) impedance were cross-plotted and the x - and y -axes are represented by the Runsum seismic and filtered shear (S-wave) impedance respectively (Figures 4.12a-4.12d). The result shows that there is no correlation between two data types. All four wells show the correlation coefficient less than 0.1 for all rock types (Table 4.10). This implies that the Runsum data cannot be correlated with the filtered shear impedance (S-wave).

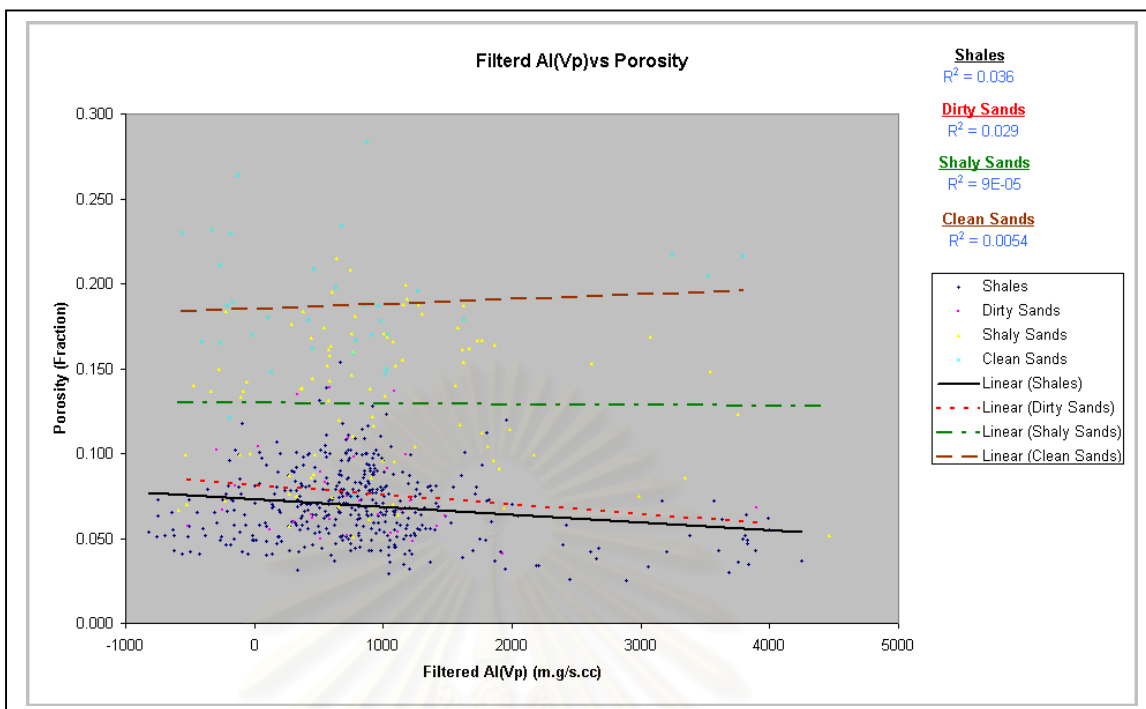


Figure 4.9a A cross-plot showing a relationship between filtered acoustic (P-wave) impedance ($AI(Vp)$) and porosity in well NTM-C01

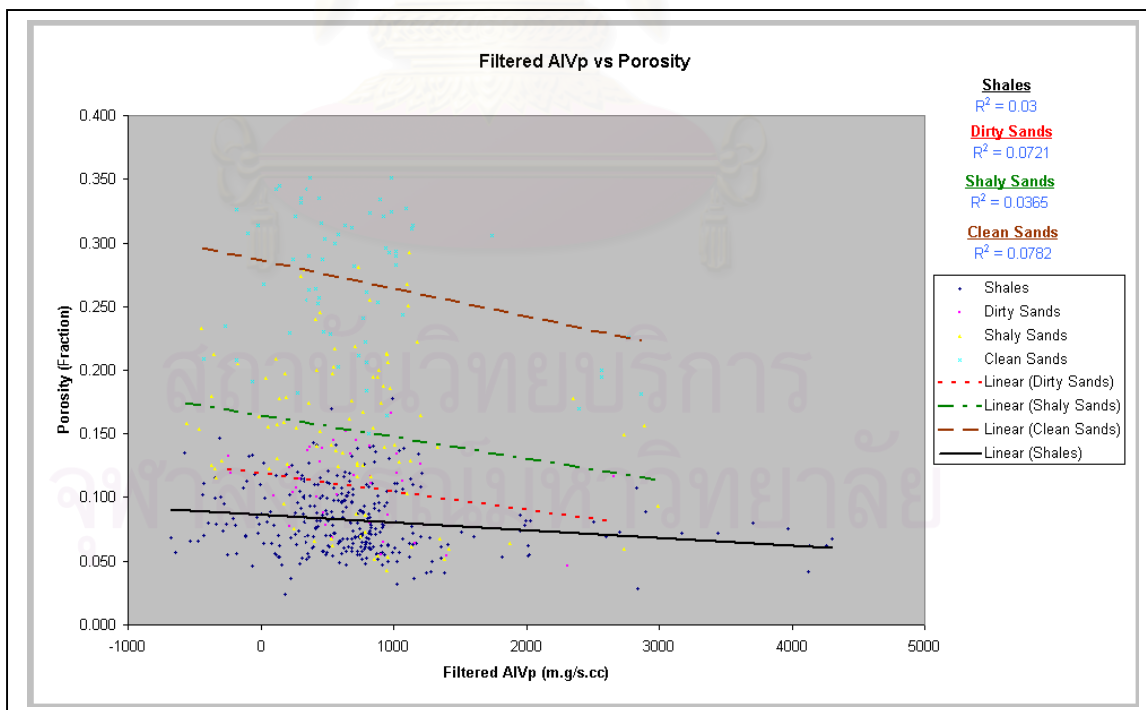


Figure 4.9b A cross-plot showing a relationship between filtered acoustic (P-wave) impedance ($AI(Vp)$) and porosity in well WTN-B01

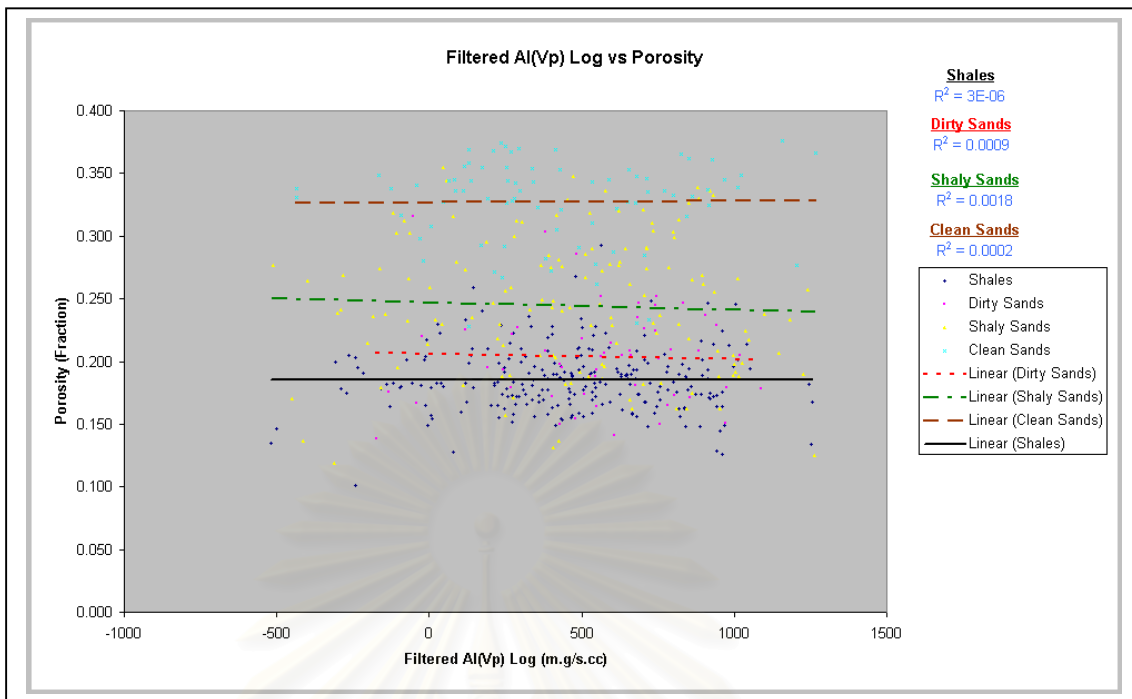


Figure 4.9c A cross-plot showing a relationship between filtered acoustic (P-wave) impedance ($AI(Vp)$) and porosity in well NOH-A01

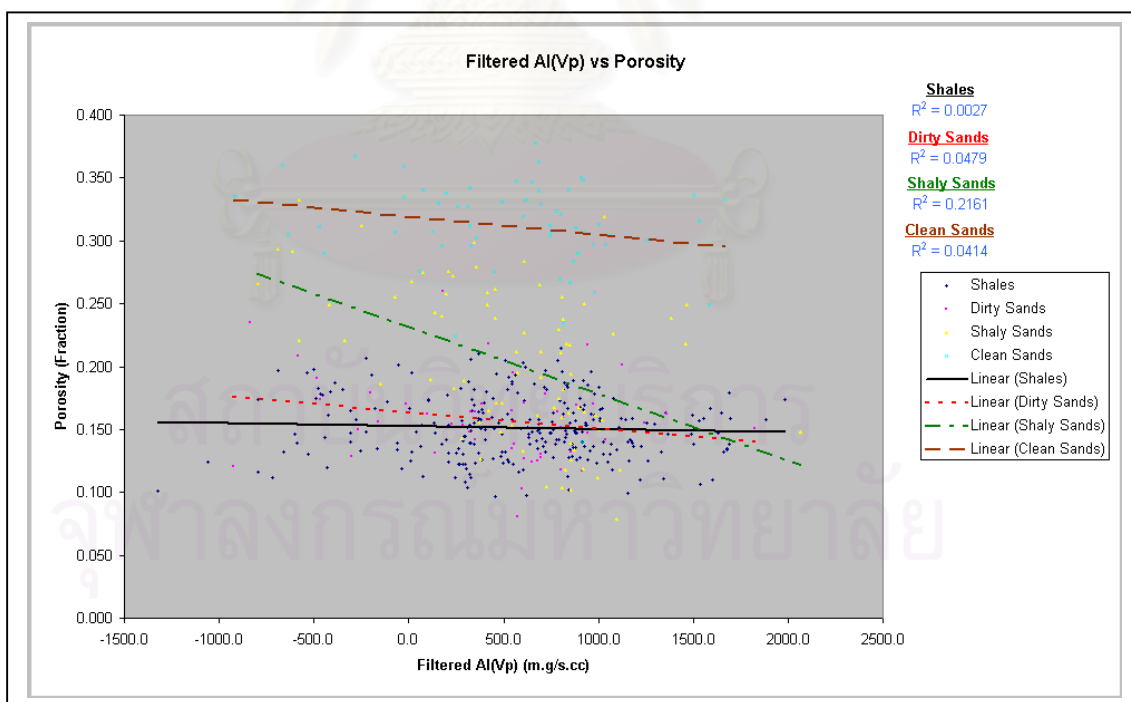


Figure 4.9d A cross-plot showing a relationship between filtered acoustic (P-wave) impedance ($AI(Vp)$) and porosity in well NOH-A02

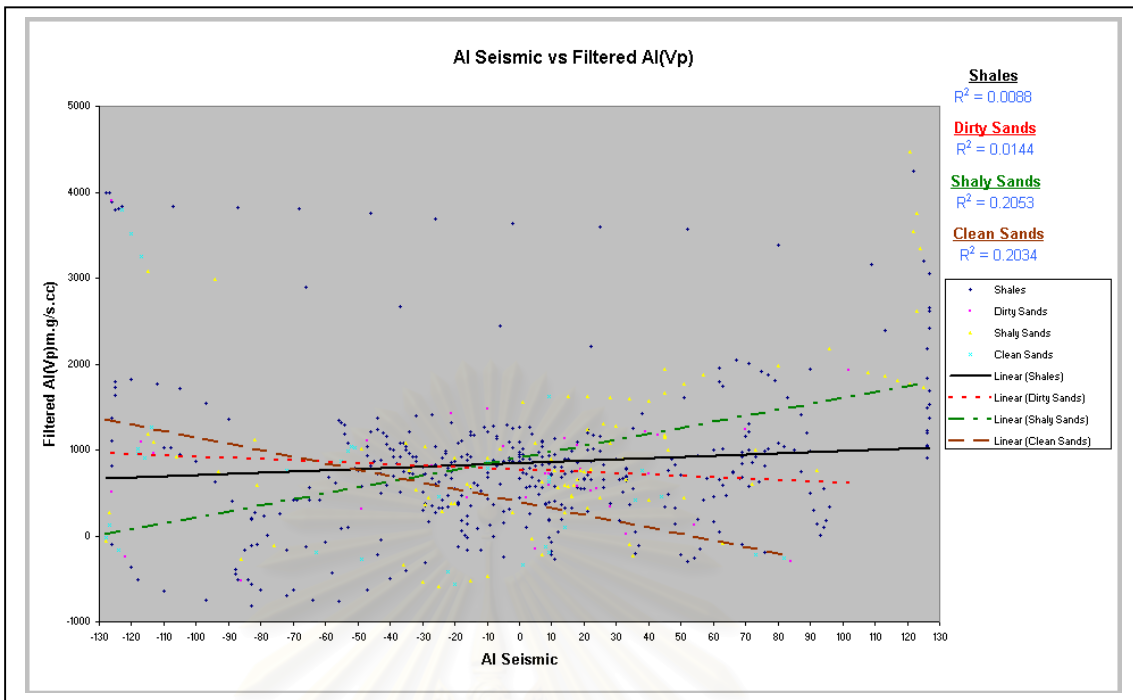


Figure 4.10a A cross-plot showing a relationship between Runsum seismic ($AI(seismic)$) and filtered acoustic (P-wave) impedance ($Filtered AI(Vp)$) in well NTM-C01

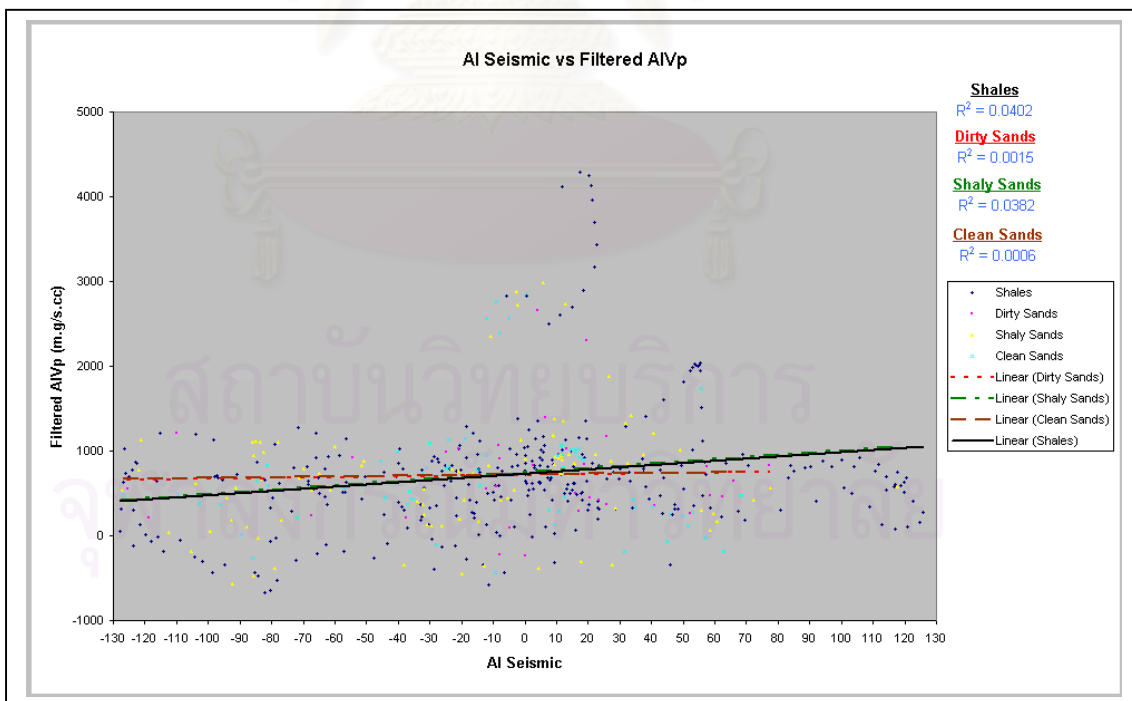


Figure 4.10b A cross-plot showing a relationship between Runsum seismic ($AI(seismic)$) and filtered acoustic (P-wave) impedance ($Filtered AI(Vp)$) in well WTN-B01

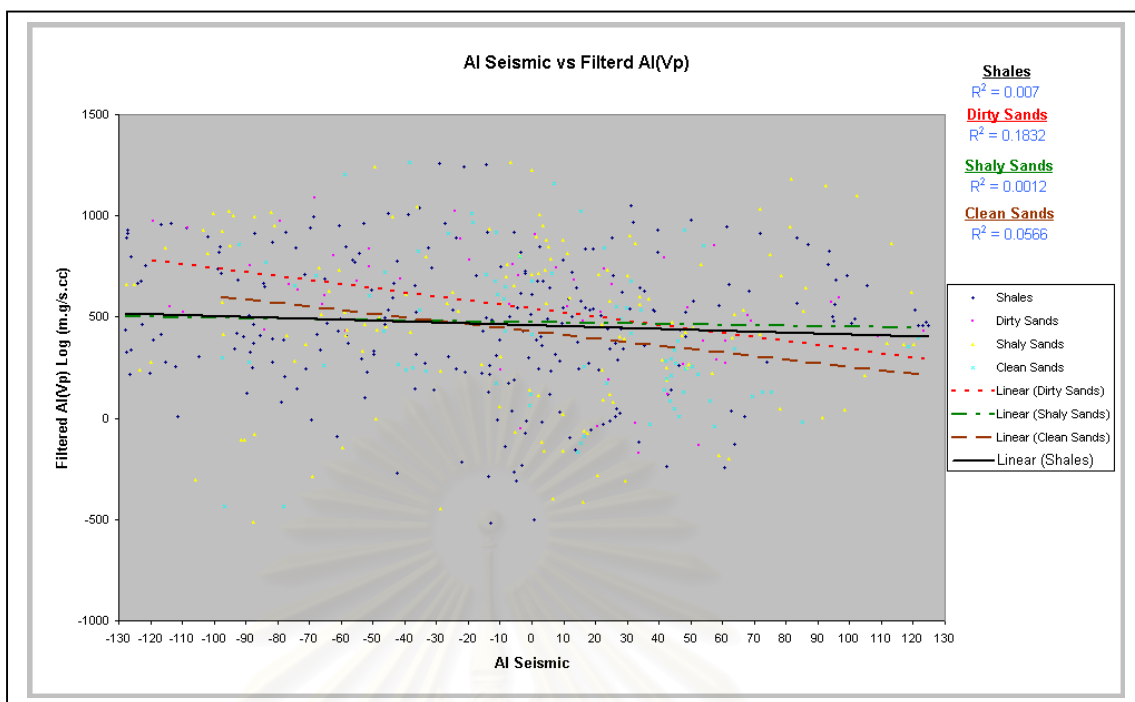


Figure 4.10c A cross-plot showing a relationship between Runsum seismic ($AI(seismic)$) and filtered acoustic (P-wave) impedance ($Filtered AI(Vp)$) in well NOH-A01

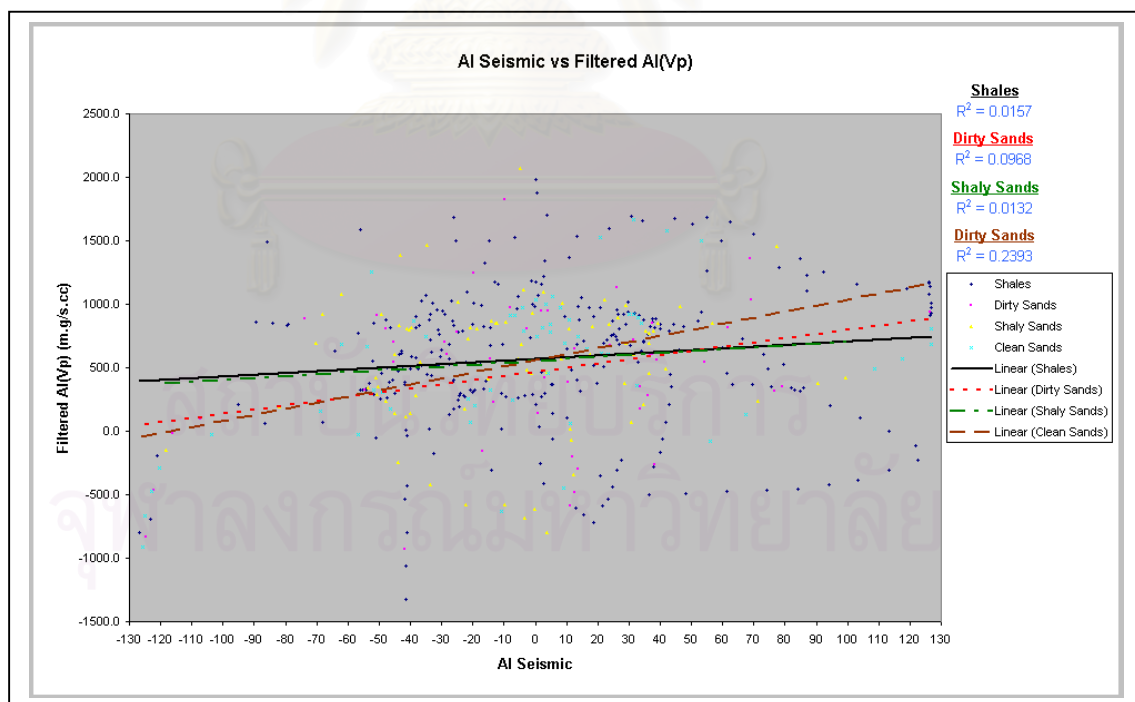


Figure 4.10d A cross-plot showing a relationship between Runsum seismic ($AI(seismic)$) and filtered acoustic (P-wave) impedance ($Filtered AI(Vp)$) in well NOH-A02

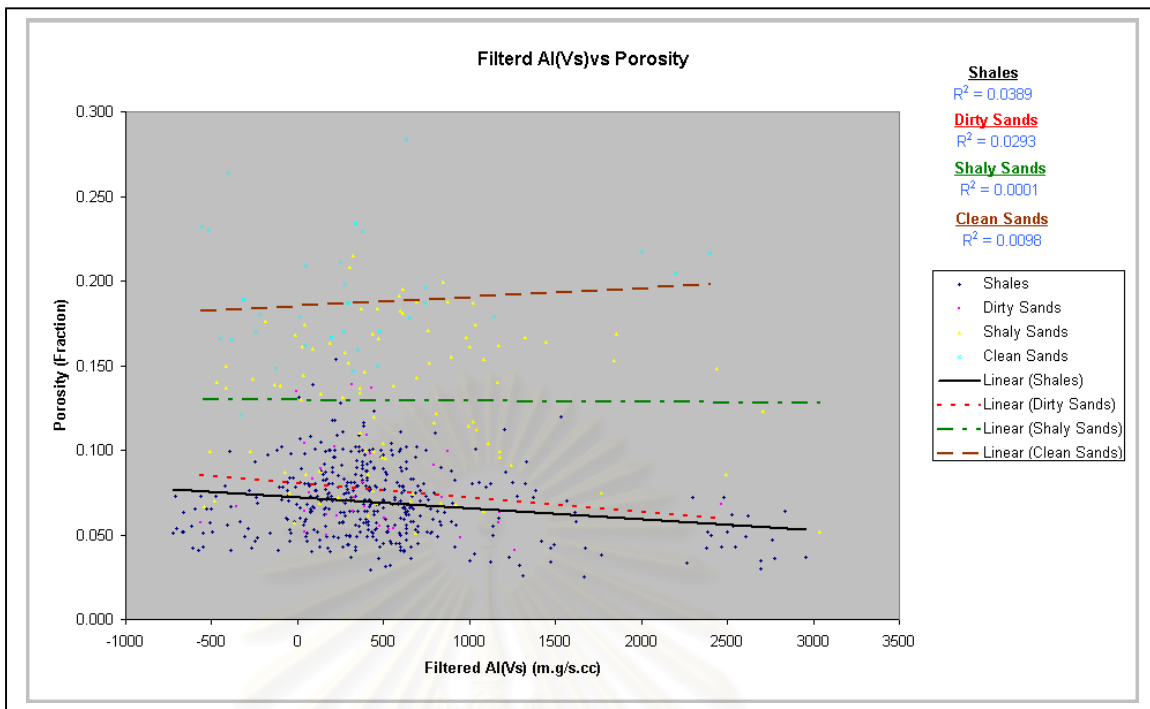


Figure 4.11a A cross-plot showing a relationship between filtered shear (S-wave) impedance (*Filtered AI(Vs)*) and porosity in well NTM-C01

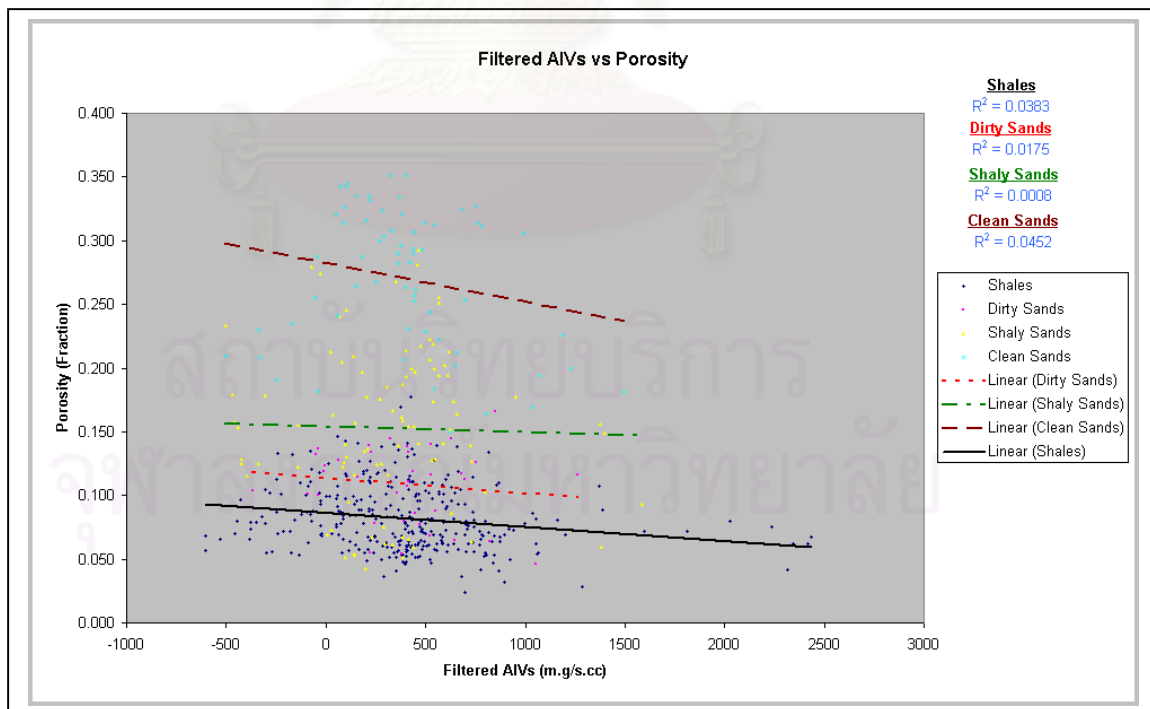


Figure 4.11b A cross-plot showing a relationship between filtered shear (S-wave) impedance (*Filtered AI(Vs)*) and porosity in well WTN-B01

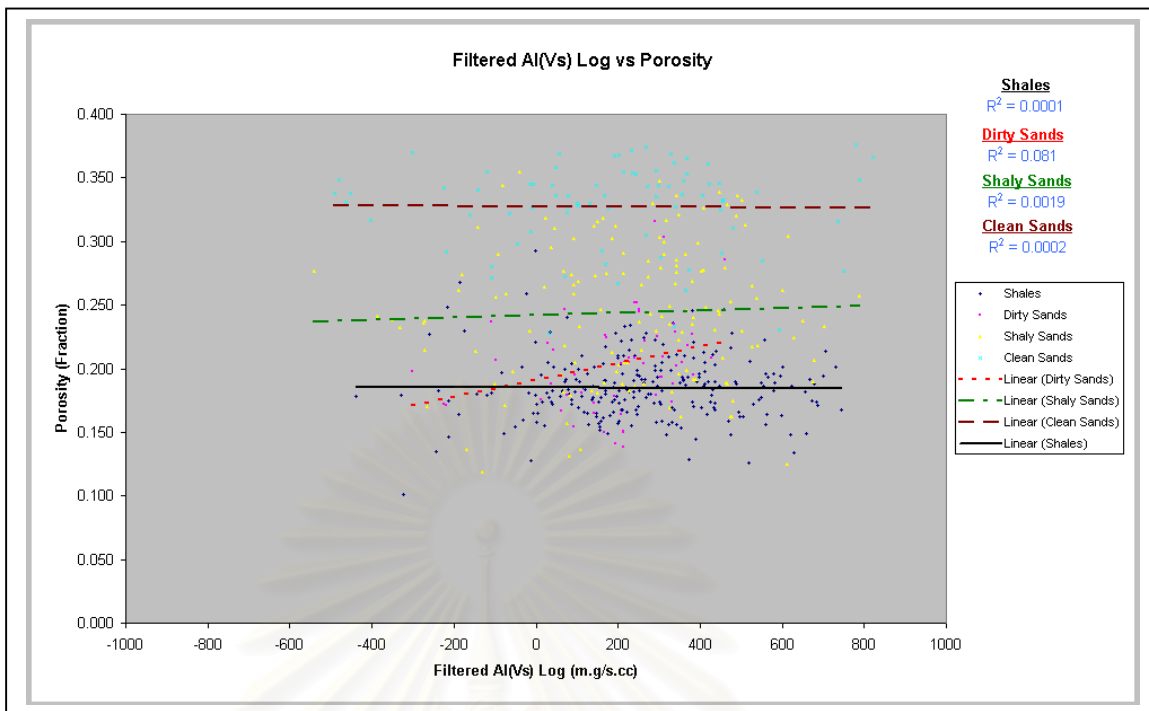


Figure 4.11c A cross-plot showing a relationship between filtered shear (S-wave) impedance (*Filtered AI(Vs)*) and porosity in well NOH-A01

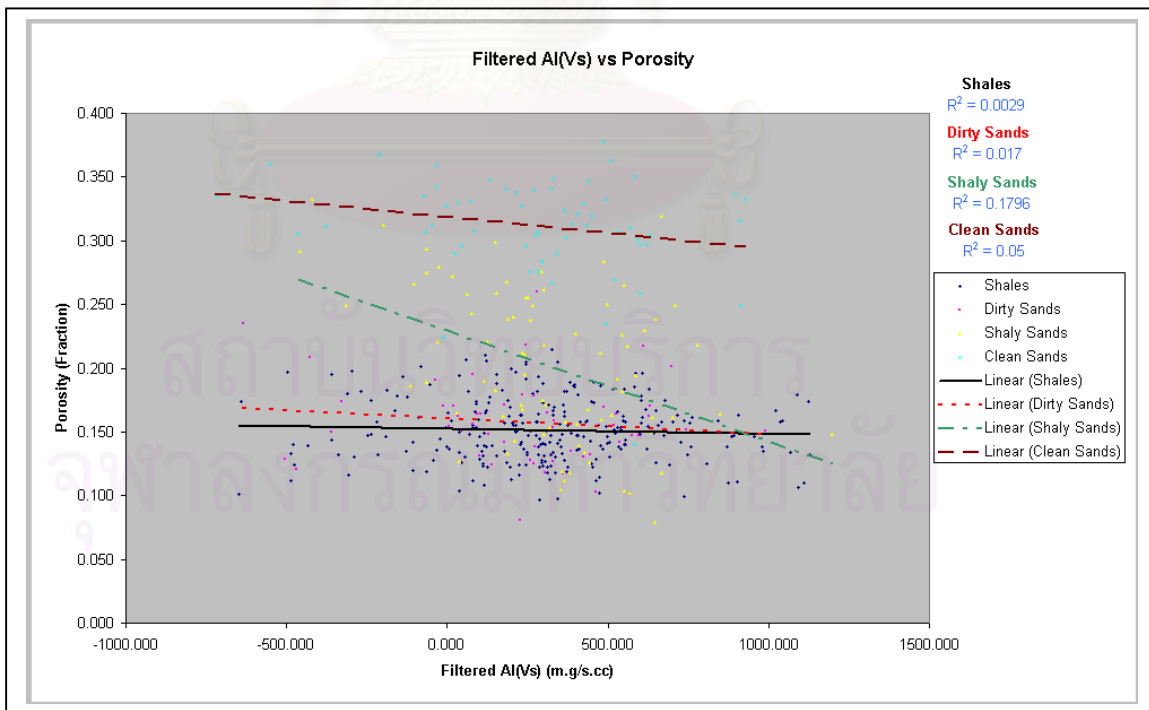


Figure 4.11d A cross-plot showing a relationship between filtered shear (S-wave) impedance (*Filtered AI(Vs)*) and porosity in well NOH-A02

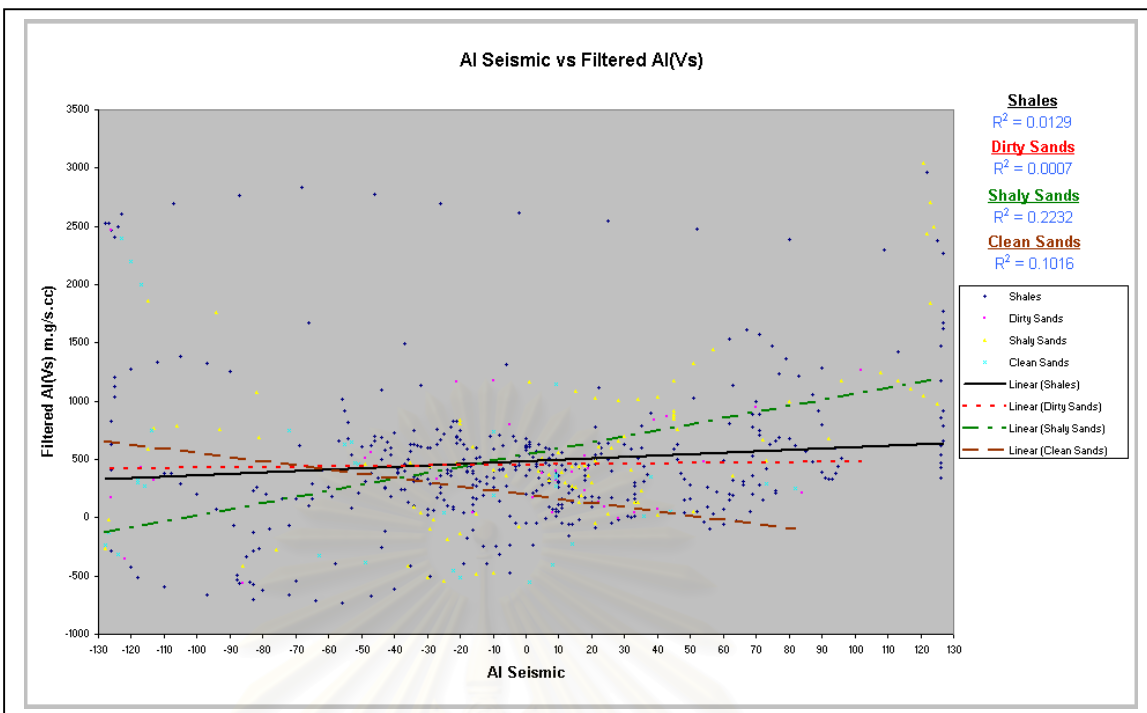


Figure 4.12a A cross-plot showing a relationship between Runsum seismic ($AI(seismic)$) and filtered shear (S-wave) impedance ($Filtered AI(Vs)$) in well NTM-C01

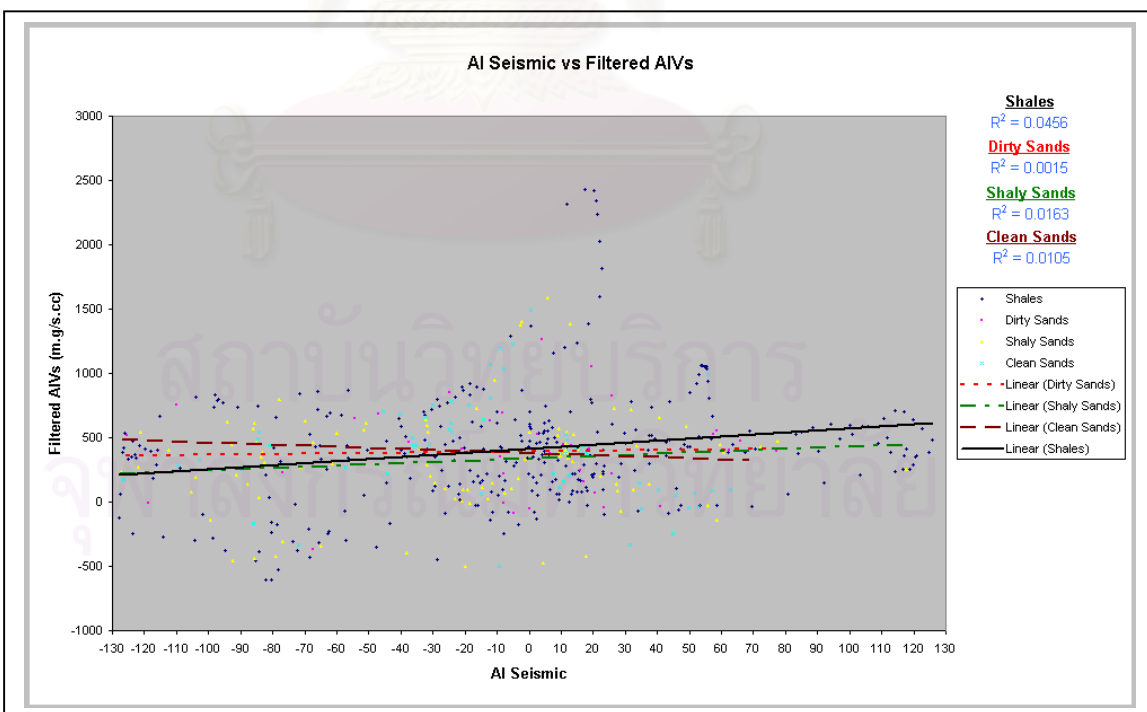


Figure 4.12b A cross-plot showing a relationship between Runsum seismic ($AI(seismic)$) and filtered shear (S-wave) impedance ($Filtered AI(Vs)$) in well WTN-B01

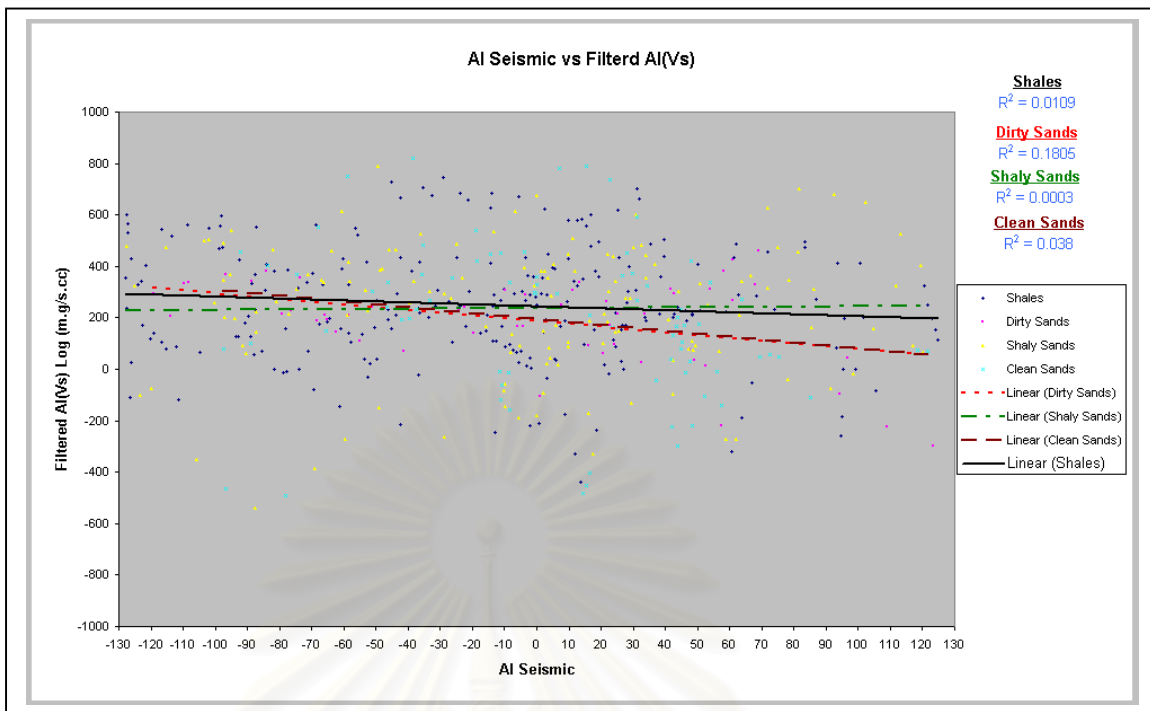


Figure 4.12c A cross-plot showing a relationship between Runsum seismic ($AI(seismic)$) and filtered shear (S-wave) impedance ($Filtered AI(Vs)$) in well NOH-A01

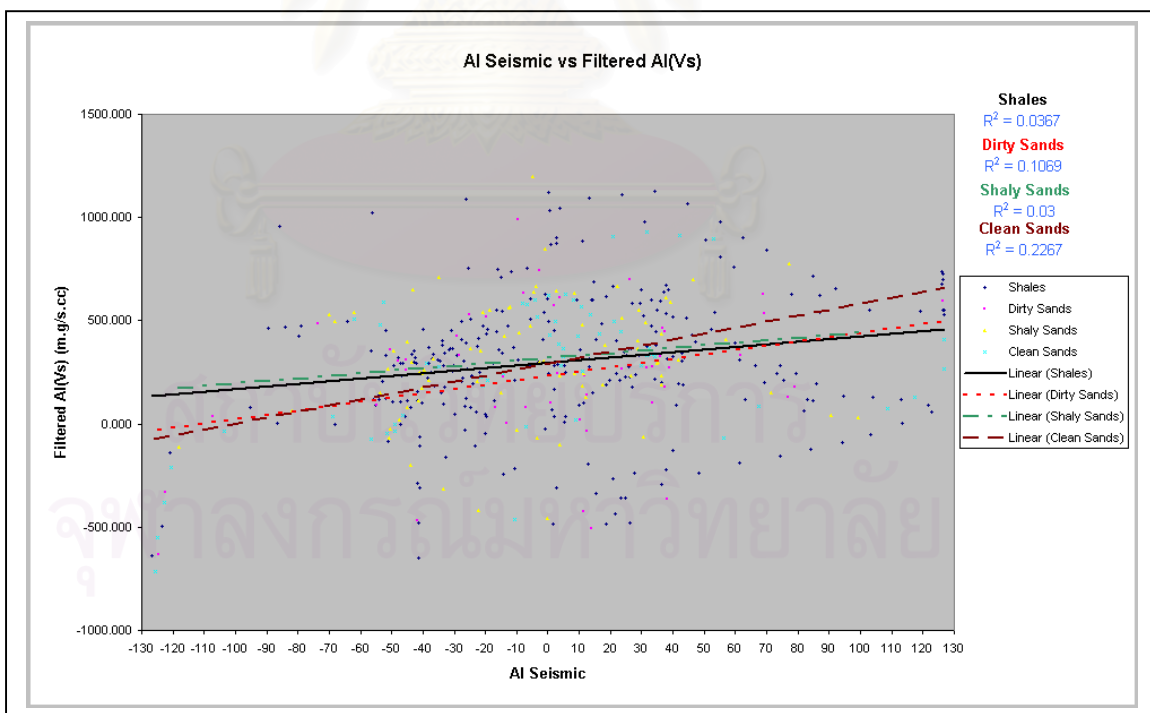


Figure 4.12d A cross-plot showing a relationship between Runsum seismic ($AI(seismic)$) and filtered shear (S-wave) impedance ($Filtered AI(Vs)$) in well NOH-A02

4.1.11 Relationship between Filtered Acoustic (P-wave) and Filtered Shear (S-wave) Impedance

The dataset of filtered acoustic (P-wave) and filtered shear (S-wave) impedance were cross-plotted and the x - and y -axes are represented by filtered acoustic (P-wave) impedance and filtered shear (S-wave) impedance respectively (Figures 4.13a-4.13d). The cross-plots show that the correlation coefficients are, in general, greater than 0.5 (Table 4.11) and, therefore, there is a linear relationship between filtered acoustic (P-wave) and filtered shear (S-wave) impedance.

4.2 Qualitative Analysis

Due to the limited lateral extent and variable nature of the Pratu Tao Formation, there is no significant detail available for the sequence stratigraphy study of in this area at Thai Shell. Moreover, it is very difficult to determine the sequence stratigraphy with any certainty in the wells drilled before 2001 as the sections are incomplete due to faulting, and the resultant log quality correlation is poor owing to wash-out.

In this study, the gamma ray, acoustic (P-wave) and shear (S-wave) impedance data from the four wells drilled in 2001, generally drilled parallel to the fault blocks, has been mainly used to determine the lithological units in the Pratu Tao Formation in the Greater Pratu Tao area. The porosity and Runsum seismic data has been employed as the supporting information. This data was cross-plotted on a graph, on which the x -axis represents the value of the gamma ray, acoustic (P-wave) and shear (S-wave) impedance, Runsum seismic and porosity data and the y -axis represents the depth. The lithological units can be sub-divided into subsidiary sub-units using the break between shale trend lines displayed in the acoustic (P-wave) and shear (S-wave) impedance dataset. This break is also present in the gamma ray cross-plot for the studied wells. Therefore, four distinct lithological units are recognised using this method (Tables 4.12-4.15). The ratios of net clean sand to shale and net clean sand to gross were also calculated for each unit (Tables 4.16-4.19). The lithological units for each well are as follows:

Unit 1

This unit is topmost of the Pratu Tao Formation. The gamma ray data shows very thin and spiky log characteristics with coarsening-upward and fining-upward

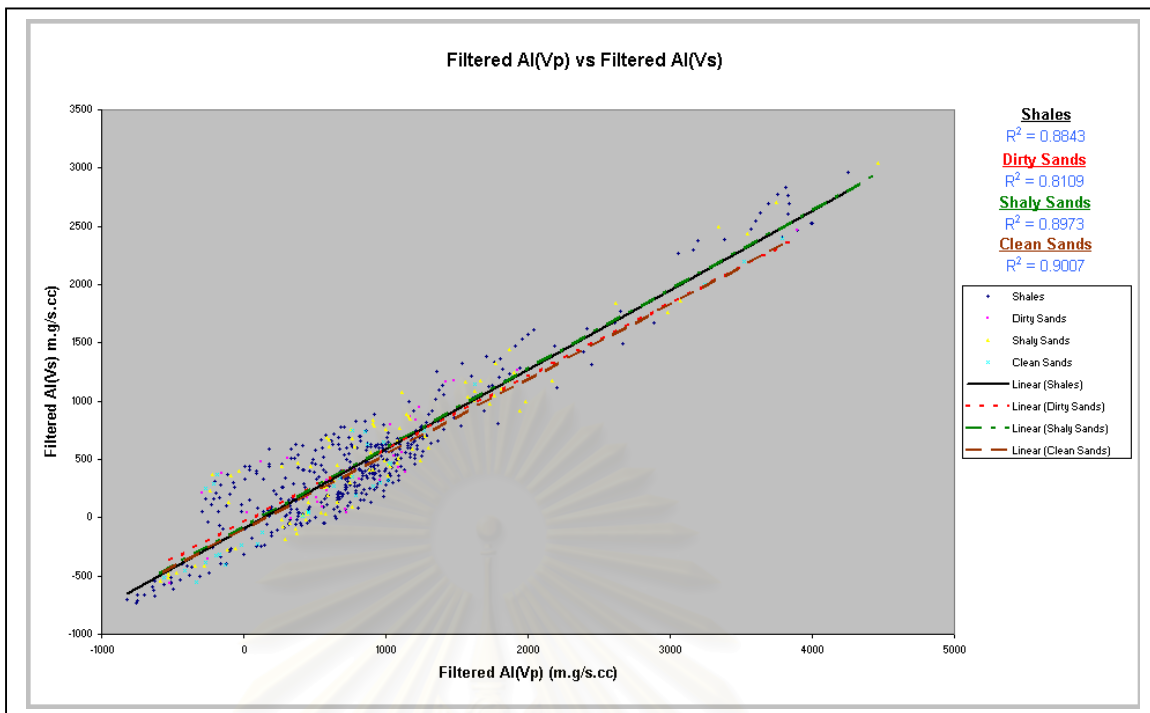


Figure 4.13a A cross-plot showing a relationship between filtered acoustic (P-wave) (*Filtered AI(Vp)*) and filtered shear (S-wave) impedance (*Filtered AI(Vs)*) in well NTM-C01

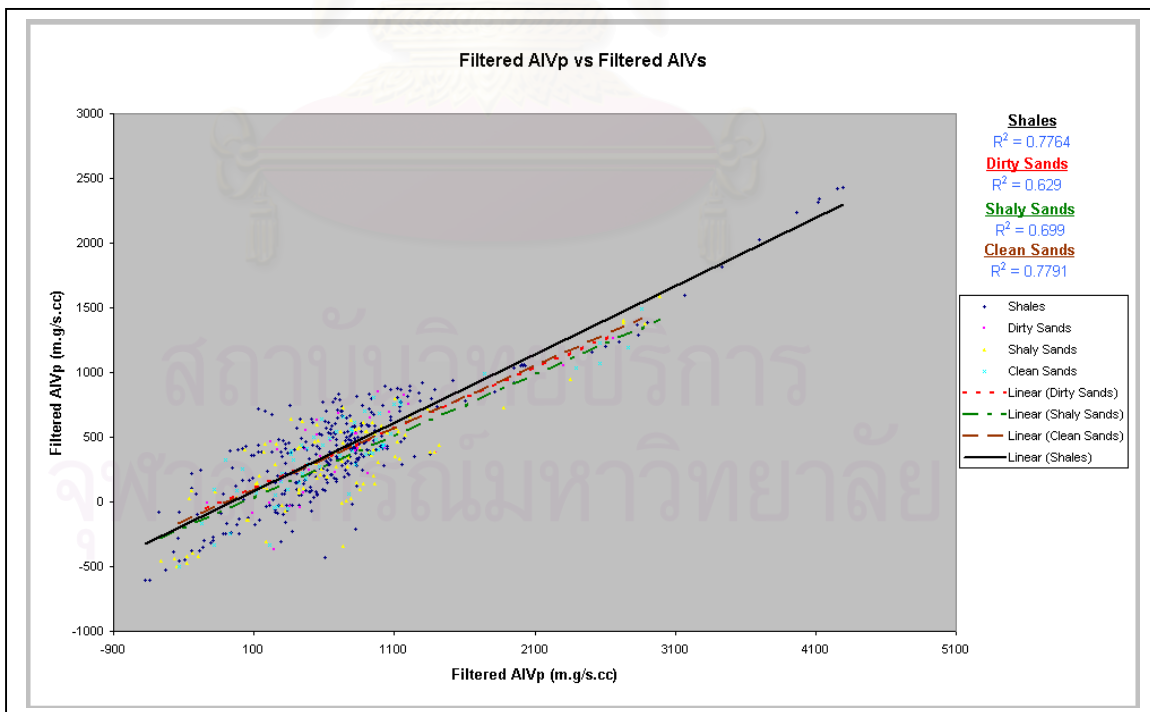


Figure 4.13b A cross-plot showing a relationship between filtered acoustic (P-wave) (*Filtered AI(Vp)*) and filtered shear (S-wave) impedance (*Filtered AI(Vs)*) in well WTN-B01

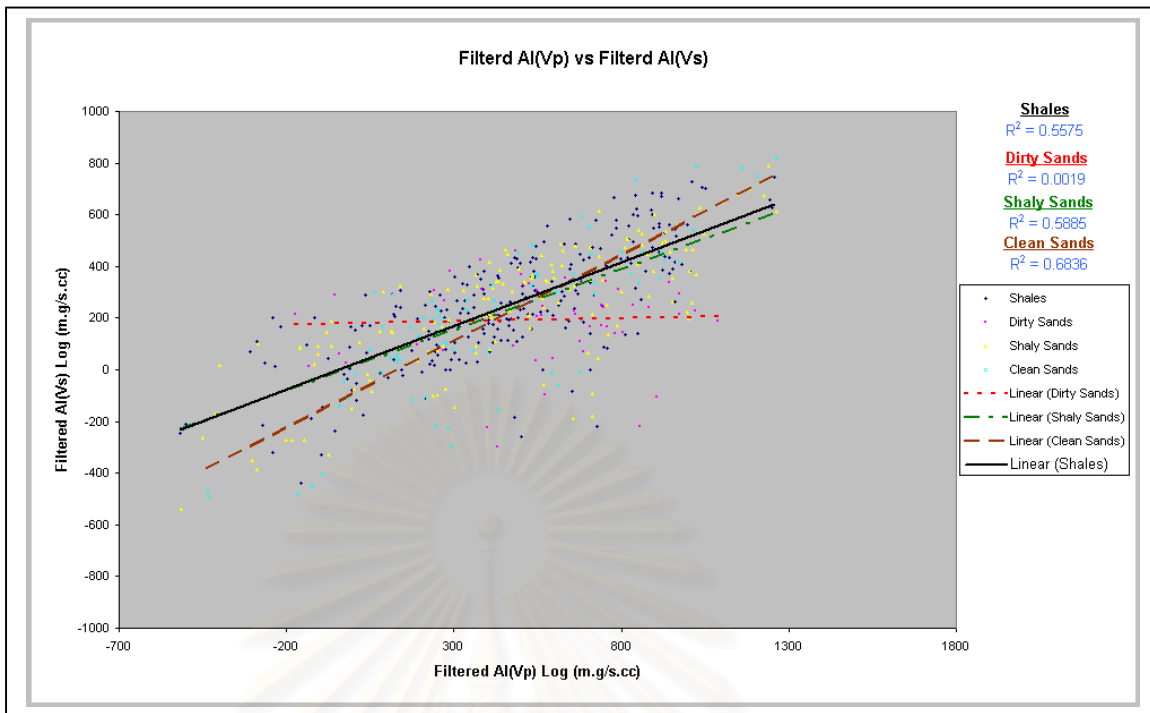


Figure 4.13c A cross-plot showing a relationship between filtered acoustic (P-wave) (*Filtered AI(Vp)*) and filtered shear (S-wave) impedance (*Filtered AI(Vs)*) in well NOH-A01

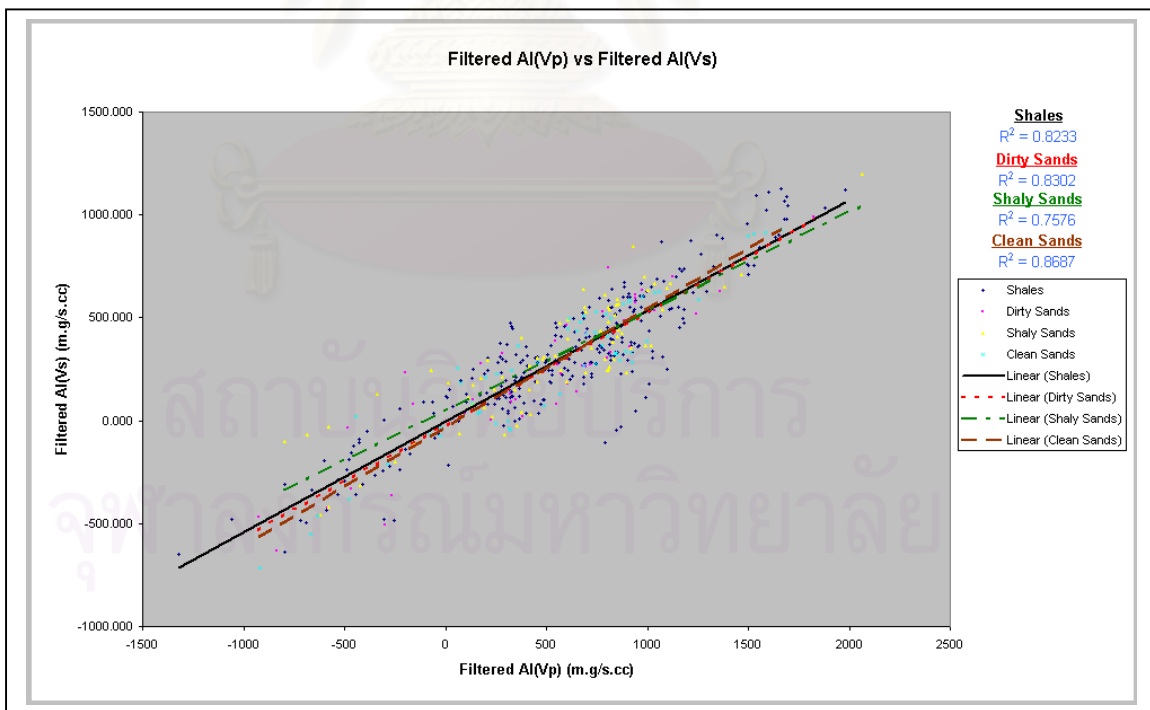


Figure 4.13d A cross-plot showing a relationship between filtered acoustic (P-wave) (*Filtered AI(Vp)*) and filtered shear (S-wave) impedance (*Filtered AI(Vs)*) in well NOH-A02

Table 4.12 Lithological units classified in NTM-C01

Well	Lithological Unit	Depth (mTVDSS)	Gamma Ray Characteristics	Acoustic Impedance Characteristics		Runsum Seismic Characteristics	Porosity Characteristics
				AI(Vp)	AI(Vs)		
NTM-C01	1	2059.86 - 2290.22	Very thin and spiky log with coarsening-upward profile, and fining-upward profile in the middle of this unit	Increasing trend line from top to bottom; 8800-10000 m.g/s.cc	Increasing shale's trend line from top to bottom; approx. 4600-5200 m.g/s.cc	Various amplitudes; max 90 and min -90	Porosity in shale approx. from 0.040 to 0.150
	2	2290.22 - 2493.61	Very thin and spiky profile with coarsening-upward trend	Increasing shale's trend line from top to bottom; 9800-13000 m.g/s.cc	Increasing shale's trend line from top to bottom; approx. 2500-3500 m.g/s.cc	Low to medium amplitudes; approx. between from -120 to 70	Porosity in shale approx. from 0.030 to 0.120
	3	2493.61 - 2685.18	Spiky log with fining-upward trend	Increasing shale's trend line from top to bottom; 9700-18000 m.g/s.cc	Increasing shale's trend line in wide range from top to bottom; approx. 5000-5700 m.g/s.cc	Low to high amplitudes; approx. between from -100 to 90	Porosity in shale approx. from 0.020 to 0.120
	4.1	2685.18 - 2910.31	Spiky log with bell-shaped profile	Increasing trend line in narrow range from top to bottom; 10000-11000 m.g/s.cc	Increasing shale's trend line in wide range from top to bottom; approx. 5300-5700 m.g/s.cc	Wide range amplitudes; approx. between from -127 to 126	Same as unit 3
	4.2	2910.31 - 3108.39	Clearly fining-upward profile	Increasing trend line in wide range from top to bottom; 9800-11700 m.g/s.cc	Increasing shale's trend line range from top to bottom; approx. 5200-6800 m.g/s.cc	Medium amplitudes; approx. between from -50 to 80	Same as unit 3

Table 4.13 Lithological units classified in WTN-B01

Well	Lithological Unit	Depth (mTVDSS)	Gamma Ray Characteristics	Acoustic Impedance Characteristics		Runsum Seismic Characteristics	Porosity Characteristics
				AI(Vp)	AI(Vs)		
WTN-B01	1	1374.80 - 1594.84	Very thin and spiky log with coarsening-upward profile, and fining-upward profile on the top of this unit	Increasing shale's trend line in narrow range from top to bottom; approx. 7200-8200 m.g/s.cc	Increasing shale's trend line from top to bottom; approx. 3800-4800 m.g/s.cc	Various amplitudes; max 60 and min -126	Porosity in shale approx. from 0.050 to 0.200
	2	1594.84 - 1704.41	Very thin and spiky profile with fining-upward trend	Increasing shale's trend line from top to bottom; approx. 7900-9200 m.g/s.cc	Increasing shale's trend line from top to bottom; approx. 2500-3500 m.g/s.cc	Low to medium amplitudes; approx. between from -110 to 80	Porosity in shale approx. from 0.050 to 0.150
	3	1704.41 - 1796.39	Spiky log with bell-shaped profile	Increasing shale's trend line in wide range from top to bottom; approx. 7300-11000 m.g/s.cc	Increasing shale's trend line in wide range from top to bottom; approx. 2500-3700 m.g/s.cc	Low to high amplitudes; approx. between from -126 to 120	Porosity in shale approx. from 0.025 to 0.150
	4.1	1796.39 - 1979.70	Spiky log with fining-upward profile	Increasing shale's trend line in narrow range from top to bottom; approx. 9000-9300 m.g/s.cc	Increasing shale's trend line in wide range from top to bottom; approx. 3800-5600 m.g/s.cc	Medium to high amplitudes; approx. between from -80 to 126	Same as unit 3
	4.2	1979.70 - 2344.77	Fining-upward profile	Increasing shale's trend line in narrow range from top to bottom; approx. 8800-9000 m.g/s.cc	Increasing shale's trend line range from top to bottom; approx. 4000-4700 m.g/s.cc	Medium amplitudes; approx. between from -60 to 20	Same as unit 3

Table 4.14 Lithological units classified in NOH-A01

Well	Lithological Unit	Depth (mTVDSS)	Gamma Ray Characteristics	Acoustic Impedance Characteristics		Runsum Seismic Characteristics	Porosity Characteristics
				AI(Vp)	AI(Vs)		
NOH-A01	1	891.93 - 1007.86	Generally, coarsening-upward profile, and fining-upward profile on the top of this unit	Increasing shale's trend line from top to bottom; 6200-6500 m.g/s.cc	Increasing shale's trend line from top to bottom; 2200-3500 m.g/s.cc	Wide range of amplitudes; max 100 and min -100	Porosity in shale approx. from 0.150 to 0.300
	2	1007.86 - 1096.89	Very thin and spiky profile with fining-upward trend	Increasing shale's trend line from top to bottom; 6400-7000 m.g/s.cc	Increasing shale's trend line from top to bottom; 2500-3500 m.g/s.cc	Low to medium amplitudes; between from -110 to 70	Porosity in shale approx. from 0.150 to 0.250
	3	1096.89 - 1229.98	Spiky log with bell-shaped profile	Increasing shale's trend line from top to bottom; 6200-7200 m.g/s.cc	Increasing shale's trend line from top to bottom; 2500-3700 m.g/s.cc	Various amplitudes; approx. between from -126 to 110	Decreasing porosity in shale from top to bottom; approx. from 0.250 to 0.100
	4	1229.98 - 1329.57	Spiky log with funnel-shaped profile	Decreasing shale's trend line from top to bottom; 7300-6500 m.g/s.cc	Decreasing shale's trend line in very narrow range from top to bottom; approx. 3200-3300 m.g/s.cc	Low to high amplitudes; approx. between from -100 to 126	Porosity in shale approx. from 0.100 to 0.200

Table 4.15 Lithological units classified in NOH-A02

Well	Lithological Unit	Depth (mTVDSS)	Gamma Ray Characteristics	Acoustic Impedance Characteristics		Runsum Seismic Characteristics	Porosity Characteristics
				AI(Vp)	AI(Vs)		
NOH-A02	1	1099.48 - 1234.31	Generally, coarsening-upward profile, and a small fining-upward profile in the middle of this unit	Increasing shale's trend line from top to bottom; approx. 6800-7500 between m.g/s.cc	Increasing shale's trend line from top to bottom; approx. 2900-3700 between m.g/s.cc	Wide range of amplitudes; max 126 and min -127	Porosity in shale approx. from 0.250 to 0.120
	2	1234.31 - 1339.51	Very thin and spiky profile with fining-upward trend	Increasing shale's trend line from top to bottom; approx. 7200-8200 between m.g/s.cc	Increasing shale's trend line from top to bottom; approx. 3400-3900 between m.g/s.cc	Various amplitudes; approx. between from -75 to 126	Same as unit1
	3	1339.51 - 1482.66	Spiky log with bell-shaped profile	Increasing shale's trend line from top to bottom; approx. 7500-8500 between m.g/s.cc	Increasing shale's trend line from top to bottom; approx. 3400-4400 between m.g/s.cc	Medium amplitudes; approx. between from -100 to 60	Decreasing porosity from top to bottom in shale from 0.250 to 0.070
	4	1482.66 - 1609.60	Spiky log with funnel-shaped profile	Decreasing shale's trend line from top to bottom; approx. 8500-7800 between m.g/s.cc	Decreasing shale's trend line from top to bottom; approx. 3900-4200 between m.g/s.cc	Medium to high amplitudes; approx. between from -60 to 90	Porosity in shale approx. from 0.100 to 0.200

Table 4.16 Summary table of net clean sand-to-shale and net clean sand-to-gross for well NTM-C01

Unit	Interval (mTVSS)		Gross	Shale	Dirty Sand	Shaly Sand	Clean Sand	Clean Sand/Shale	Clean Sand/Gross
	Top	Base							
1	2059.86	2290.22	230.36	159.21	21.58	36.44	13.12	0.08	0.06
2	2290.22	2493.61	203.39	148.36	14.65	31.65	8.61	0.06	0.04
3	2493.61	2685.18	191.57	135.27	9.34	27.04	15.64	0.12	0.08
4.1	2685.18	2910.31	225.13	119.03	10.87	51.04	15.64	0.13	0.07
4.2	2910.31	3108.39	198.08	116.42	14.41	32.08	22.95	0.20	0.12
TOTAL			1048.53	678.29	70.85	178.25	75.96	0.11	0.07

Table 4.17 Summary table of net clean sand-to-shale and net clean sand-to-gross for well WTN-B01

Unit	Interval (mTVSS)		Gross	Shale	Dirty Sand	Shaly Sand	Clean Sand	Clean Sand/Shale	Clean Sand/Gross
	Top	Base							
1	1374.80	1594.84	220.04	128.23	19.81	34.12	37.88	0.30	0.17
2	1594.84	1704.41	109.57	78.10	7.84	12.46	11.18	0.14	0.10
3	1704.41	1796.39	91.98	57.82	9.23	20.13	4.80	0.08	0.05
4.1	1796.39	1979.70	183.31	137.51	9.11	24.29	12.27	0.09	0.07
4.2	1979.70	2344.77	365.07	253.24	11.04	22.74	73.34	0.29	0.20
TOTAL			969.97	654.90	57.03	113.74	139.47	0.21	0.14

Table 4.18 Summary table of net clean sand-to-shale and net clean sand-to-gross for well NOH-A01

Unit	Interval (mTVSS)		Gross	Shale	Dirty Sand	Shaly Sand	Clean Sand	Clean Sand/Shale	Clean Sand/Gross
	Top	Base							
1	891.93	1007.86	115.93	52.76	9.51	31.91	21.75	0.41	0.19
2	1007.86	1096.89	89.03	34.93	10.60	28.29	15.21	0.44	0.17
3	1096.89	1229.98	133.09	57.17	14.36	30.25	31.31	0.55	0.24
4	1229.98	1329.57	99.59	58.07	13.16	24.05	4.31	0.07	0.04
TOTAL			437.64	202.93	47.63	114.50	72.58	0.36	0.17

Table 4.19 Summary table of net clean sand-to-shale and net clean sand-to-gross for well NOH-A02

Unit	Interval (mTVSS)		Gross	Shale	Dirty Sand	Shaly Sand	Clean Sand	Clean Sand/Shale	Clean Sand/Gross
	Top	Base							
1	1099.48	1234.31	134.83	85.04	14.90	17.92	16.98	0.20	0.13
2	1234.31	1339.51	105.20	56.29	10.64	18.92	19.37	0.34	0.18
3	1339.51	1482.66	143.15	64.21	15.71	32.96	30.28	0.47	0.21
4	1482.66	1609.60	126.94	95.04	11.78	15.62	2.75	0.03	0.02
TOTAL			510.12	300.58	53.03	85.42	69.38	0.23	0.14

profiles interbedded (Figures 4.14a, 4.15a, 4.16a and 4.17a). The shale trend lines, displayed on the cross-plots for acoustic (P-wave), and shear (S-wave) impedance data against depth, show a clear break between the unit 1 and 2 for the WTN-A01, NOH-A01 and NOH-A02 (Figures 4.15b-c, 4.16b-c and 4.17b-c). The ratios of net clean sand-to-gross and net clean sand-to-shale for these wells are generally greater than 0.13. However, a break of the shale trend line is not seen clearly in NTM-C01 (Figures 4.14b-c). The net clean sand-to-gross and net clean sand-to-shale ratios are less than 0.1. The Runsum seismic characteristics are displayed with various amplitudes (Figures 4.14d, 4.15d, 4.16d and 4.17d). The shale porosity for all wells is higher in the unit 1 than in the other units (Figures 4.14e, 4.15e, 4.16e and 4.17e).

Unit 2

This unit is underneath of the unit 1. The gamma ray data presents very thin and spiky log characteristics with fining-upward profile in WTN-B01, NOH-A01 and NOH-A02 (Figures 4.15a, 4.16a and 4.17a), but shows coarsening-upward trend in NTM-C01 (Figures 4.14a). The shale trend lines, displayed on the cross-plots for the acoustic (P-wave) and shear (S-wave) impedance data against depth, show a clear break between unit 2 and 3 for WTN-A01, NOH-A01 and NOH-A02 (Figures 4.15b-c, 4.16b-c and 4.17b-c). The ratios of net clean sand-to-gross and net clean sand-to-shale for these wells are generally between 0.14 to 0.34 and 0.10 to 0.18 respectively. However, the shale trend line in this unit is not been observed clearly in NTM-C01 (Figures 4.14b-c). The net clean sand-to-gross and net clean sand-to-shale are less than 0.1. The Runsum seismic characteristic is displayed on one loop in WTN-B01 and various amplitudes in the others (Figures 4.14d, 4.15d, 4.16d and 4.17d). The shale porosity for all wells is high in NOH-A01 and NOH-A02, but low in the NTM-C01 and WTN-B01 (Figures 4.14e, 4.15e, 4.16e and 4.17e).

Unit 3

This unit is underneath of the unit 2. The gamma ray data shows very thin and spiky log characteristics with fining-upward profiles in the well NOH-A01 and NOH-A02. (Figures 4.16a and 4.17a), but it is not clearly seen in the others (Figures 4.14a and 4.15a). The shale trend lines, displayed on the cross-plots for the acoustic (P-wave) and shear (S-wave) impedance data against depth, show a clear break between

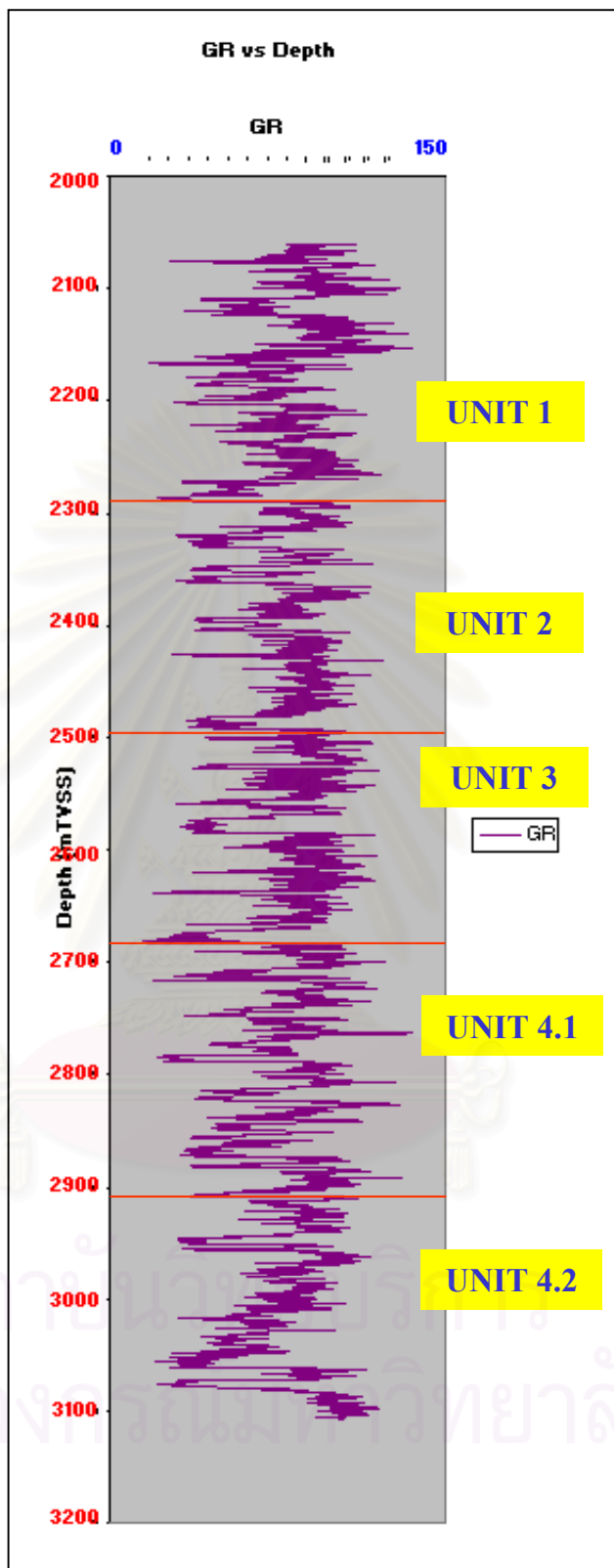


Figure 4.14a A cross-plot between gamma ray and depth showing the lithological units in well NTM-C01

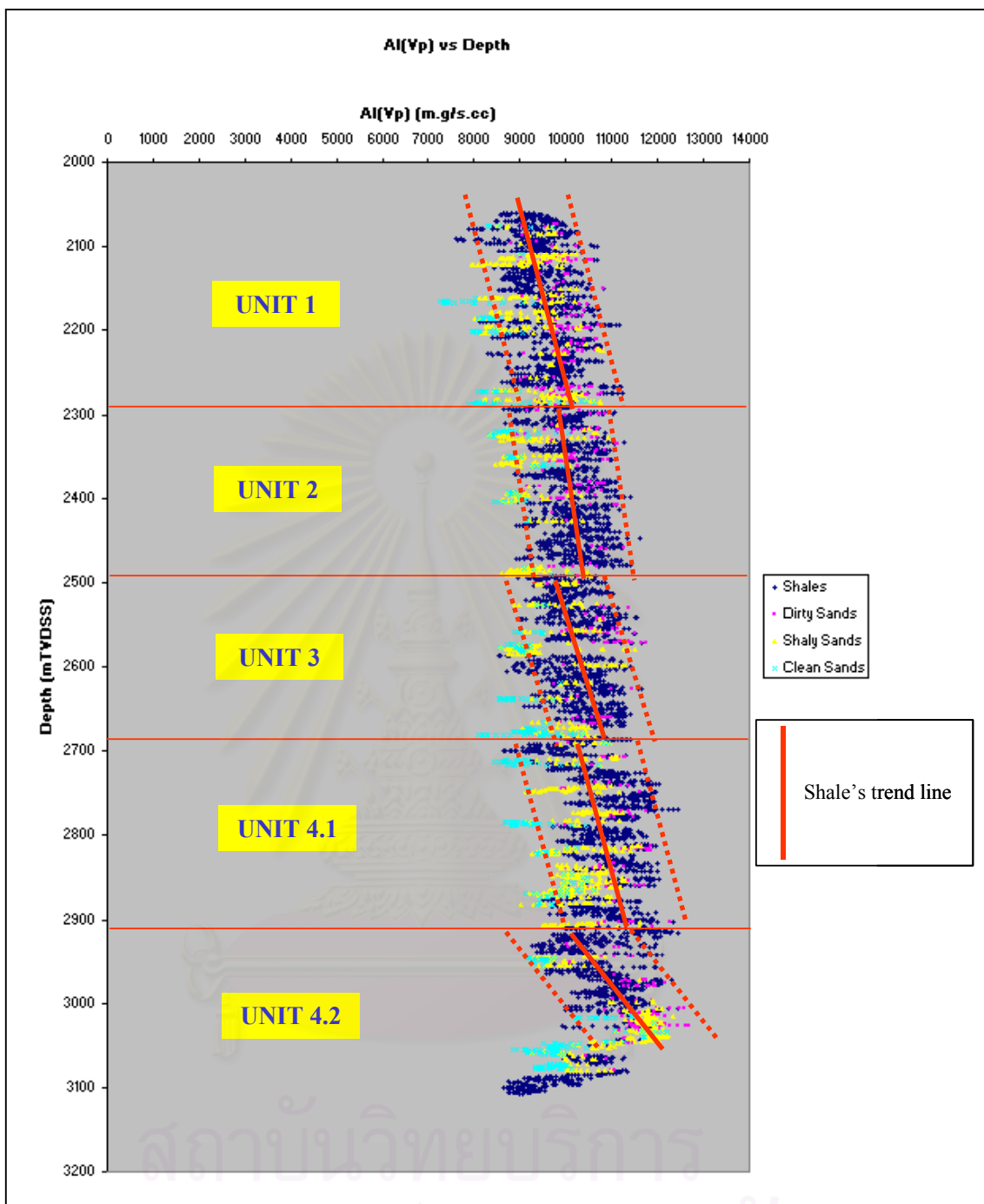


Figure 4.14b A cross-plot between acoustic (P-wave) impedance (AI(Vp)) and depth showing the lithological units in well NTM-C01

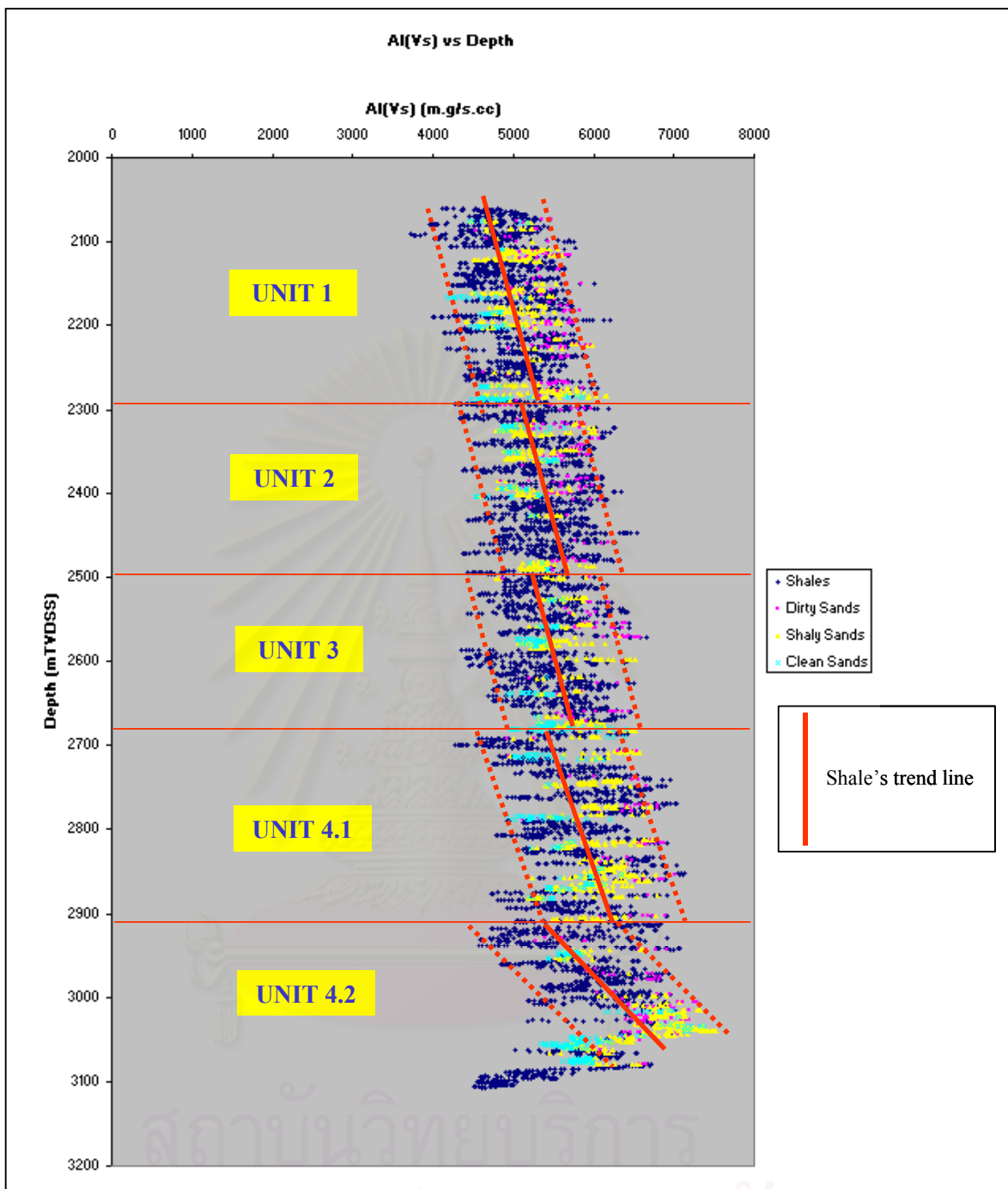


Figure 4.14c A cross-plot between shear (S-wave) impedance (AI(Vs)) and depth showing the lithological units in well NTM-C01

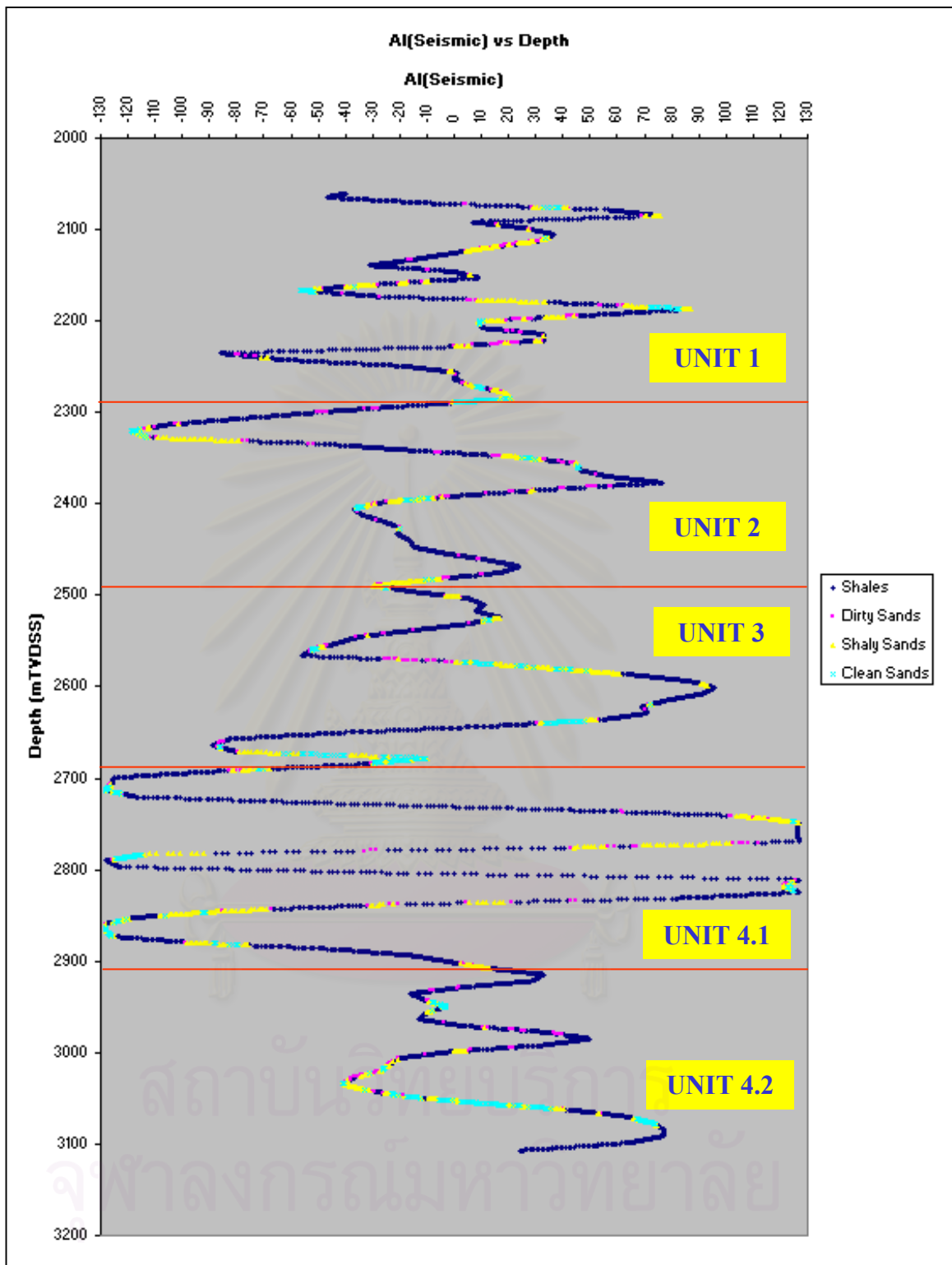


Figure 4.14d A cross-plot between Runsum seismic (AI(Seismic)) and depth showing the lithological units in well NTM-C01

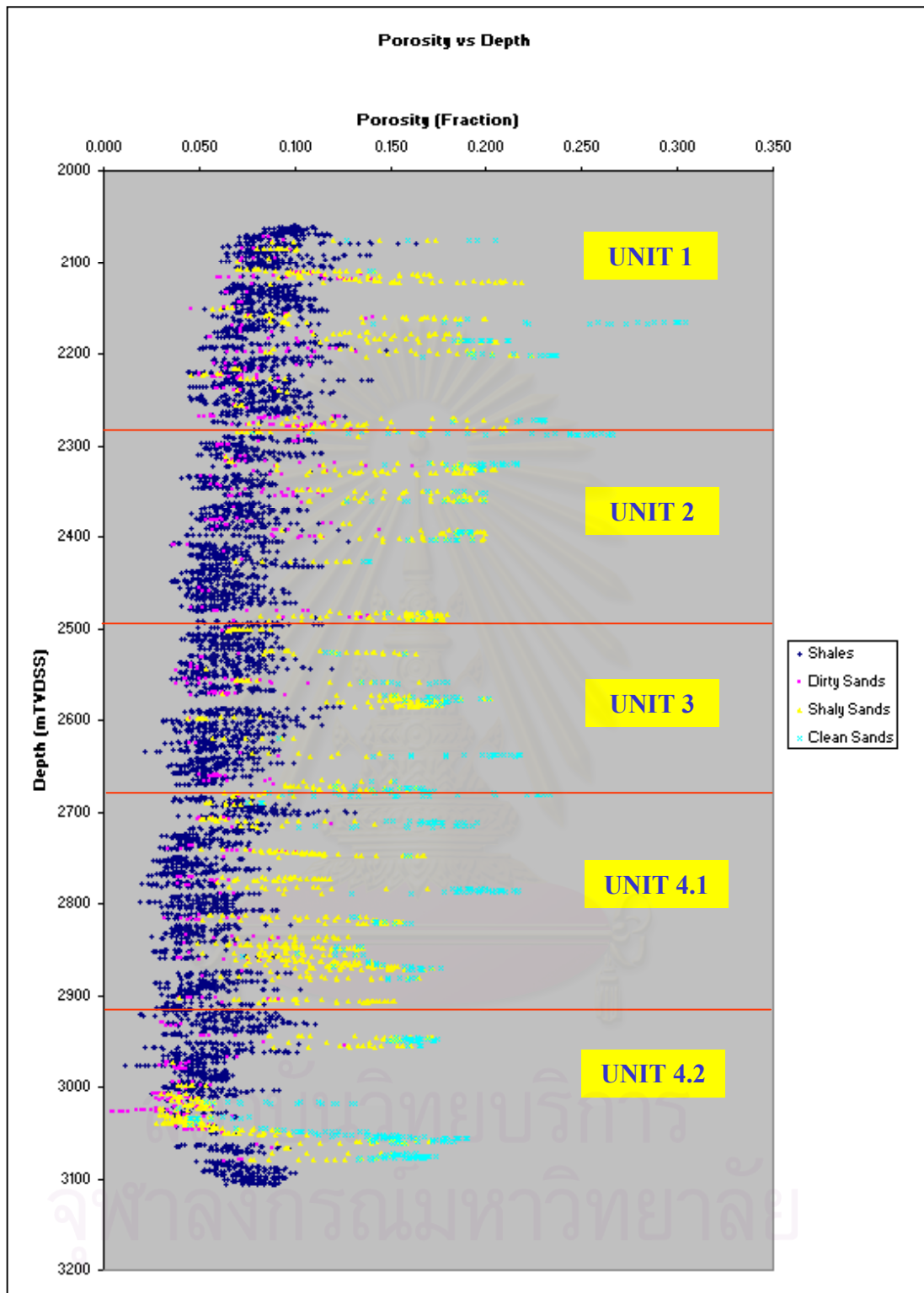


Figure 4.14e A cross-plot between porosity and depth showing the lithological units in well NTM-C01

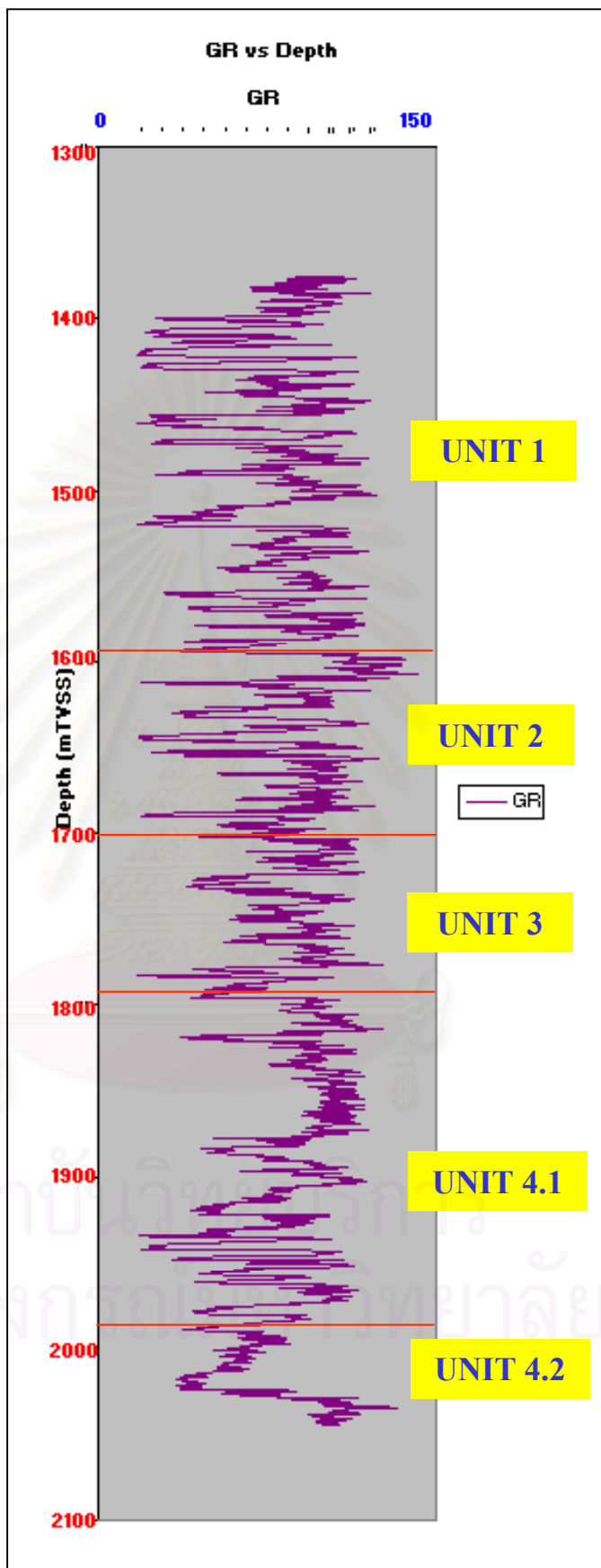


Figure 4.15a A cross-plot between gamma ray and depth showing the lithological units in well WTN-B01

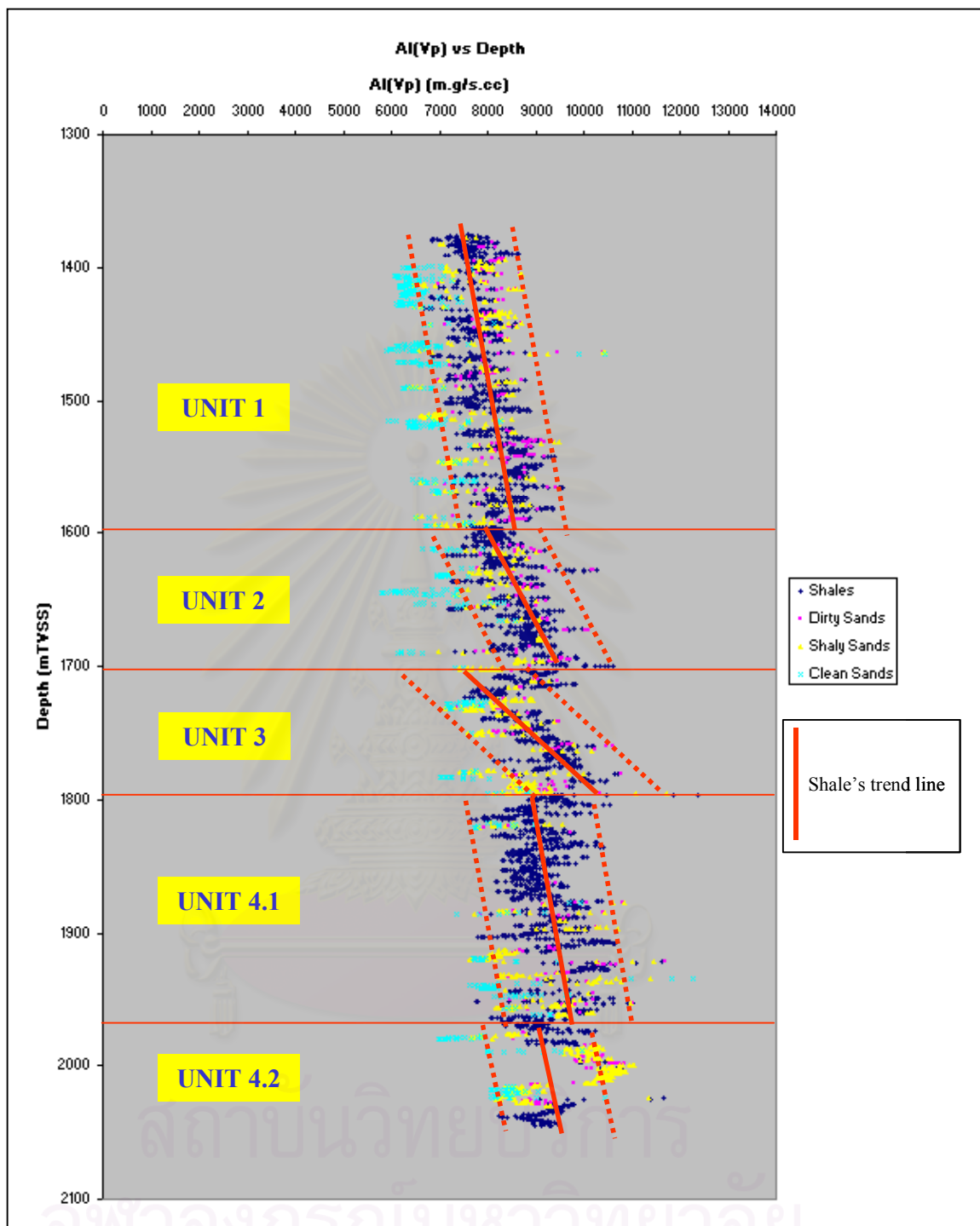


Figure 4.15b A cross-plot between acoustic (P-wave) impedance (AI(Vp)) and depth showing the lithological units in well WTN-B01

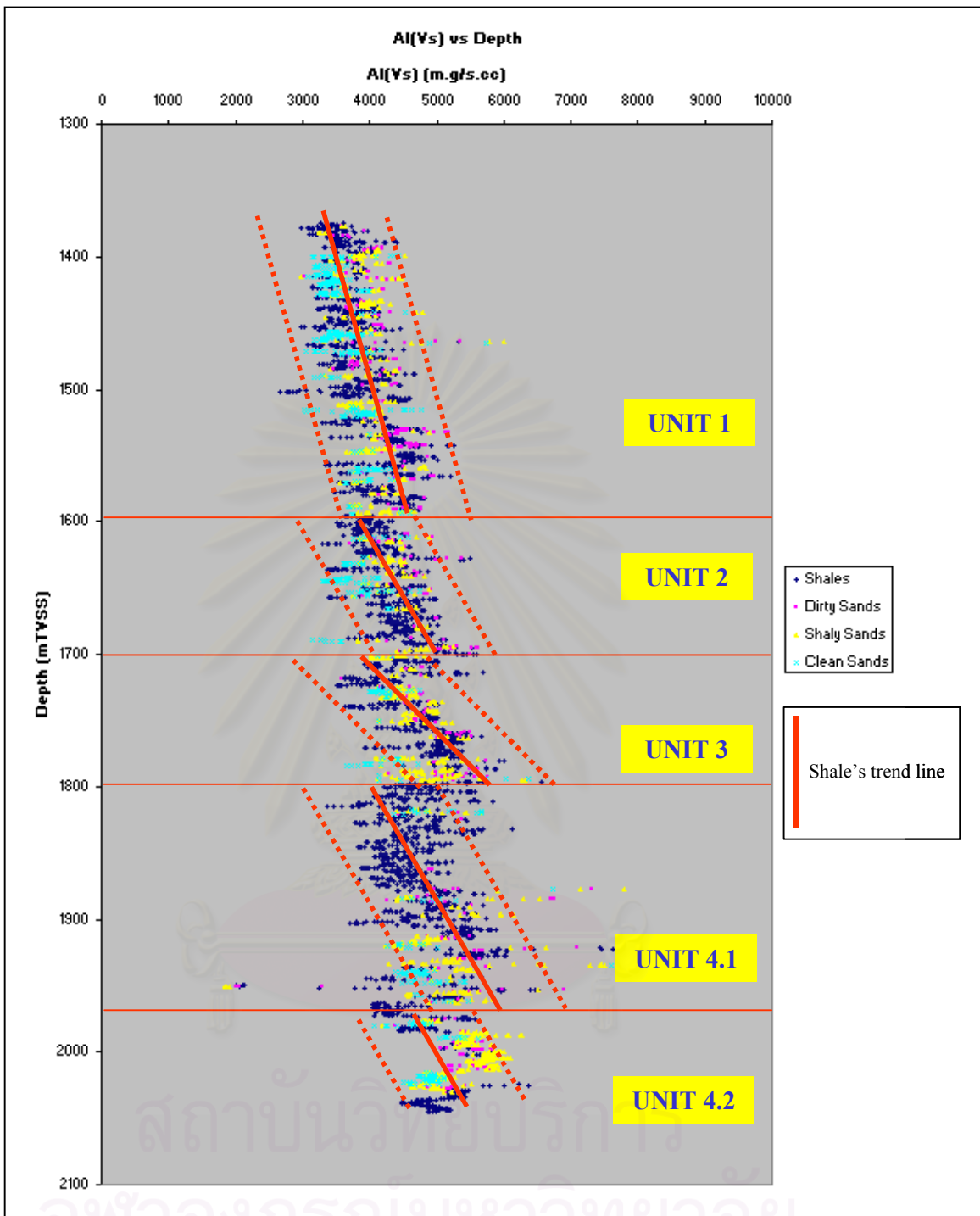


Figure 4.15c A cross-plot between shear (S-wave) impedance (AI(Vs)) and depth showing the lithological units in well WTM-B01

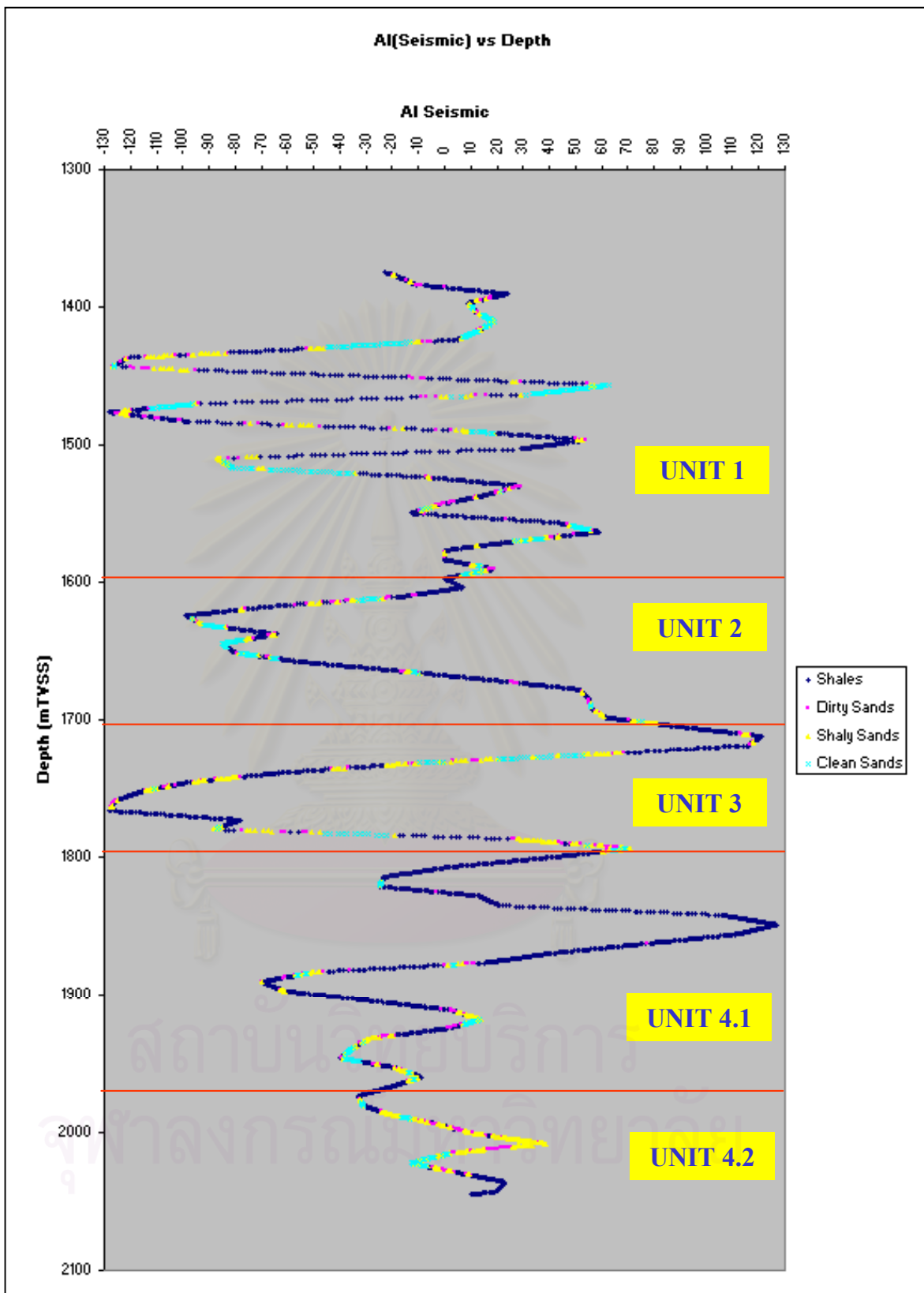


Figure 4.15d A cross-plot between Runsum seismic (AI(Seismic)) and depth showing the lithological units in well WTN-B01

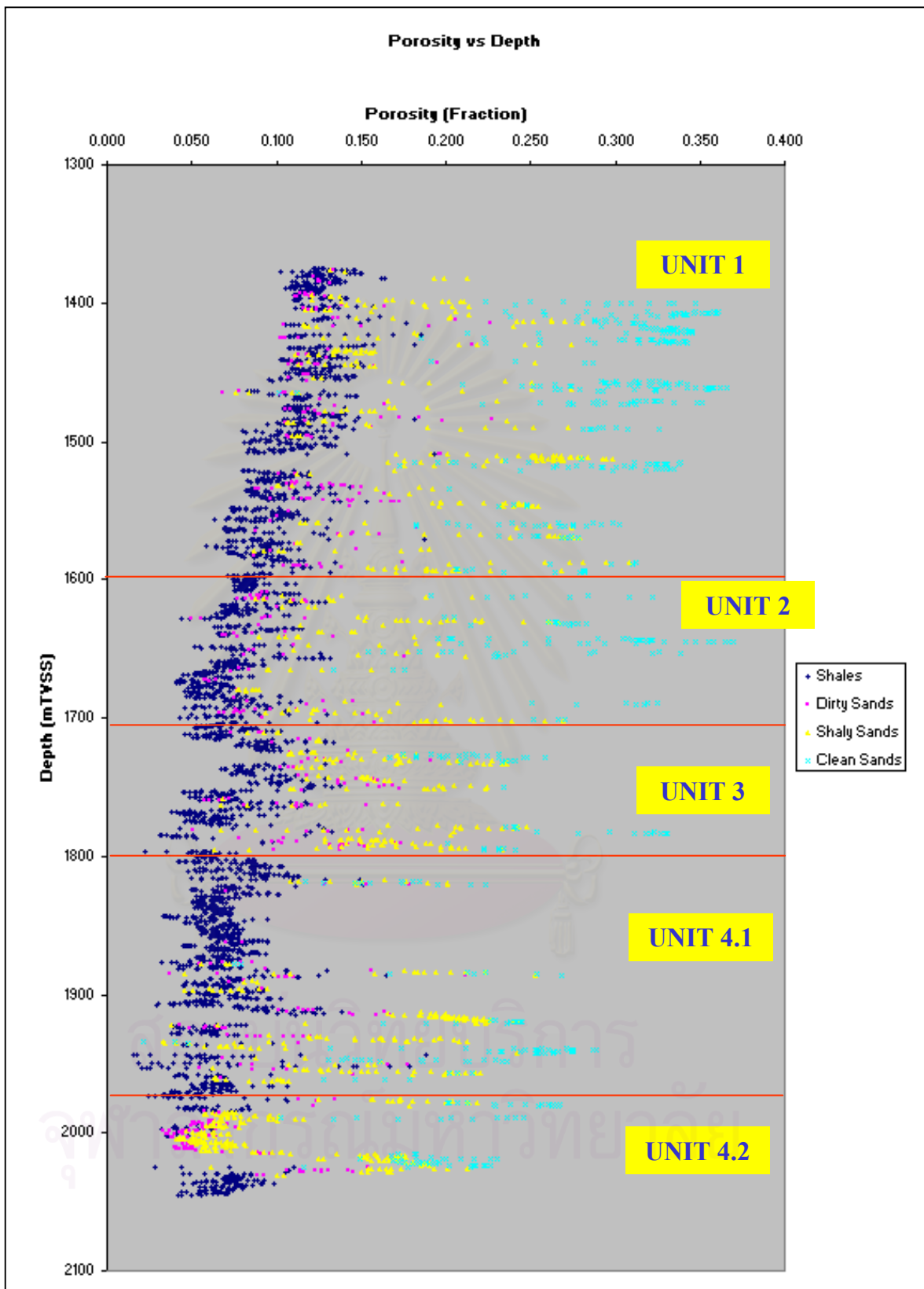


Figure 4.15e A cross-plot between porosity and depth showing the lithological units in well WTN-B01

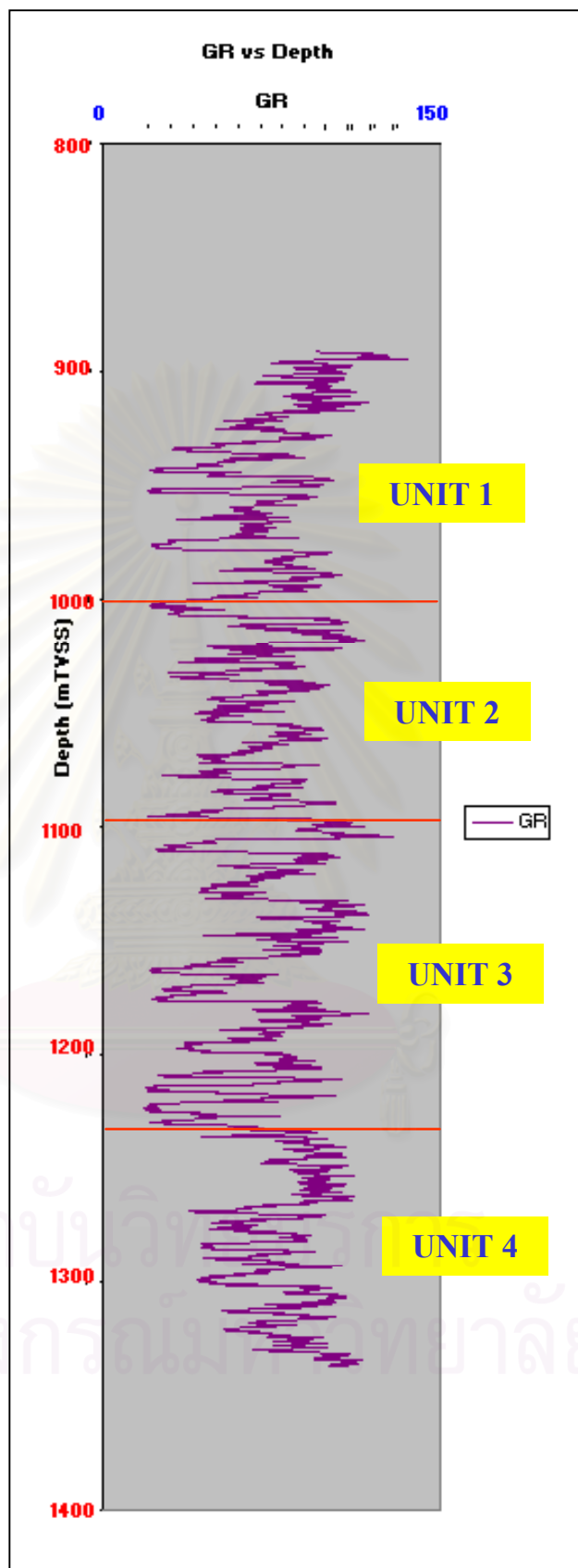


Figure 4.16a A cross-plot between gamma ray and depth showing the lithological units in well NOH-A01

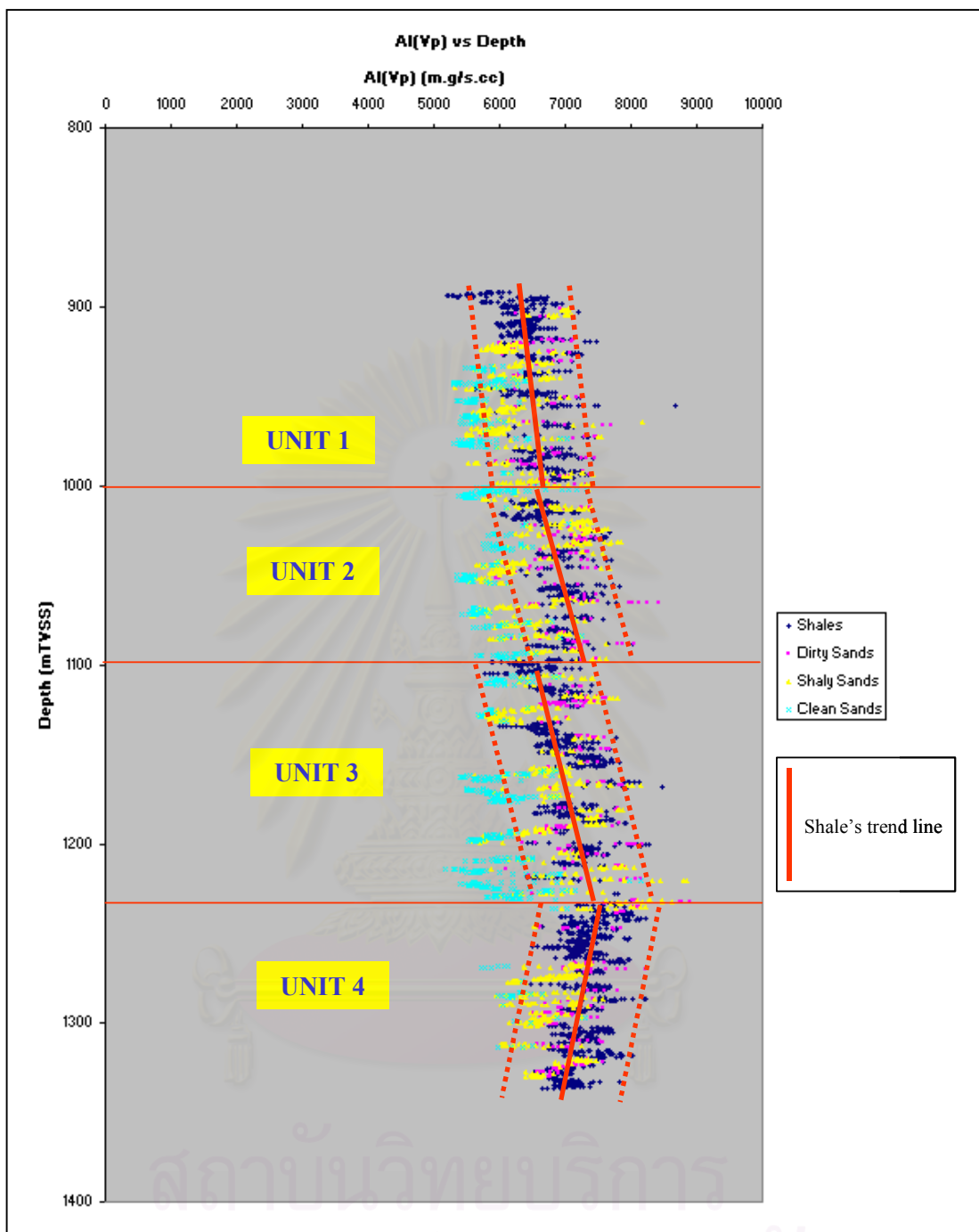


Figure 4.16b A cross-plot between acoustic (P-wave) impedance (AI(Vp)) and depth showing the lithological units in well NOH-A01

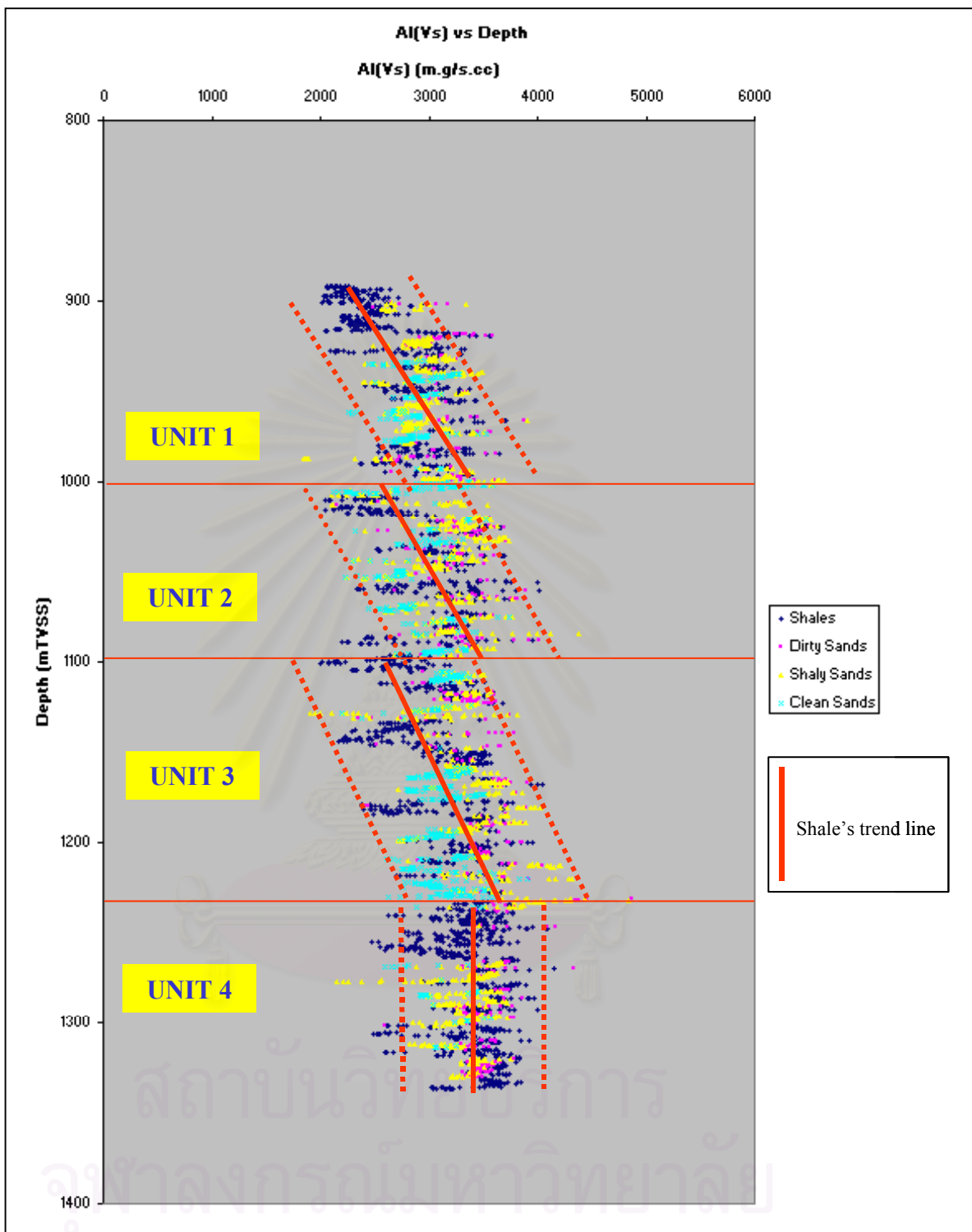


Figure 4.16c A cross-plot between shear (S-wave) impedance (AI(Vs)) and depth showing the lithological units in well NOH-A01

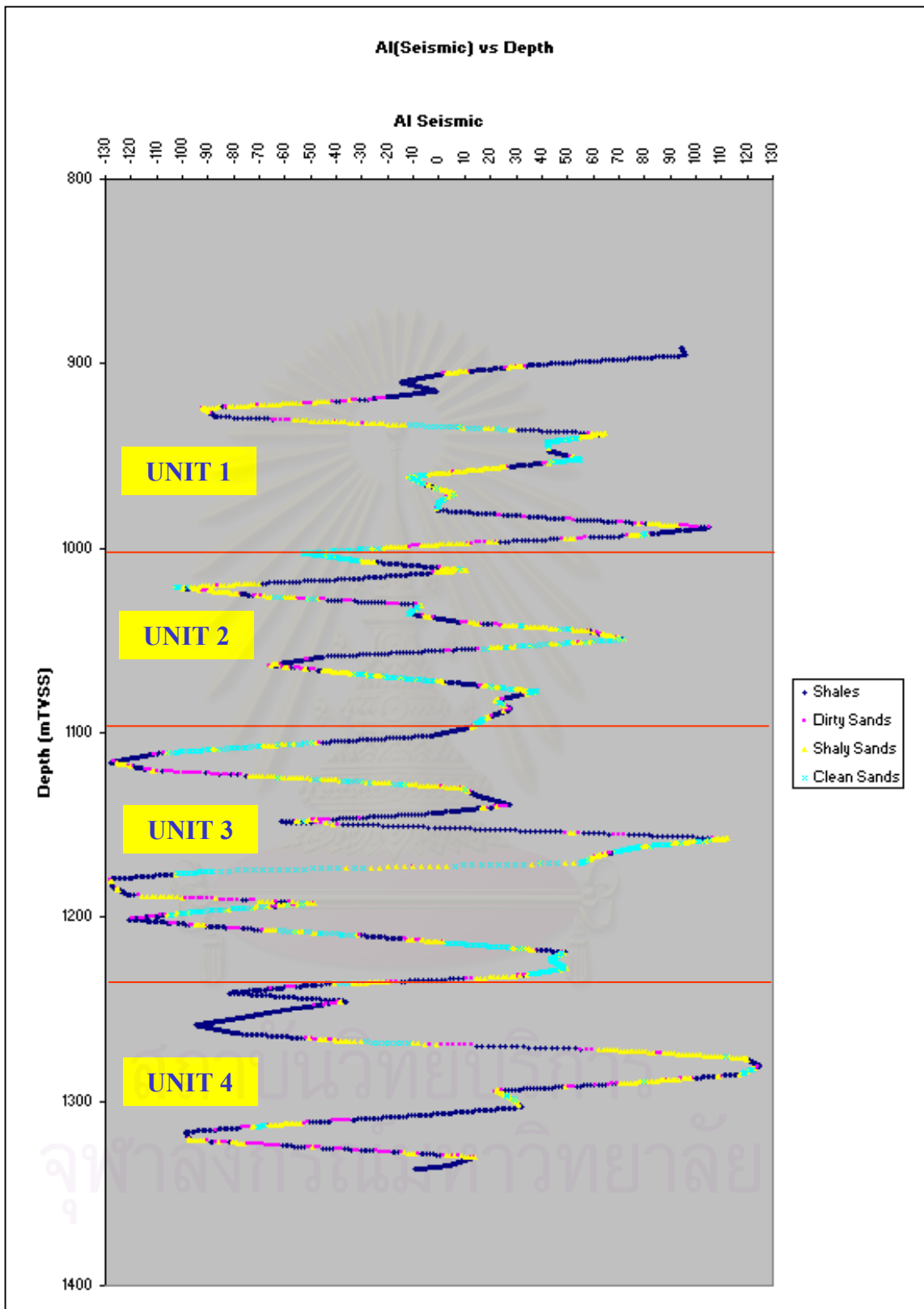


Figure 4.16d A cross-plot between Runsum seismic (AI(Seismic)) and depth showing the lithological units in well NOH-A01

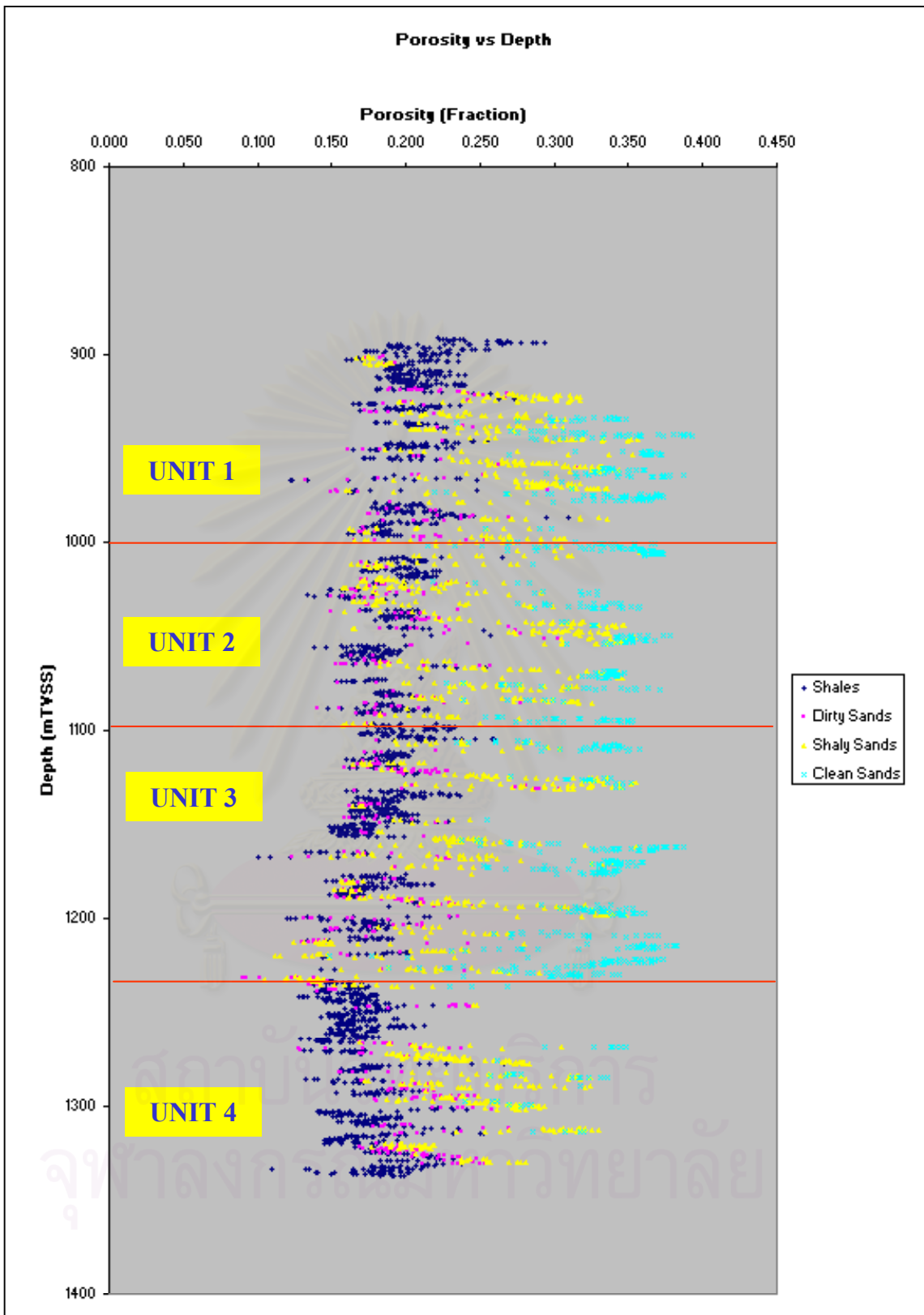


Figure 4.16e A cross-plot between porosity and depth showing the lithological units in well NOH-A01

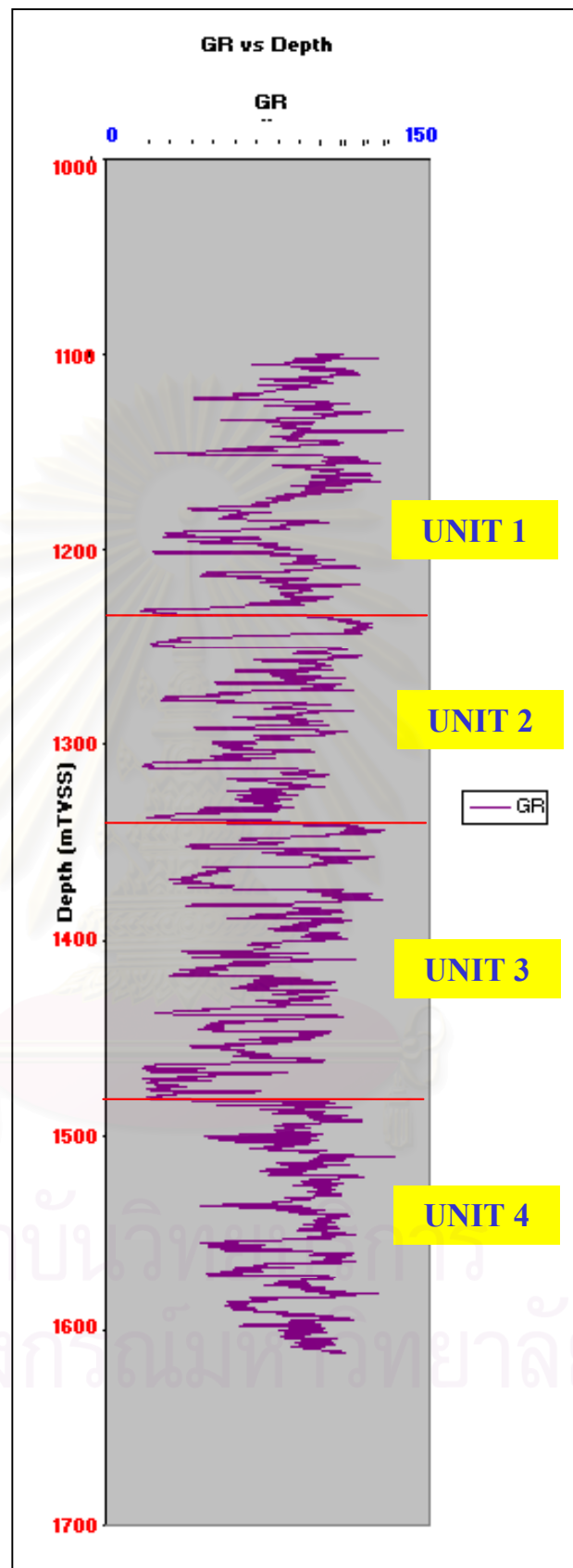


Figure 4.17a A cross-plot between gamma ray and depth showing the lithological units in well NOH-A02

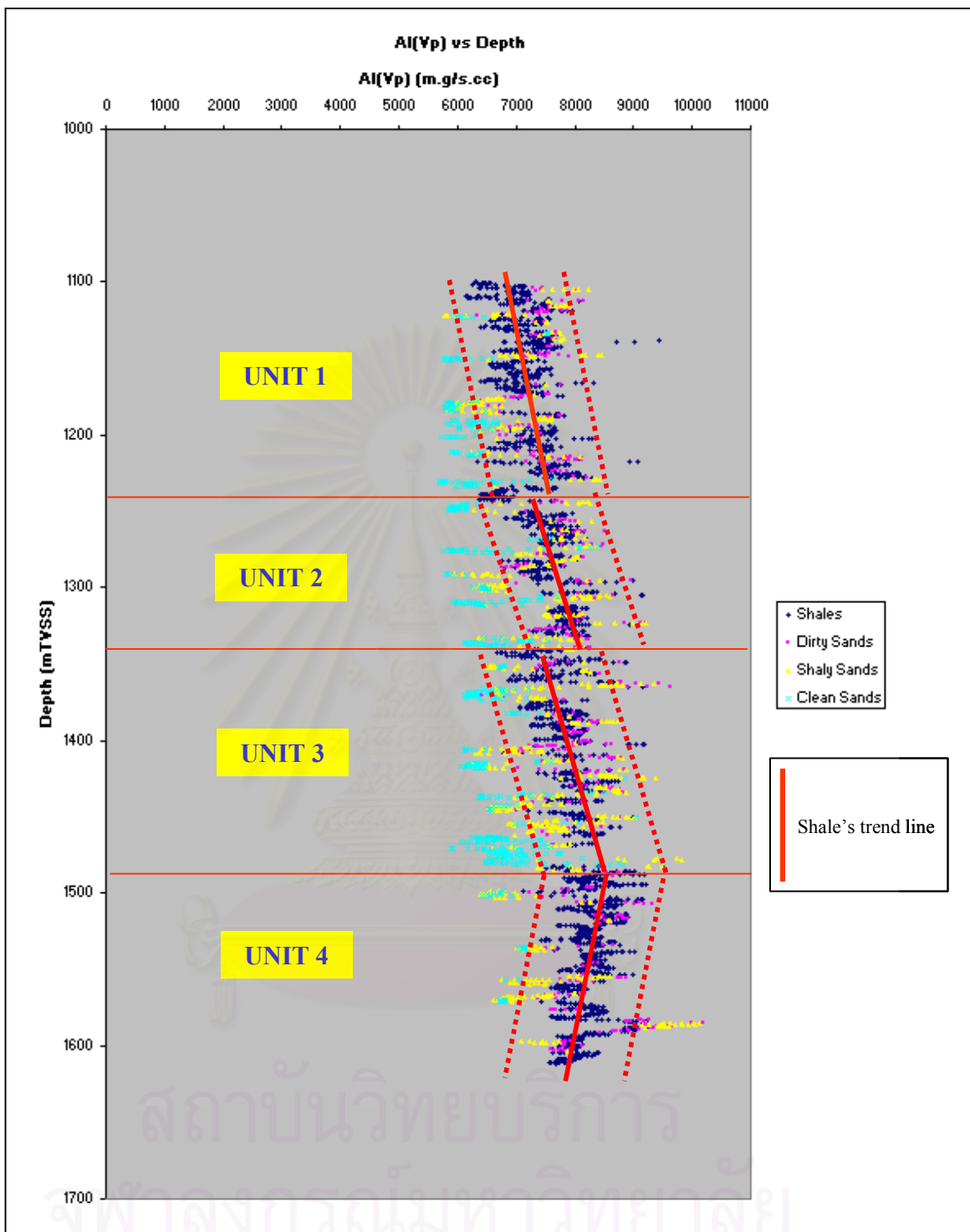


Figure 4.17b A cross-plot between acoustic (P-wave) impedance (AI(Vp)) and depth showing the lithological units in well NOH-A02

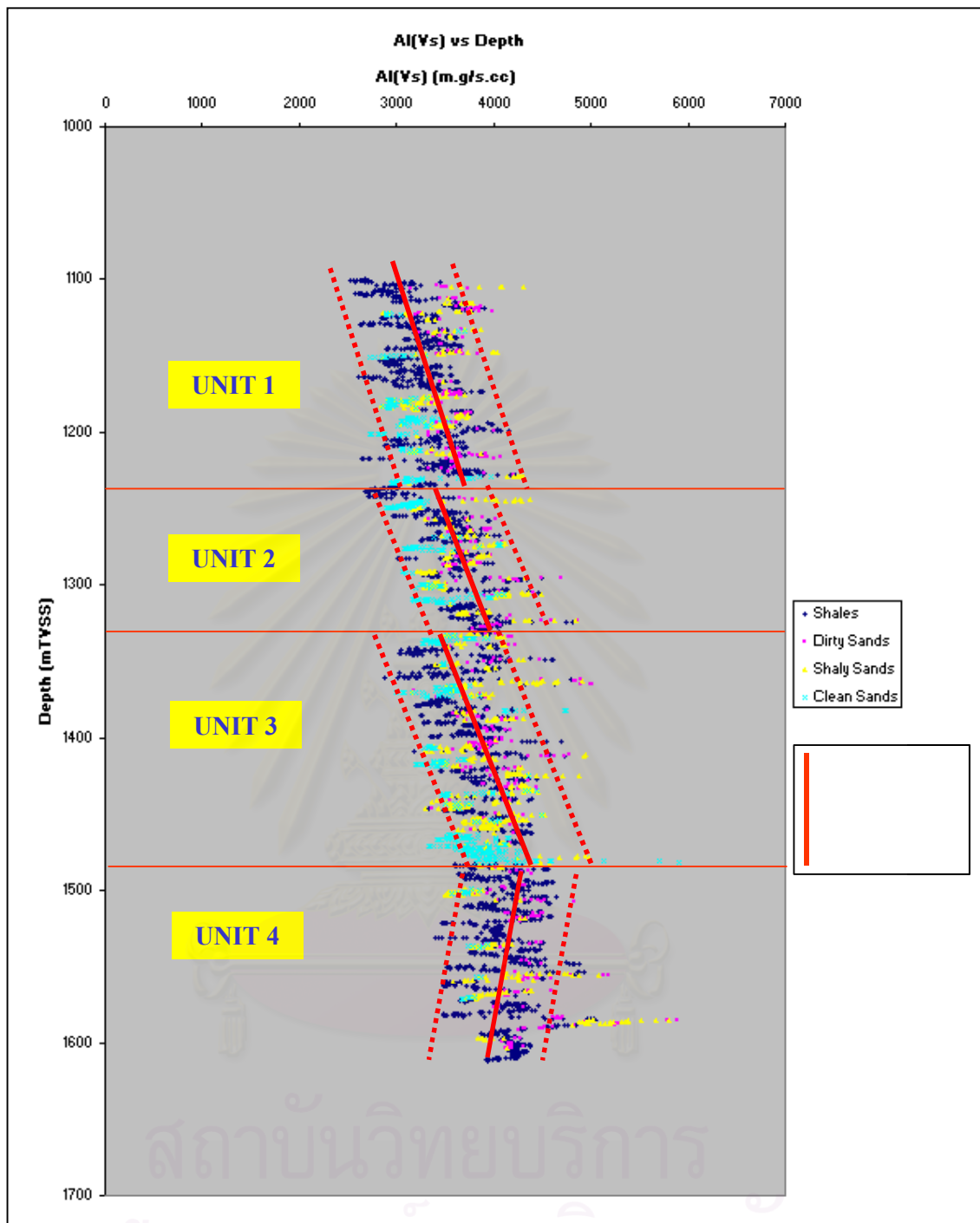


Figure 4.17c A cross-plot between shear (S-wave) impedance (AI(Vs)) and depth showing the lithological units in well NOH-A02

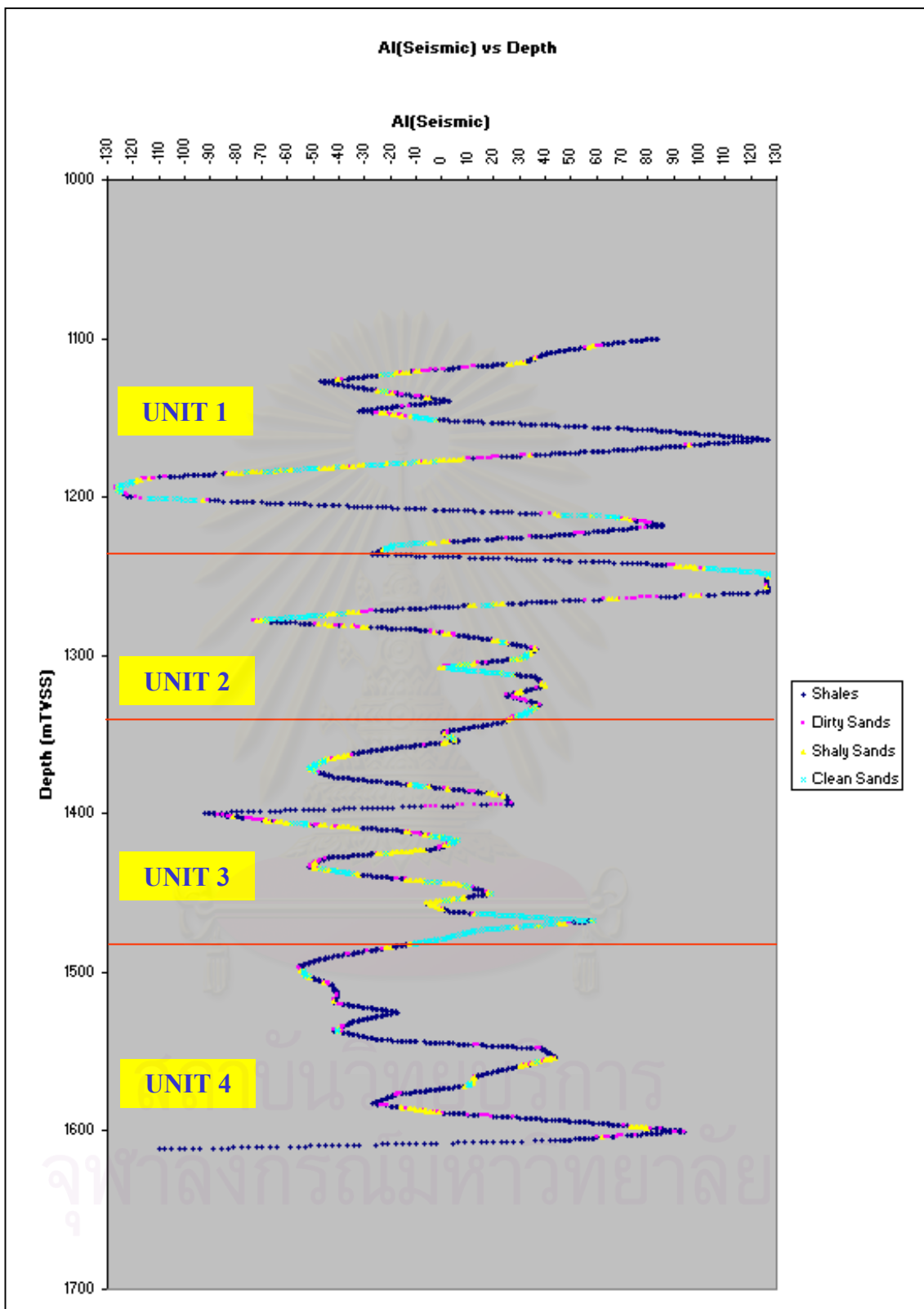


Figure 4.17d A cross-plot between Runsum seismic (AI(Seismic)) and depth showing the lithological units in well NOH-A01

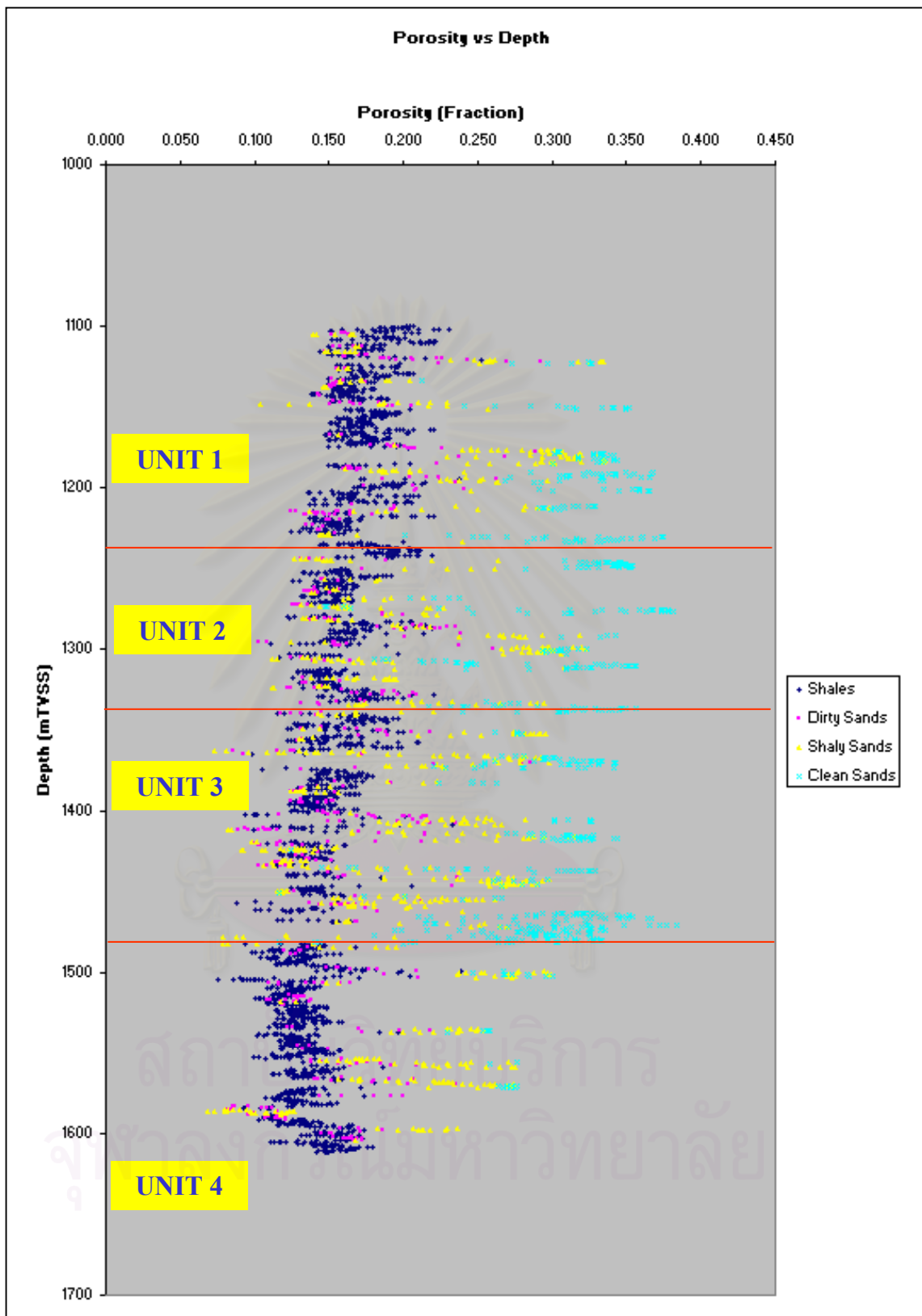


Figure 4.17e A cross-plot between porosity and depth showing the lithological units in well NOH-A02

unit 3 and 4 for all wells (Figures 4.14b-c, 4.15b-c, 4.16b-c and 4.17b-c). The ratios of net clean sand-to-gross and net clean sand-to-shale are high in NOH-A01 and NOH-A02 between 0.47 to 0.55 and 0.21 to 0.24 respectively. However, they show the lower net clean sand-to-gross and net clean sand-to-shale ratios between 0.08 to 0.12 and 0.05 to 0.08 respectively in the others. The Runsum seismic characteristics are displayed with various amplitudes (Figures 4.14d, 4.15d, 4.16d and 4.17d). The shale porosity for all wells shows the same as the unit 2 (Figures 4.14e, 4.15e, 4.16e and 4.17e).

Unit 4

This unit is observed only in the well NOH-A01 and NOH-A02. The gamma ray of these wells shows coarsening-upward profiles (Figures 4.16a and 4.17a). The shale trend lines, displayed on the cross-plots for the acoustic (P-wave) and shear (S-wave) impedance data against depth, show a clear break for these wells (Figures 4.16b-c and 4.17b-c). The ratios of net clean sand-to-gross and net clean sand-to-shale are less than 0.07. The Runsum seismic characteristics are displayed with various amplitudes (Figures 4.16d and 4.17d). The shale porosity for these wells shows decreasing trend from top to bottom (Figures 4.16e and 4.17e).

Unit 4.1

This unit is found only in the well NTM-C01 and WTN-B01. The gamma ray of these wells shows fining-upward profiles. (Figures 4.14a and 4.15a. The shale trend lines, displayed on the cross-plots for the acoustic (P-wave) and shear (S-wave) impedance data against depth, show a clear break for these wells (Figures 4.14b-c and 4.15b-c). The ratios of net clean sand-to-gross and net clean sand-to-shale are higher than 0.07. The Runsum seismic characteristics are displayed with various amplitudes (Figures 4.14d and 4.15d). The shale porosity for all wells shows the same as the unit 3 (Figures 4.14e and 4.15e).

Unit 4.2

This unit is found only in the well NTM-C01 and WTN-B01. The gamma ray of these wells shows fining-upward profiles. (Figures 4.14a and 4.15a. The shale trend lines, displayed on the cross-plots for the acoustic (P-wave) and shear (S-wave) impedance data against depth, show a clear break for these wells (Figures 4.14b-c and

4.15b-c). The ratios of net clean sand-to-gross and net clean sand-to-shale are between 0.20 to 0.29 and 0.12 to 0.20 respectively. The Runsum seismic characteristics are displayed with various amplitudes (Figures 4.14d and 4.15d). The shale porosity for these wells shows decreasing trend from top to bottom (Figures 4.14e and 4.15e).



สถาบันวิทยบริการ
จุฬาลงกรณ์มหาวิทยาลัย

CHAPTER V

DISCUSSION

5.1 Discussion of the Quantitative Results

- *Comparison between the quality of logging data acquired in the 1980s and 2001*

The logging data acquired in the 1980s have been limited in use due to poor data quality caused by poor borehole condition. The data acquired in 2001 is of higher quality because these recent wells are drilled quickly, allowing logging before deterioration in borehole occurred. The type of drilling mud is another reason for the poor borehole condition. In the 1980s, water based drilling mud was used, which caused swelling in shale units. Due to the change to oil based drilling mud, shale swelling has been much reduced. The comparison between data acquired in the 1980s and 2001, represented by wells PTO-A03 and WTN-B01, can be observed in the Figures 4.3g and 4.3i respectively.

- *Relationship between the acoustic and shear impedances, Runsum seismic and porosity*

The results from the quantitative study, focusing on the Pratu Tao Formation in the Greater Pratu Tao area, show that there are linear relationships between the well impedance data, either from P- or S- waves, and porosity of all study wells. Moreover, the clear separation between clean sand and shale has been observed for each well. This implies that the porosity can be predicted from the acoustic impedances data, which are derived from both P- and S- wave sonic logging data. It suggests that further amplitude variation with offset study would be worthwhile.

However, a linear relationship between Runsum seismic data, porosity and acoustic impedance data, either from P- or S- waves, cannot be observed. This implies that the porosity, related to lithological variation, cannot be predicted from Runsum seismic data in this study. There are some limitations of using Runsum seismic data. Firstly, the Runsum data is a low grade seismic inversion. The completed seismic inversion needs to remove the earth's wavelet, which can be estimated from the well acoustic impedance and band limited component. This has not been done in the

current Runsum processing. Moreover, the time-depth conversion could cause an effect.

- *Limitation of data caused by the reservoir geometry and thickness*

From this study, there are some limitations due to the physical properties of reservoir. In the Pratu Tao Formation, the thickness of sand reservoirs is normally lower than 10 m. Their geometry cannot be observed from Runsum seismic because they are below seismic resolution. However, there are two previous studies using Runsum seismic data that recognised the reservoir geometry and distribution. The first study, carried out by Lechner et al. (1994) of Shell UK Expro, aimed to enhance the interpretability of lithological packages for better understanding of the Nelson turbidite reservoir (Figure 5.1). The extremely good recognition and resolution of the lithological boundaries on impedance displays was observed on formation boundaries between more uniform packages on the Nelson survey. The reservoir comprises thick discrete sand packages and the frequency of lithology changes fall nicely within the observed seismic bandwidth. The second study was carried out by Muggli (2000) over the Barik reservoir in the Greater Makarem area, Oman. The purpose of the study was to predict reservoir properties using generation of a Runsum bandlimited impedance cube. The impedance cube was a result of integration of the seismic data. The result presented a trend of sand distribution and was useful for reducing the uncertainty of the Barik reservoir property prediction. Figure 5.2 shows a map of Barik net sand thickness in the Greater Makarem area. However, this measure equates roughly to the whole Barik reservoir interval when the reservoir thickness is in the order of 40-50 m.

This proves that the Runsum seismic data works successfully with the reservoirs near tuning thickness. If the reservoirs are substantially thicker than the tuning thickness, then the Runsum data can cause interpretive difficulties. Therefore, the Runsum seismic data of the Greater Pratu Tao survey cannot be applied as a practical tool for quantitative interpretation due to limitation of data caused by reservoir geometry and thickness. However, they can be used as the supporting information for horizon interpretation together with the normal seismic data interpretation.

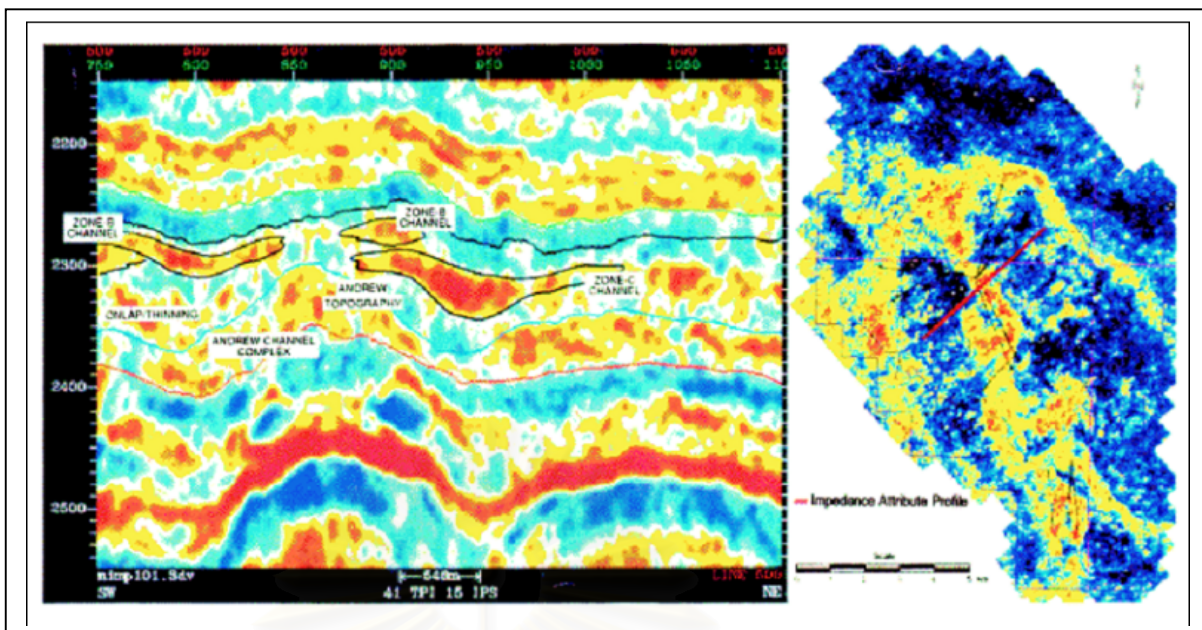


Figure 5.1 Impedance (Runsum) attribute of Nelson survey displays reservoir architecture (Eocene channels) (Lechner et al.,1994).

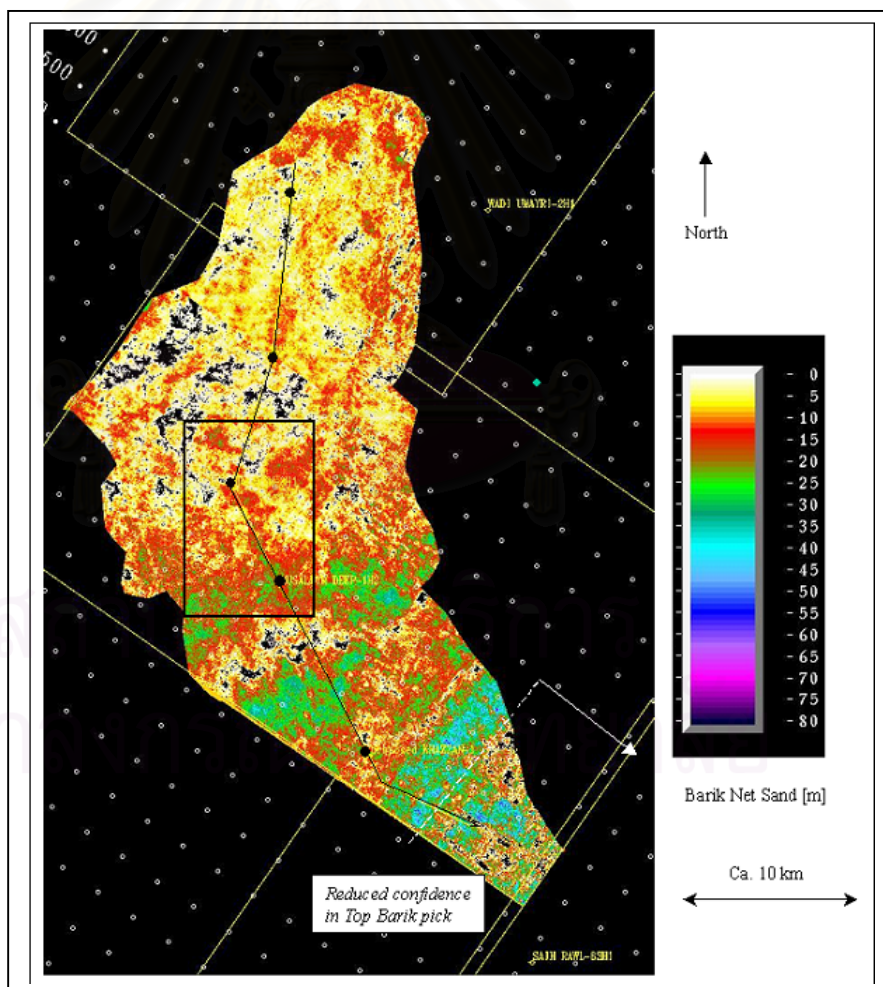


Figure 5.2 Map showing Barik net sand thickness in the Greater Makarem area, Oman (Muggli, 2000).

- *Limitation of data caused by processing without earth's wavelet removal*

As mentioned in the Chapter III, the Runsum data are generated by the low grade seismic inversion without removing the earth's wavelet. This would indicate that the Greater Pratu Tao 3D survey could be used for lithology prediction and reservoir distribution by applied completed inversion method. There is a study of acoustic impedance interpretation for sand distribution adjacent to a rift boundary fault by Ronghe and Surarat (2002). This reports on a seismic inverse modelling study from an oil-producing field in the Suphan Buri Basin, Thailand. Seismic data made the inverse modelling study feasible, with the objective of imaging distributions of lithology and/or hydrocarbons, depending on the data-specific discriminatory capability of acoustic impedance. This is a good example for a complete seismic inversion process. The study was applied the constrained sparse spike inversion, which resulted in good comparisons between the derived impedance traces and band-filtered wire-line impedance. The outcomes from the study were the seismic-derived impedance maps imaging sand distribution, and the evaluation of the tectonic influences on sedimentation in the Suphan Buri Basin (Figure 5.3). For the filtering process, it was applied to the acoustic (P-wave) and shear (S-wave) impedance data. This process aimed to adjust the frequency resolution of the logging data by using the Runsum seismic bandwidth. However, this filtered data cannot be related to the Runsum seismic data. The log reflectivity normally contains all frequencies from lowest up to highest measurable with the logging tools, whereas seismic data is missing both high and low frequencies. This limits resolution achievable from filtering process.

5.2 Discussion of the Qualitative Results

- *New approach to recognise lithological units*

The impedance data reflects the physical properties of the rocks. A break of shale impedance trend line is a good indicator to recognise the lithological unit. There are at least 4 cycles of deposition observed from this method. The units 1, 2, and 3 exist in the Nong Tum, Wat Taen and Nong Ooh area. The unit 4 is only found in Nong Ooh area, which is equivalent to units 4.1 and 4.2 in the Nong Tum and Wat Taen (Figure 5.4). This study can provide the supporting information for future detailed study in the sequence stratigraphy and can be a guidance of reservoir development in the Pratu Tao Formation.

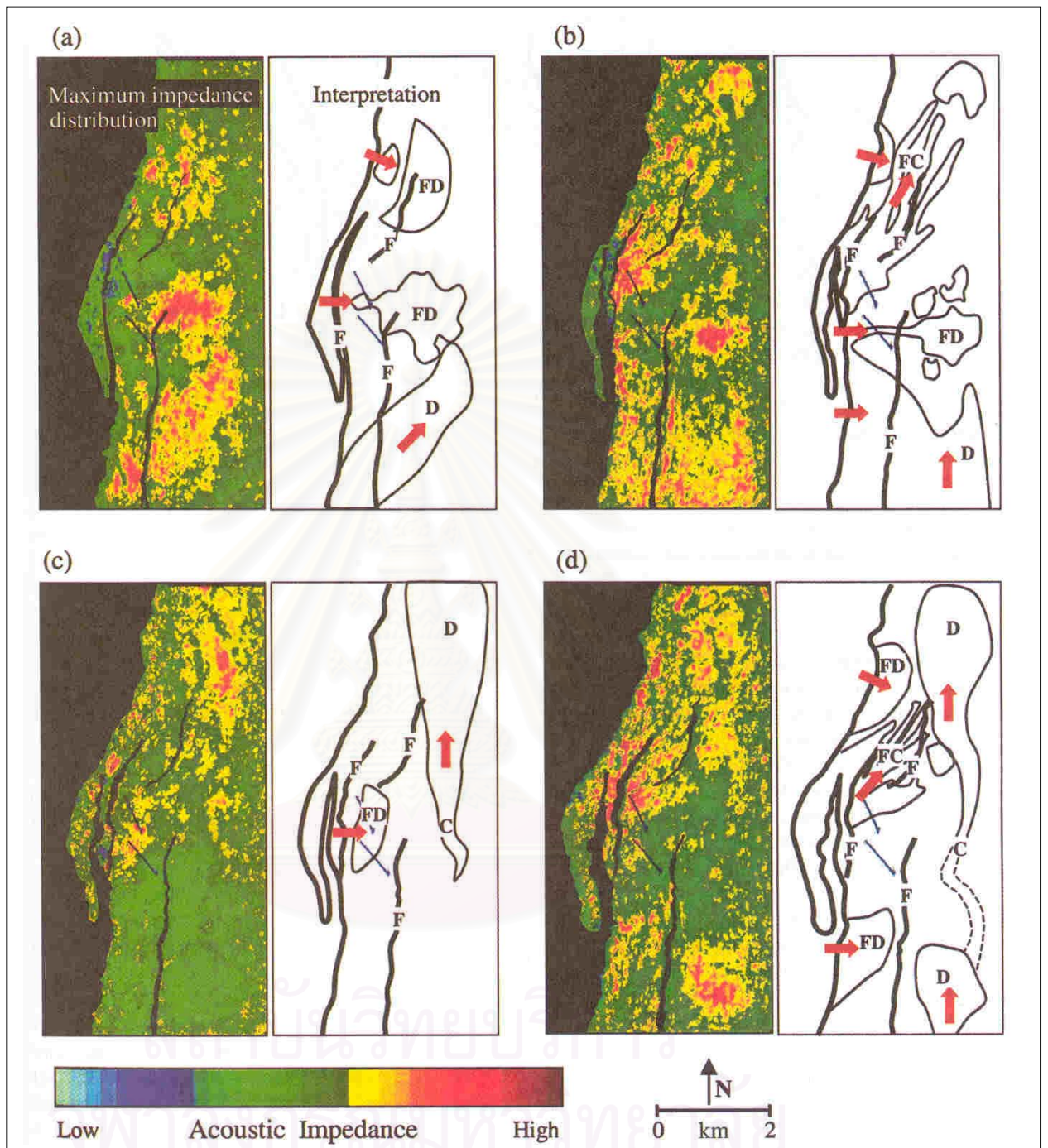


Figure 5.3 Impedance maps with line-drawing interpretations of sand distribution and the inferred directions of sediment transport in Suphan Buri Basin, Thailand (Ronghe and Surarat, 2002).

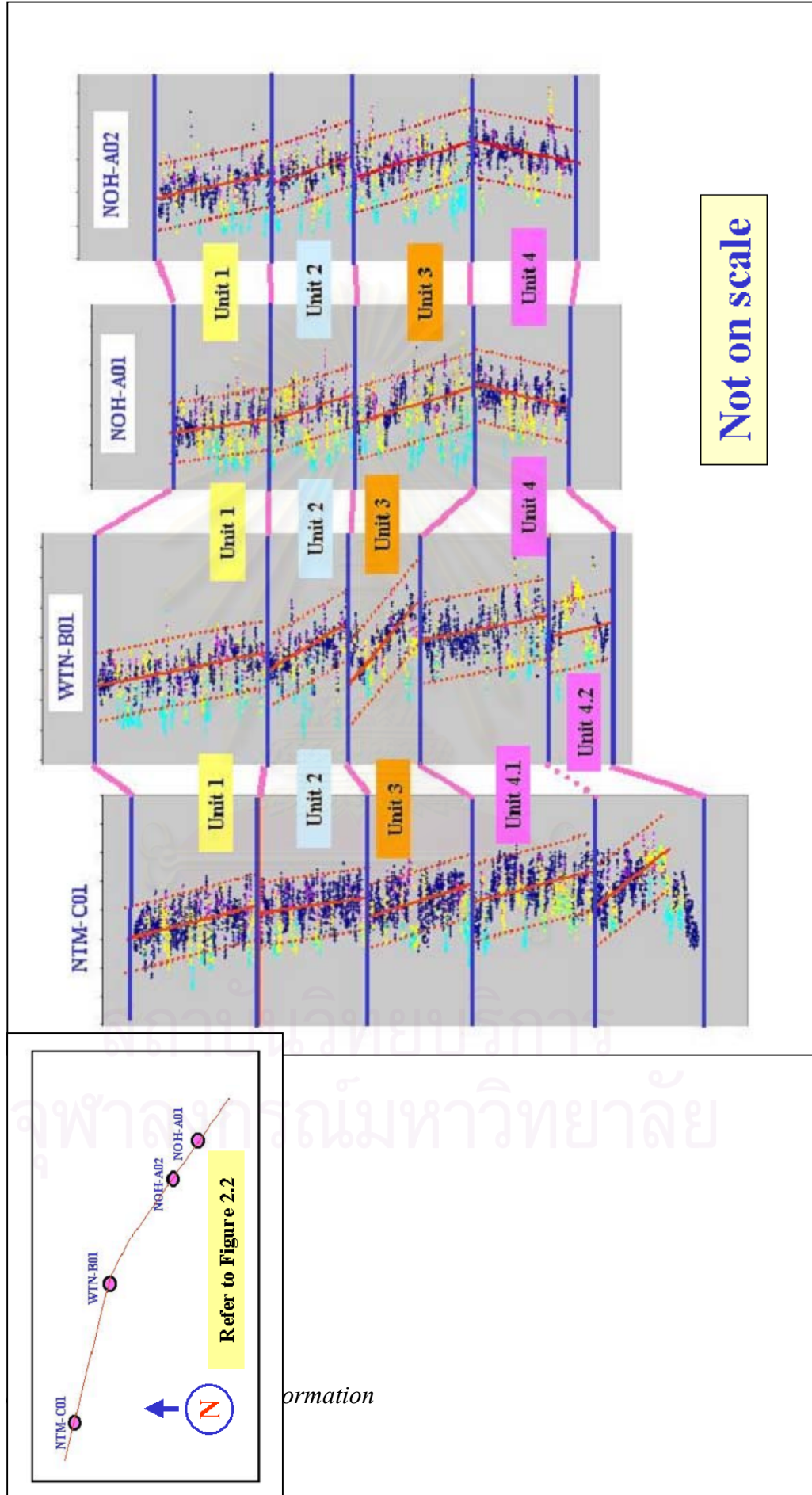


Figure 5.4 The schematic plots between acoustic impedance (P-wave) against depths for wells drilled in 2001 showing the new approach to recognise lithological units in the Pratu Tao Formation.

The results from the qualitative study in the Pratu Tao Formation are significant. Four distinct lithological units are recognised using a cross-plot of the acoustic (P-wave) and shear (S-wave) impedance data against depth. Due to the limited lateral extent and variable nature of the Pratu Tao Formation, it is difficult to use the gamma ray data for lithological recognition.

- *New possible top Chum Saeng Formation*

In well NTM-C01, it is observed from the plot between acoustic and shear impedances data against depth that the top Chum Saeng Formation might be picked deeper than reality. The possible top Chum Saeng Formation could be picked shallower at 3090 mTVDSS (Figure 5.5).

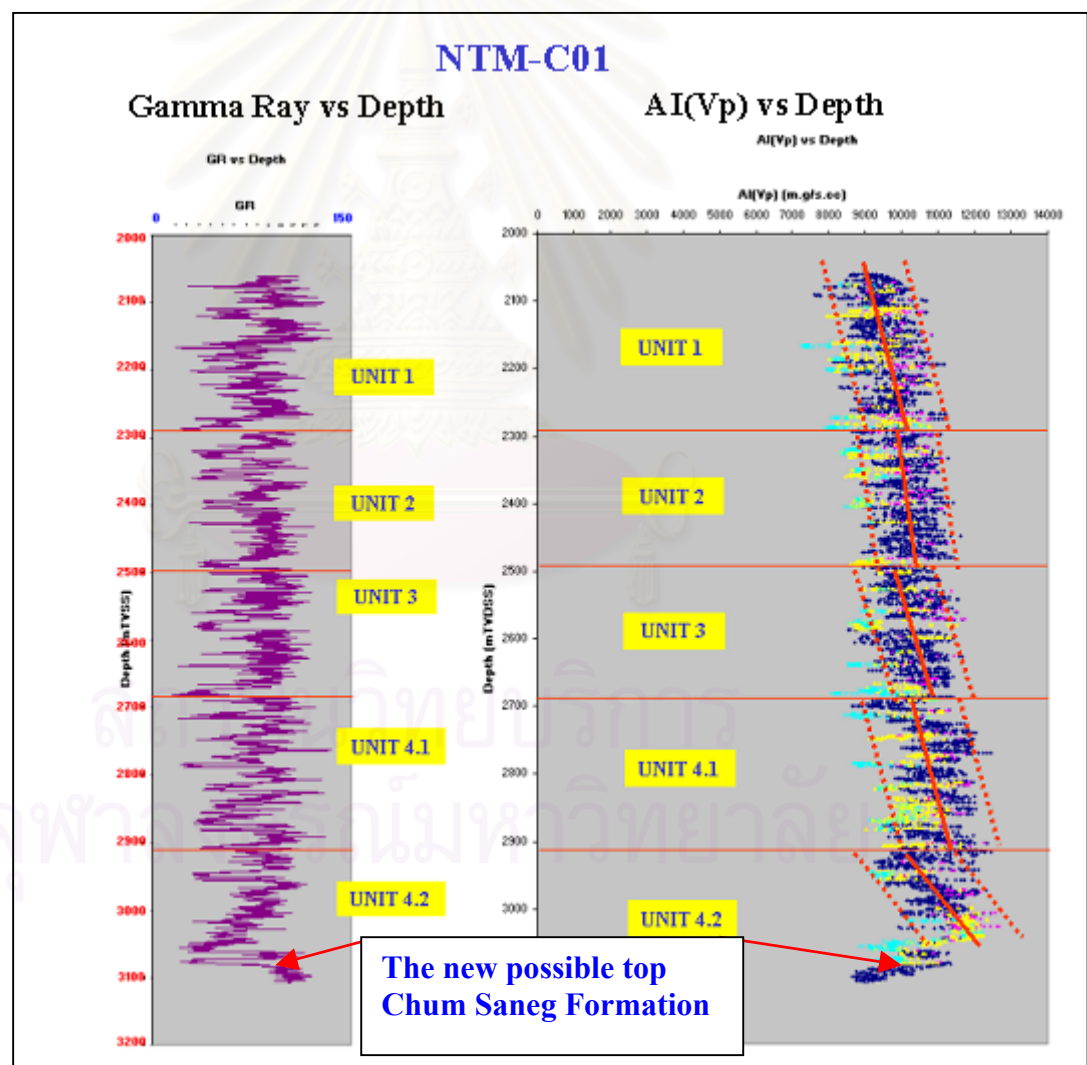


Figure 5.5 The plots of gamma ray data against depth and acoustic impedance against depth of well NTM-C01 showing the new possible top Chum Saeng Formation.

▪ *Depositional environment of Pratu Tao Formation*

Fluvial deposits can be observed from plots of gamma ray data against depth. This can be confirmed by the character of common idealised log curve shapes interpreted as facies succession (Walker, 1992). This is also related to the number of sand and shale dataset from the plots of acoustic and shear impedances data against depth (Figure 5.6). The net clean sand-to-gross of units 1, 2 and 3 are higher than units 4, 4.1 and 4.2 for all areas. This implies that the units 1, 2 and 3 could be deposited as the stacked channels, whereas the others could be deposited in the floodplain or overbank due to the lower net clean sand -to-gross presented. Moreover, the clean sand porosity trends in the units 1, 2 and 3 are also higher than the others. Most of clean sand porosity data in these units present value greater than 0.2, which indicate the good reservoir quality (Thai Shell, 2002).

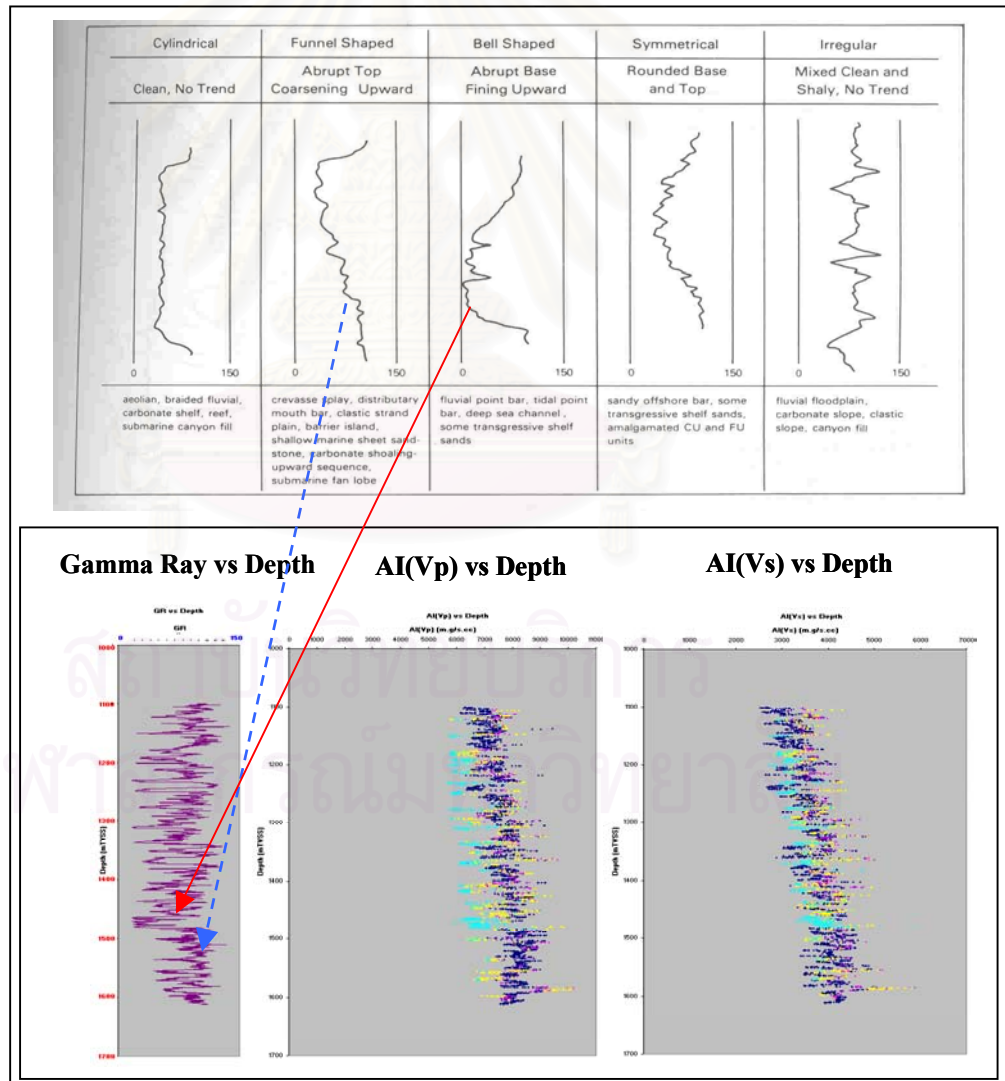


Figure 5.6 The plots showing the conformable pattern with the common idealised log curve shapes interpreted as facies succession (Walker, 1992).

REFERENCES

- Asquith, G. B. and Gibson, C. R. 1983. Basic Well Log Analysis for Geologist. Oklahoma: The American Association of Petroleum Geologists.
- Bal, A. A. and others 1988. Hydrocarbon Habitat of The Phitsanulok Basin (S1 Concession, Onshore Thailand). Bangkok: Thai Shell Exploration and Production. (Unpublished Manuscript)
- Brown, A. R. 1996. AAPG Memoir 42: Interpretation of Three-Dimensional Seismic Data. 4th ed. Oklahoma: American Association of Petroleum Geologists.
- Chaodumrong, P. and Chaimanee, Y. 2002. Tertiary Sedimentary Basins in Thailand. Proceedings of The Symposium on Geology of Thailand. pp.161-162. August 26-31, Bangkok, Thailand.
- Cordier, J. P. 1985. Velocities in Reflection Seismology. The Netherlands: D. Reidel Publishing Company.
- Davis, R. A., Jr. 1983. Depositional Systems. New Jersey: Prentice-Hall.
- Dobrin, M. B. and Savit, C. H. 1988. Introduction to Geophysical Prospecting. 4th ed. Singapore: McGraw-Hill.
- Emery, D. and Myers, K. J. 1996. Sequence Stratigraphy. Oxford: Blackwell Science.
- FM Consultants Limited. 1985. The Basement Rocks of the Phitsanulok Basin: the K/Ar and Argon-40/Argon-39 Evidence. Bangkok: Thai Shell Exploration and Production. (Unpublished Manuscript)
- Gadallah, M. R. 1994. Reservoir Seismology: Geophysics in Nontechnical Language. Oklahoma: PennWell.

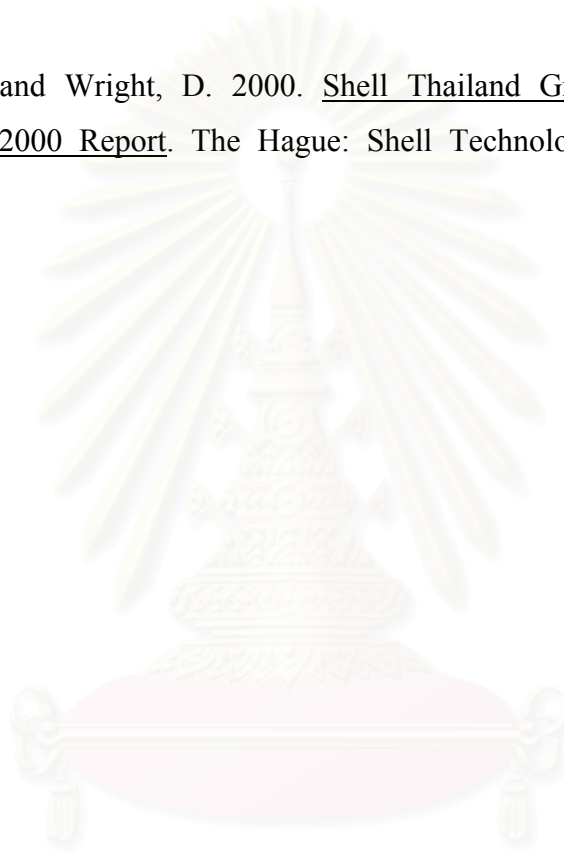
- Gardham, R. C. 2001. Prospectivity of Pratu Tao and Yom Formations, Greater Pratu Tao Area (Based on GPTO Seismic Reprocessing 2000). Bangkok: Thai Shell Exploration and Production. (Unpublished Manuscript)
- Isaaks, E. H. and Srivastava R. M. 1989. Applied Geostatistics. Oxford: Oxford University Press.
- Jensen, J. L., Corbett P. W. M., Lake, L.W. and Goggin D. J. 2000. Statistics for Petroleum Engineers and Geoscientist. 2nd ed. Amsterdam: Elsevier.
- Lechner, M. and others 1994. Enhancement of Seismic Definition in Nelson through Landmark “Impedance Conversion”. Aberdeen: Shell UK Expro. (Unpublished Manuscript)
- Leegte H. and others. 2003. Field Development Plan for the Greater Pratu Tao South Area. Bangkok: Thai Shell Exploration and Production. (Unpublished Manuscript)
- Lindseth, R. O. 1982. Digital Processing of Geophysical Data: A review. Alberta: Teknica Resource Development Ltd.
- Lowrie, W. 1997. Fundamentals of Geophysics. Cambridge: Cambridge University Press.
- Mäkel, G. and others. 1997. Sirikit Field Review 1996-1997. Bangkok: Thai Shell Exploration and Production. (Unpublished Manuscript)
- Meesook, A. and others. 2002. Mesozoic Rocks of Thailand: A summary. Proceedings of The Symposium on Geology of Thailand. pp.82-92. August 26-31, Bangkok, Thailand.
- Miall. A. M. 1996. The Geology of Fluvial Deposits: Sedimentary Facies, Basin Analysis, and Petroleum Geology. Italy: Springer-Verlag Berlin Heidelberg.

- Miall, A. M. 1997. The Geology of Stratigraphic Sequences. Germany: Springer-Verlag Berlin Heidelberg.
- Miall, A. D. 1990. Principle of Sedimentary Basin Analysis. United States of America: Springer-Verlag New York Inc.
- Muggli, R. 2000. Barik Reservoir Distribution Prediction in the Greater Makarem Area. Muscat: Petroleum Development Oman. (Unpublished Manuscript)
- Reading, H. G. 1978. Sedimentary Environment and Facies. London: Backwell Scientific.
- Rider, M. H. 1996. The Geological Interpretation of Well Logs. 2nd ed. Malta: Whittles Publishing
- Ronghe, S. and Surarat K. 2002. Acoustic Impedance Interpretation for Sand Distribution Adjacent to A Rift Boundary Fault, Suphan Buri Basin, Thailand. Bulletin of the American Association of Petroleum Geologists. V.86:1753-1771.
- Selley, R.C. 1982. An Introduction to Sedimentology. London: Academic press INC. (London) LTD.
- Selley, R.C. 1996. Ancient Sedimentary Environments. Published by Chapman & Hall:5-6.
- Sheriff, R. E. 1978. A First Course in Geophysical Exploration and Interpretation. Boston: International Human Resources Development Corporation.
- Sheriff, R. E. 1997. Encyclopedic Dictionary of Exploration Geophysics. Tulsa: Society of Exploration Geophysicists.
- Taner, M. T. 1992. Attributes Revised. [Online] Available from: http://www.rocksolidimages.com/pdf/attrib_revisited.htm [2001,November 6].

Walker, R. G. and James, N. P. 1997. Facies Models: Response to Sea Level Change. Quebec: Geological Association of Canada Publications.

Wang, F. P., Dai, J. and Kerans, C. 1998. Modeling Dolomitized Carbonate-ramp Reservoirs: A Case Study of the Seminole San Andres Unit-Part II, Seismic Modeling, Reservoir Geostatistics, and Reservoir Simulation. Geophysics Volume 63, No. 6 (November 1998): 1876-1884.

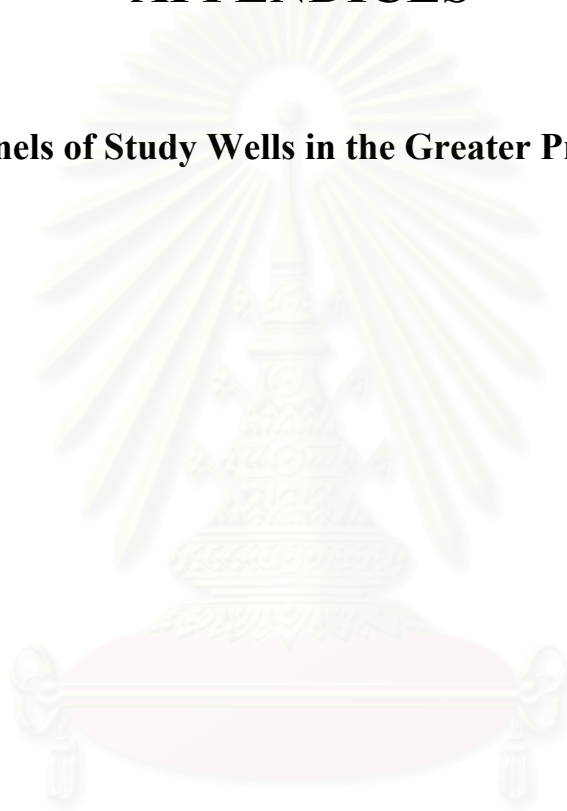
Workman, A. C. and Wright, D. 2000. Shell Thailand Greater Pratu Tao Re-Processing 2000 Report. The Hague: Shell Technology EP. (Unpublished Manuscript)



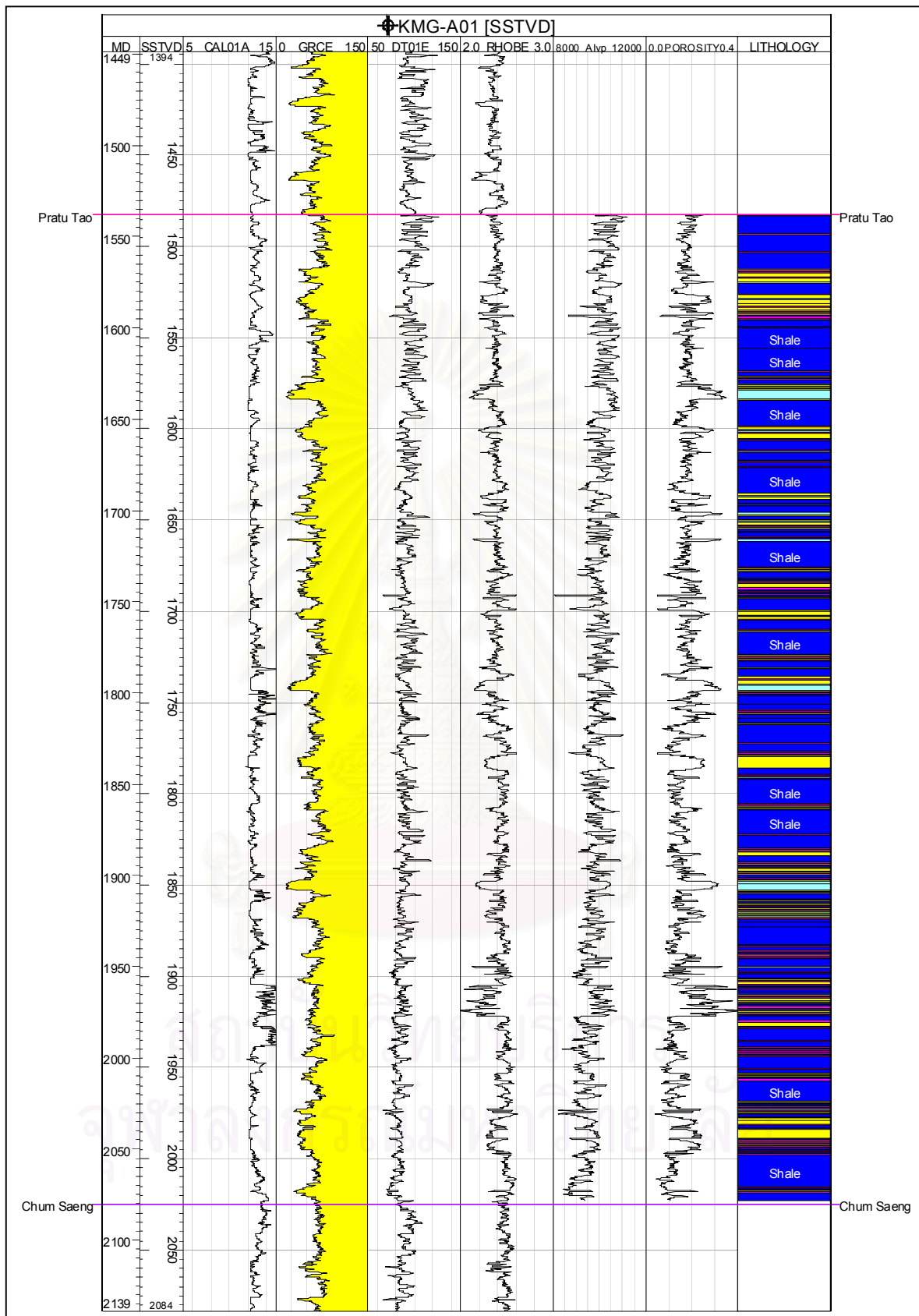
สถาบันวิทยบริการ
จุฬาลงกรณ์มหาวิทยาลัย

APPENDICES

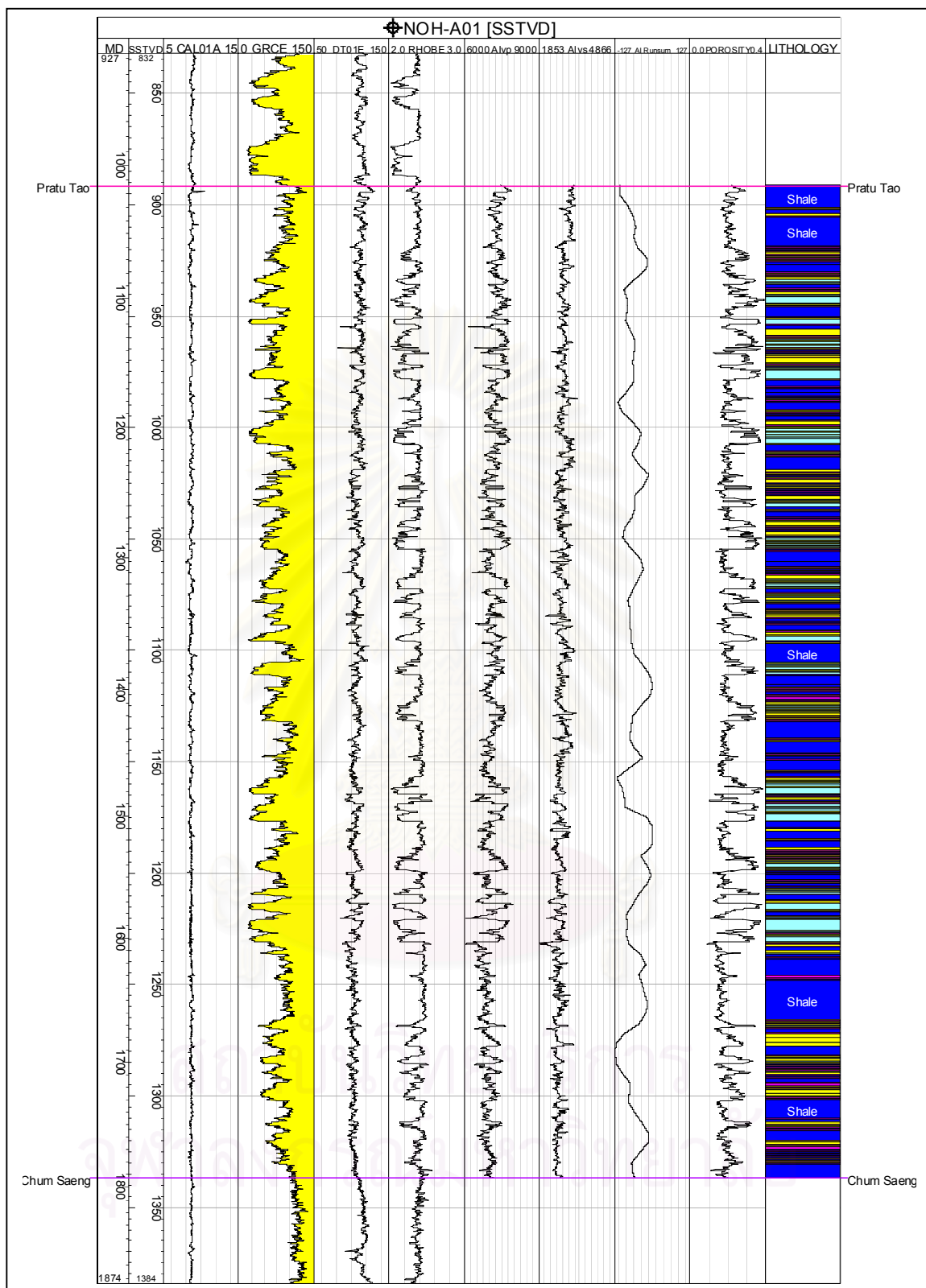
Logging Panels of Study Wells in the Greater Pratu Tao Area



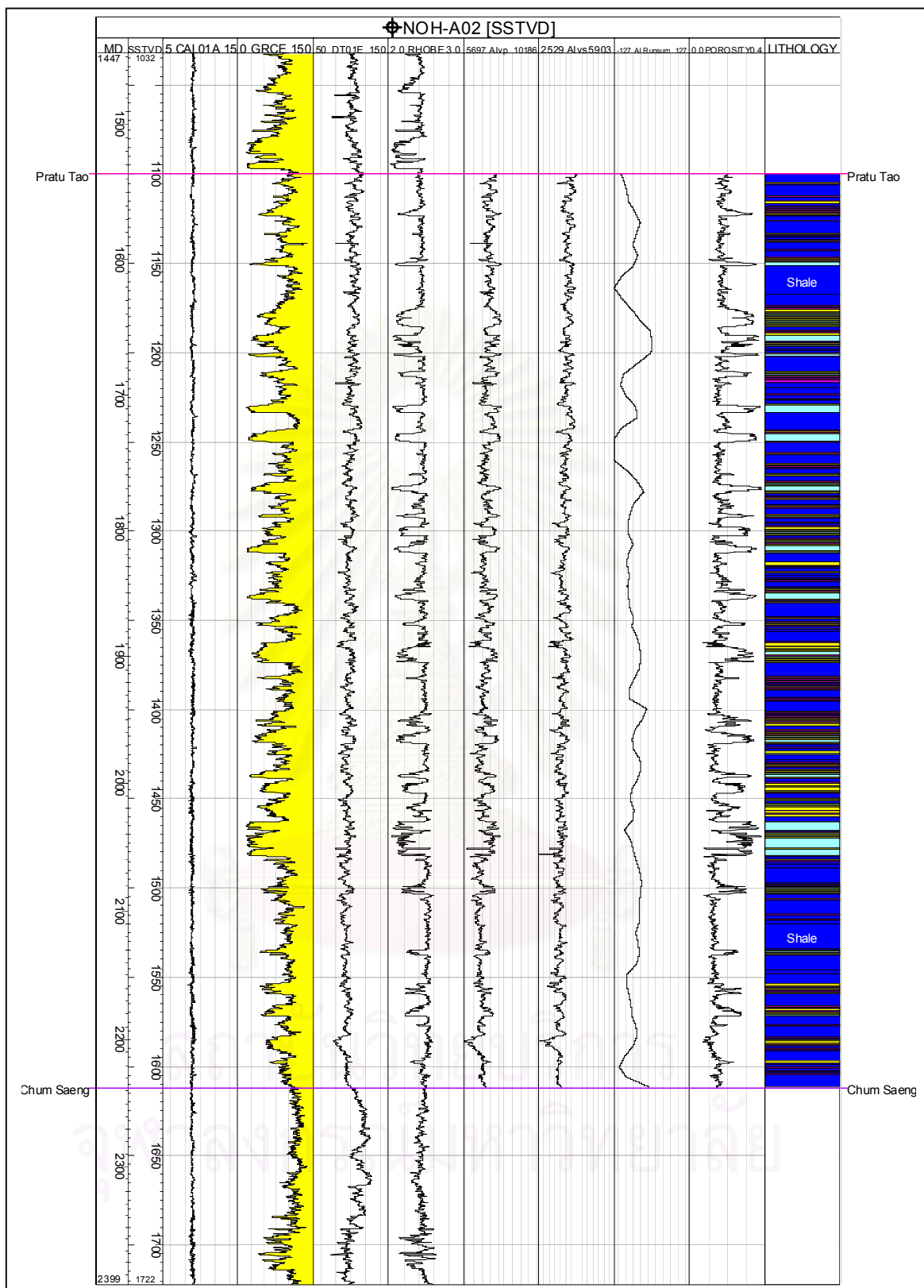
สถาบันวิทยบริการ
จุฬาลงกรณ์มหาวิทยาลัย



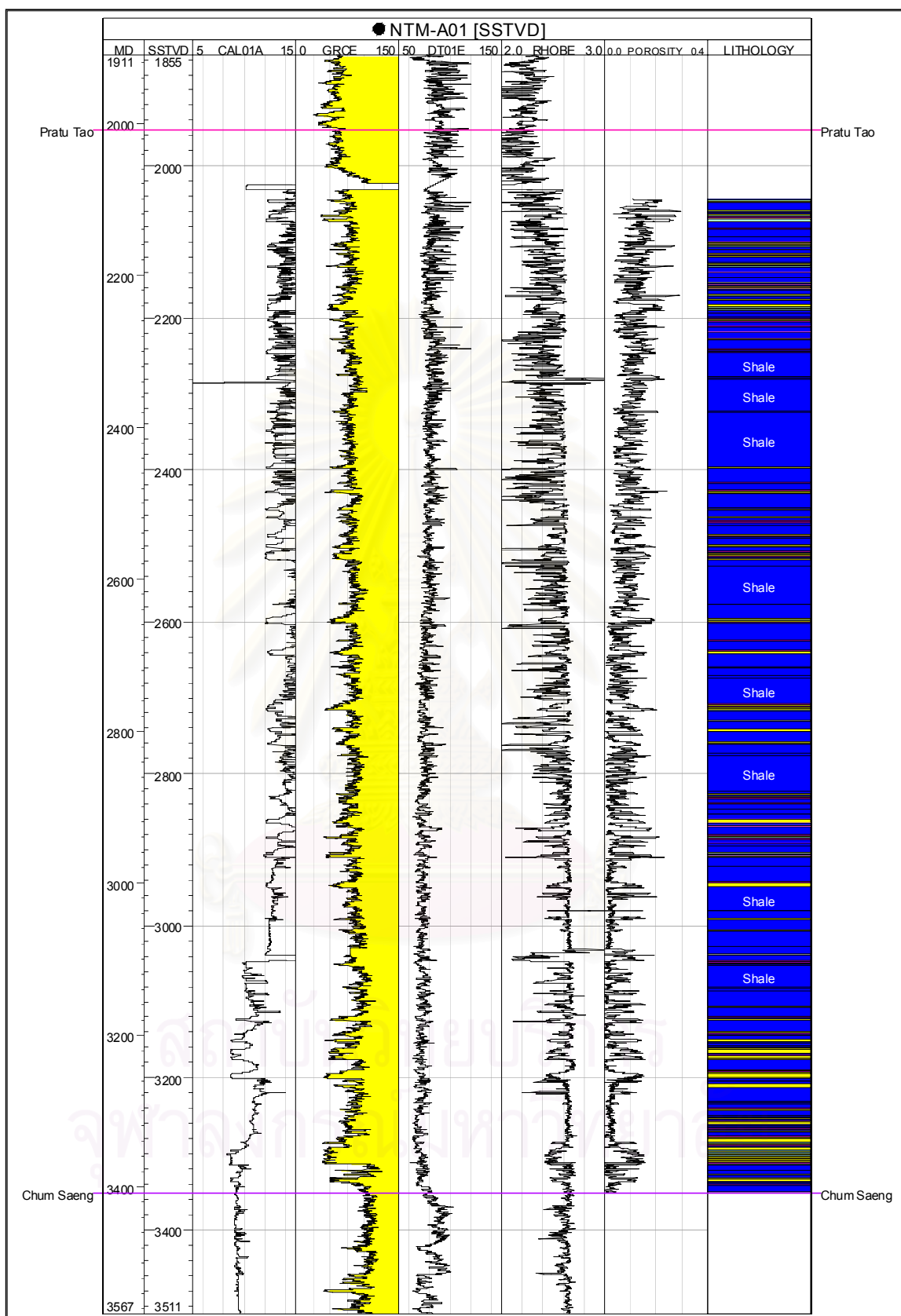
Appendix A. The logging panel of well KMG-A01



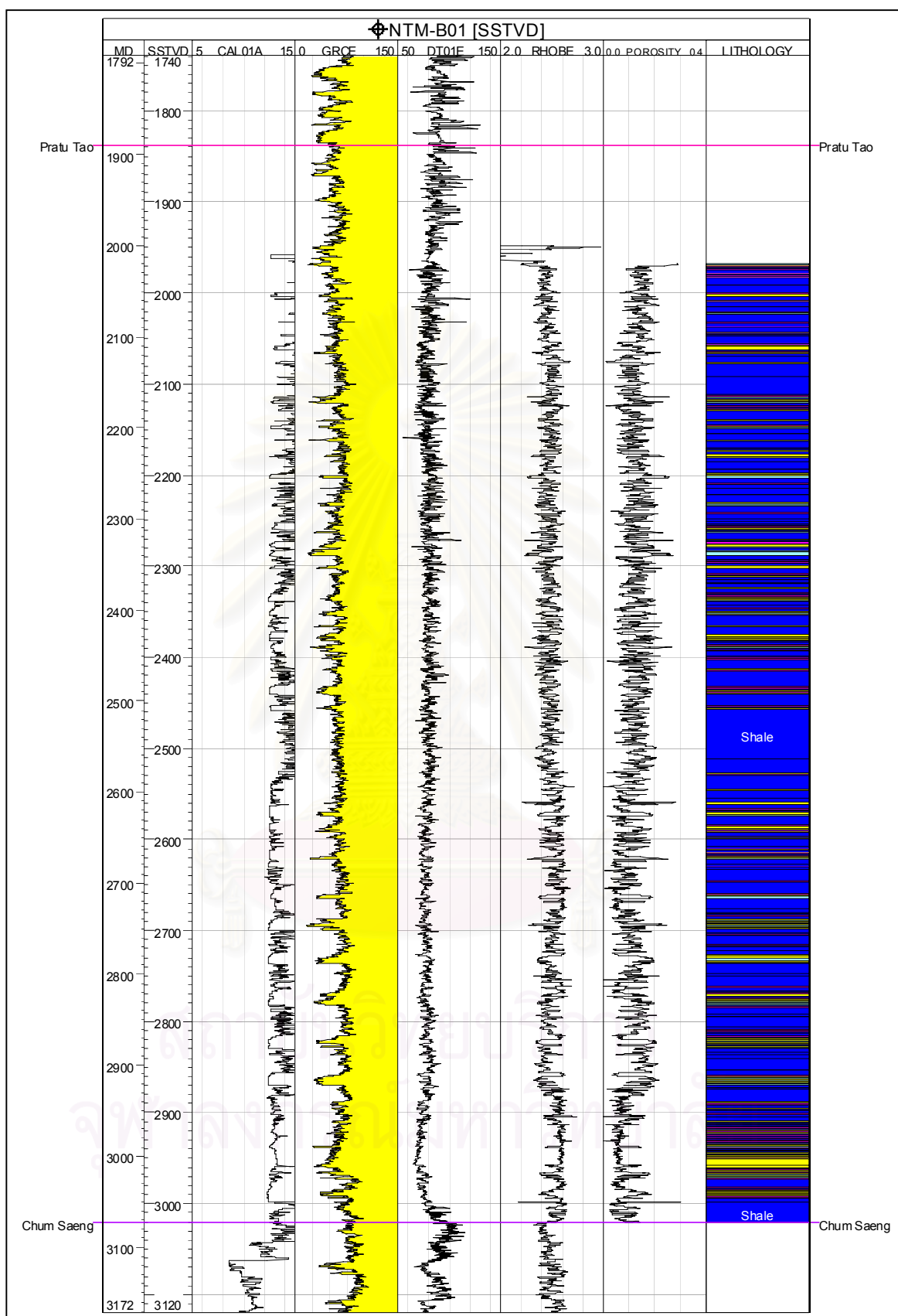
Appendix B. The logging panel of well NOH-A01



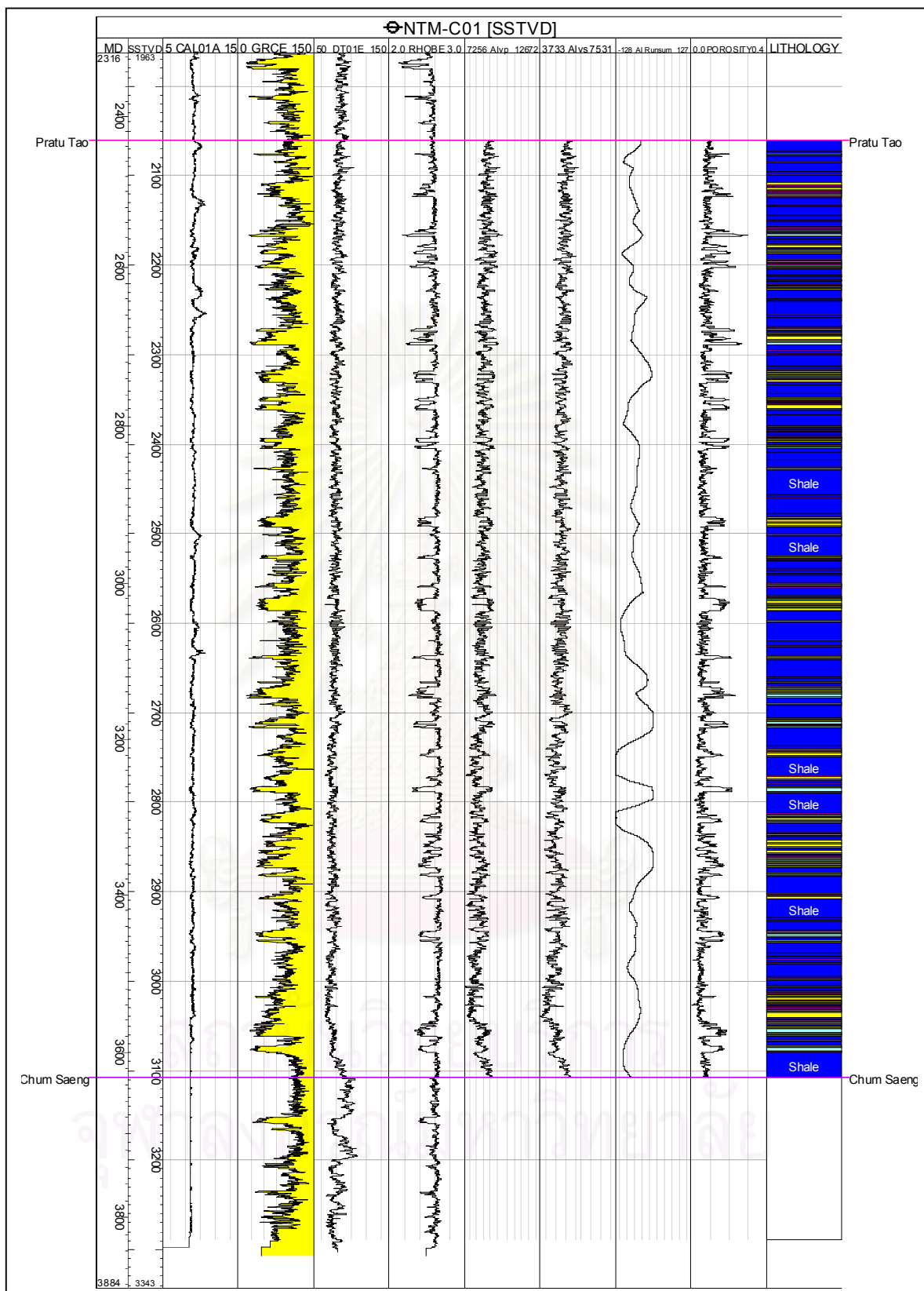
Appendix C. The logging panel of well NOH-A02



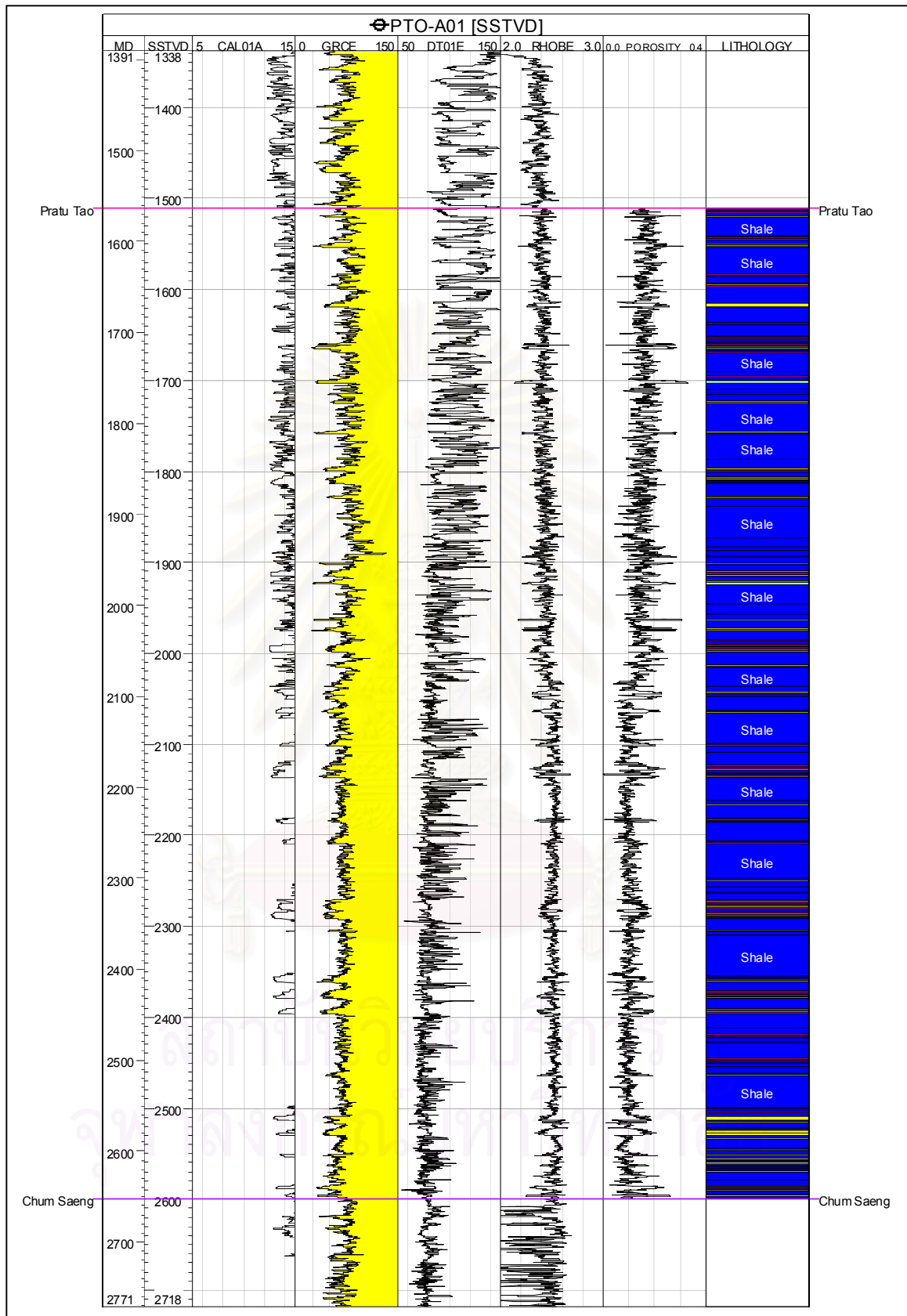
Appendix D. The logging panel of well NTM-A01



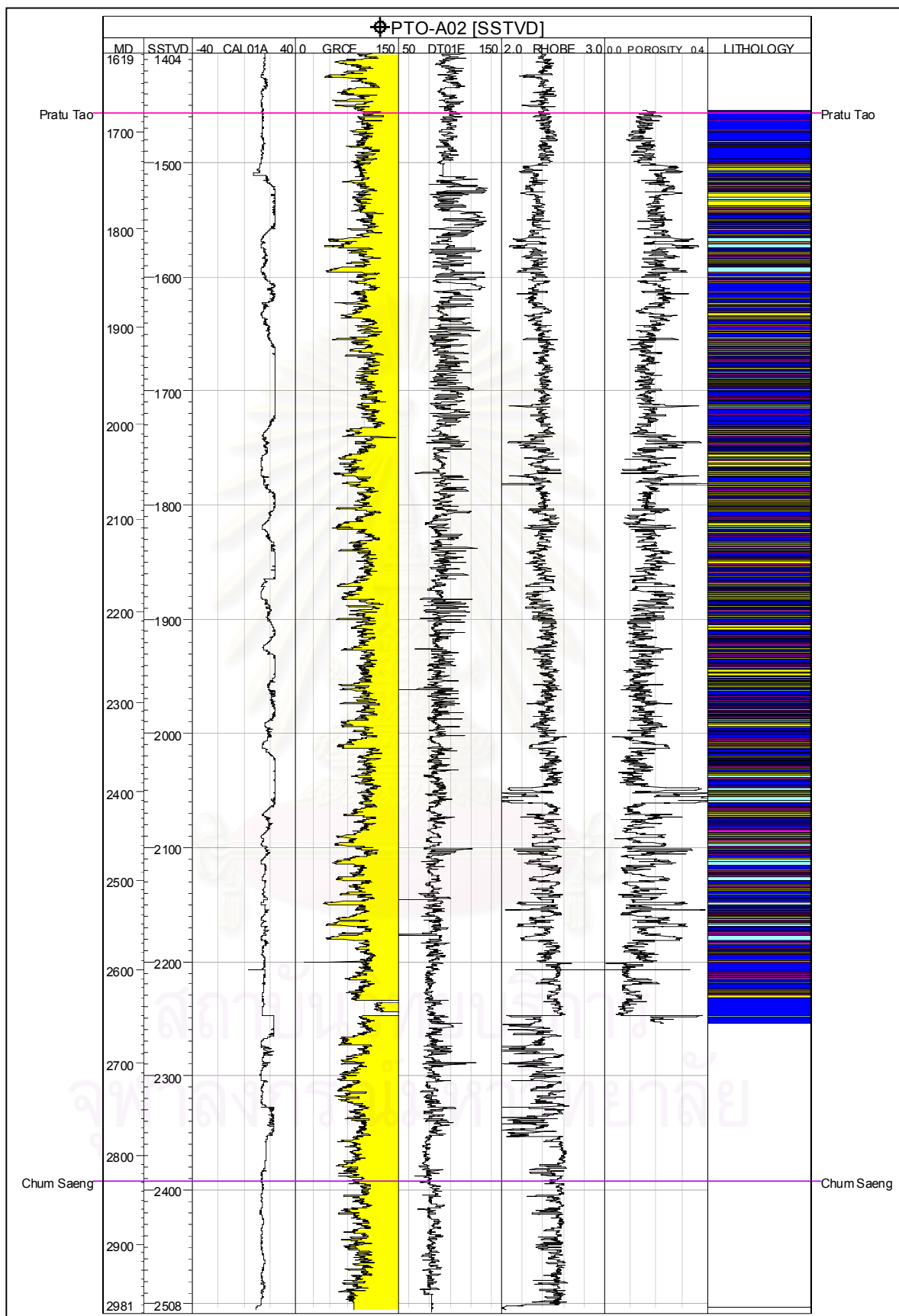
Appendix E. The logging panel of well NTM-B01



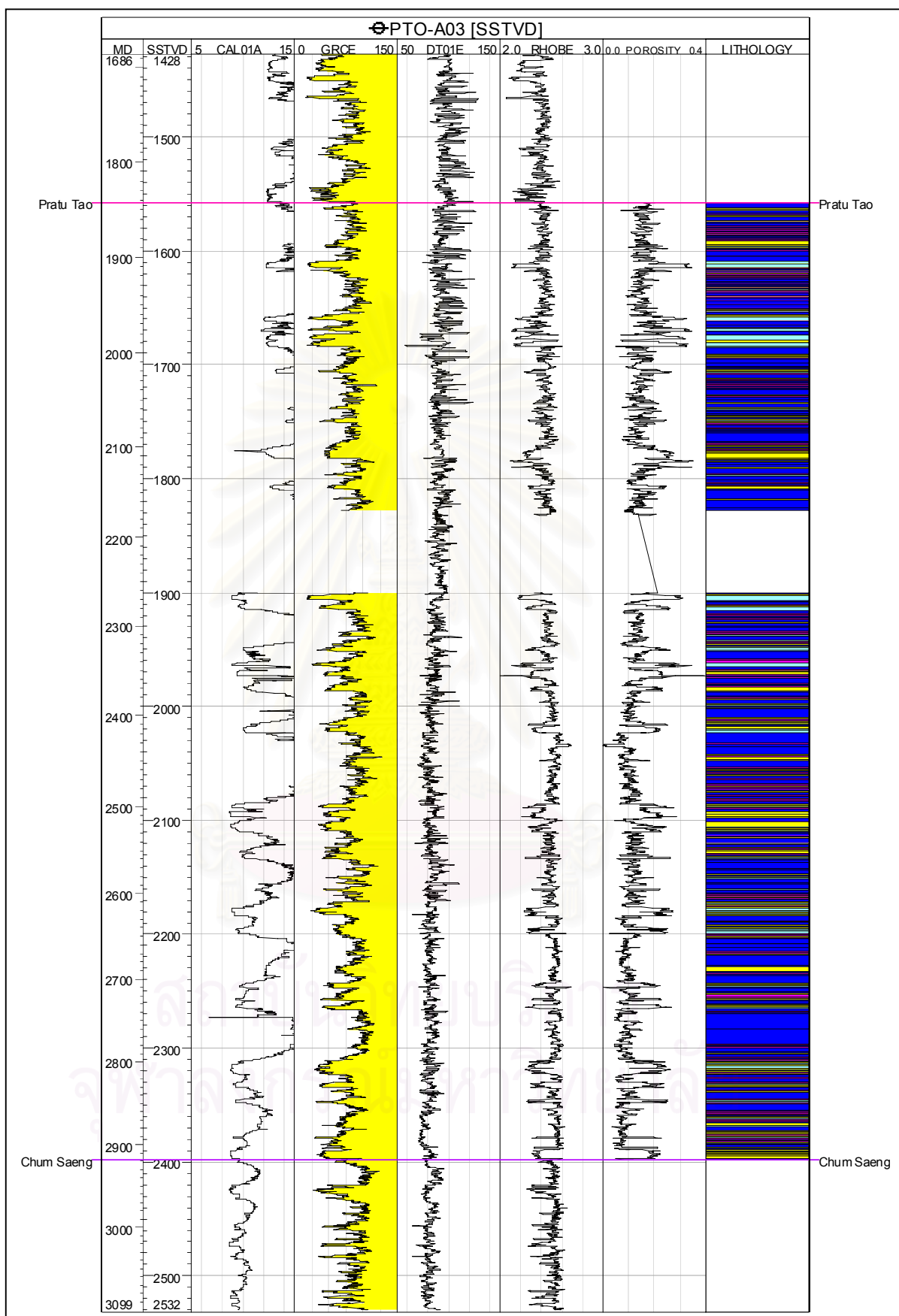
Appendix F. The logging panel of well NTM-C01



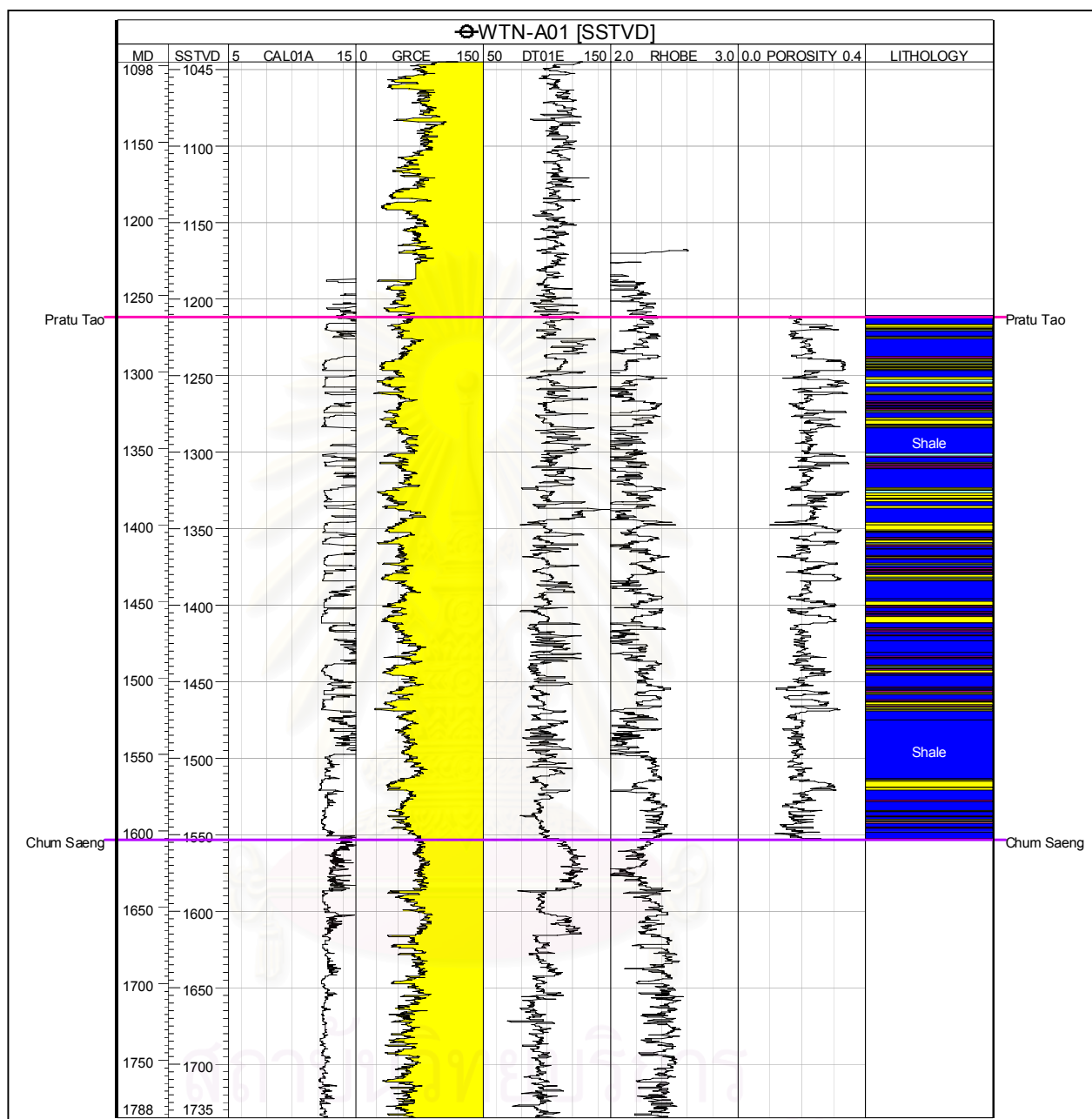
Appendix G. The logging panel of well PTO-A01



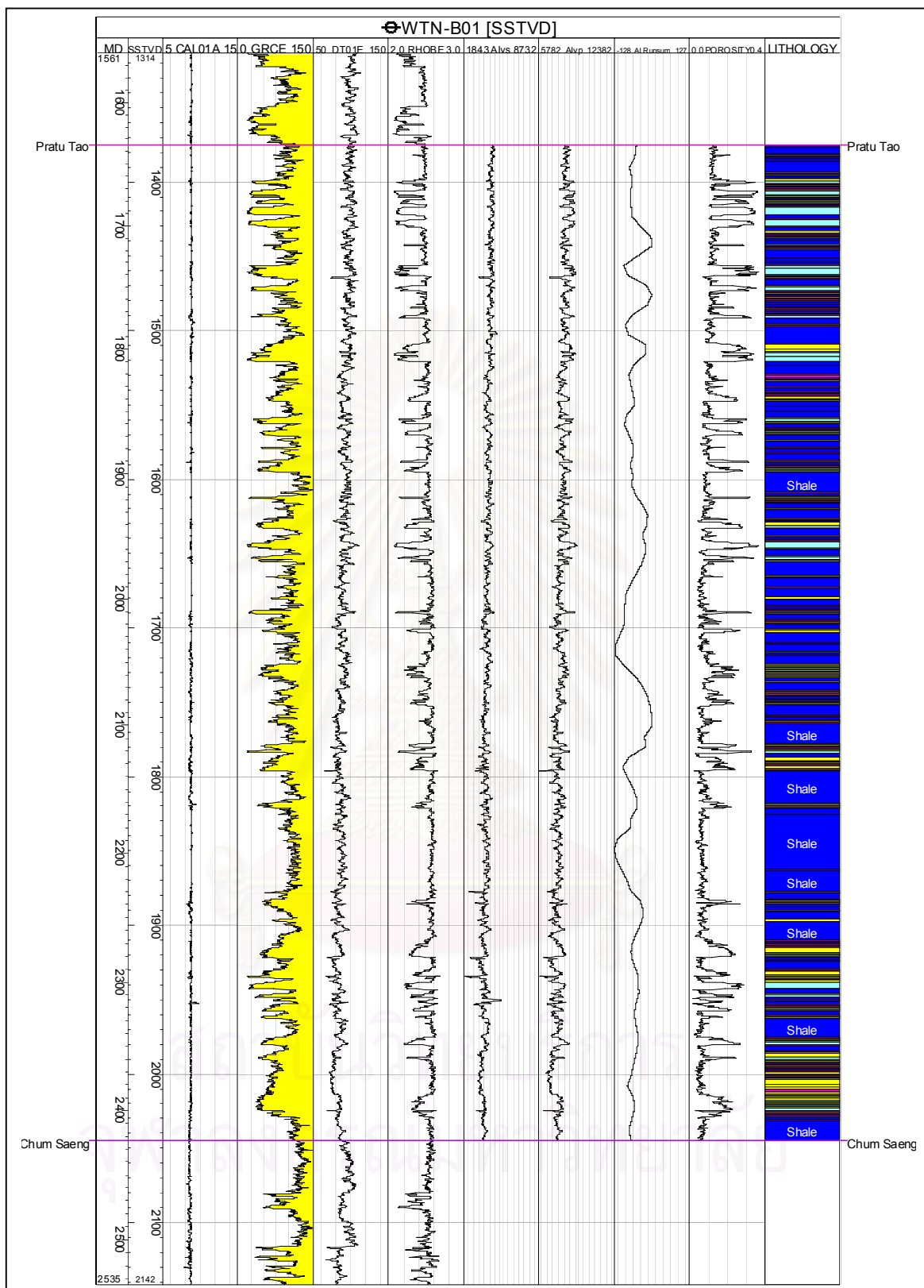
Appendix H. The logging panel of well PTO-A02



Appendix I. The logging panel of well PTO-A03



Appendix J. The logging panel of well WTN-A01



Appendix K. The logging panel of well WTN-B01

BIOGRAPHY

Miss Suhattaya Kaewla-iad was born in Bangkok, Thailand in 1971. She received a BSc (1993) in Geology from Chulalongkorn University. In 1993, she joined Thai Management Science Co., Ltd. as GIS Software Consultant. Two years later she transferred to Unocal Thailand as Senior Technical Assistant. For the last seven years, she has been working in Thai Shell Exploration and Production Co., Ltd. where she is presently a Production Seismologist in Hydrocarbon Resource Management Department. In Thai Shell, her responsibilities are mainly in seismic interpretation and prospect evaluation. She also has experiences in exploration and rehabilitation. Her main interests are in seismic and quantitative interpretation.



สถาบันวิทยบริการ
จุฬาลงกรณ์มหาวิทยาลัย